AN INVESTIGATION OF ANATOLIAN-AFRICAN SUBDUCTION
ZONE IN SOUTHWESTERN TURKEY: LITHOSPHERIC STRUCTURE
BENEATH ISPARTA ANGLE AND THE SURROUNDINGS FROM
RAYLEIGH WAVE PHASE VELOCITY INVERSION

by

Uğur Mustafa Teoman

B.S., Physics Engineering, Istanbul Technical University, 2001

M.S., Geophysics, Boğaziçi University, 2005

Submitted to the Kandilli Observatory and

Earthquake Research Institute in partial fulfillment of

the requirements for the degree of

Doctor of Philosophy

Graduate Program in Geophysics

Boğaziçi University

2016

ACKNOWLEDGEMENTS

ABSTRACT

AN INVESTIGATION OF ANATOLIAN-AFRICAN SUBDUCTION ZONE IN SOUTHWESTERN TURKEY: LITHOSPHERIC STRUCTURE BENEATH ISPARTA ANGLE AND THE SURROUNDINGS FROM RAYLEIGH WAVE PHASE VELOCITY INVERSION

Geodynamics of Turkey is complicated by the tectonic interactions between Africa, Eurasia and Arabian plates leading to high seismic activity and internal deformation beneath this region. Subduction of African Plate beneath Western Anatolia along Hellenic and Cyprus Arcs even more complicates the overall picture. In this sense, Isparta Angle (IA) plays a key role in understanding the neotectonic development of the Eastern Mediterranean. In this research, our goal is to put constraints on the upper mantle structure beneath IA and the surroundings via Rayleigh wave tomography method. In this regard, we adopted a phase velocity inversion technique named as "Two-plane wave method". With the use of this technique, we will be able to effectively map the three-dimensional velocity structure and amplitude variations to a certain extent. In August 2006 - September 2009 time frame, we recorded teleseismic earthquakes ($30° < \Delta < 120°$) with magnitudes greater than 5.5 using the permanent stations of Kandilli Observatory and Earthquake Research Institute (KOERI), Süleyman Demirel University (SDU) and IRIS/GEOFON together with temporary stations deployed with support from Missouri University and Boğaziçi University Research Fund (BAP). Following the detailed analysis of vertical component seismograms, we calculated a one-dimensional dispersion curve which served as an input for two dimensional (2-D) phase velocity inversions. Phase velocity maps were displayed in several cross sections at various periods. We also performed other series of inversions to determine the shear wave velocity distribution down to 250 km. Furthermore, construction of a 3-D shear velocity model enabled us to address the significant issues regarding the complex slab geometry of Anatolian-African subduction. These velocity anomalies provided us insights on the key elements that define the nature of subduction such as slab detachment, slab tearing, asthenospheric upwelling, and volcanism etc. The outcomes have been compared to most recent and previous studies to make reliable interpretations.

ÖZET

GÜNEYBATI TÜRKİYEDEKİ ANADOLU-AFRİKA YİTİM ZONU'NUN ARAŞTIRILMASI: ISPARTA BÜKLÜMÜ VE CİVARINDAKİ LİTOSFERİK YAPININ RAYLEIGH DALGALARI TERS ÇÖZÜM YÖNTEMİ İLE BELİRLENMESİ

Türkiye'nin jeodinamiği; Afrika, Avrasya ve Arap plakalarının birbirleriyle olan tektonik etkileşimlerinden ötürü karmaşıklık göstermektedir. Bu etkileşimler bölge ve yakın çevresinde sismisitenin yoğun olmasına ve iç deformasyona sebebiyet vermektedir. Afrika plakasının Helenik ve Kıbrıs yayları boyunca Batı Anadolu'nun altına dalması resmi daha da karmaşık hale getirmektedir. Bu çerçevede, Isparta Büklümü (IB) Doğu Akdenizdeki neotektonik gelişimlerin anlaşılması açısından önemli bir rol oynamaktadır. Bu araştırmada, IB ve çevresi altındaki üst manto yapısı hakkında yüzey dalgaları tomografisi yöntemi kullanılarak bilgi edinilmesi amaçlanmaktadır. Bu bağlamda, "İkili Düzlem Dalga" tekniğini çalışmamıza adapte ettik. Bu yöntem ile güneybatı Türkiye altındaki üç-boyutlu yapıyı güvenilir bir biçimde haritalayabilme imkanını elde ettik. Ağustos 2006 ile Eylül 2009 tarihleri arasında meydana gelen büyüklüğü 5.5 in üzerinde olan telesismik depremler (30° < episantır uzaklık < 120°) Kandilli Rasathanesi ve Deprem Araştırma Enstitüsü (KRDAE), Süleyman Demirel Üniversitesi (SDÜ) ve IRIS/GEOFON kalıcı sismik ağlarına ait kalıcı istasyonlara ek olarak, bölgede Missouri Üniversitesi ve Bilimsel Araştırma Projeleri (BAP) desteği ile kurulan geçici istasyonlar tarafından kaydedildi. Düşey sismogramların detaylı analizini takiben, iki boyutlu faz hızları ters çözümünde girdi olarak kullanılacak olan bir boyutlu dispersiyon eğrisini oluşturduk. Akabinde, faz hızı haritalarını fartkı periyodlardaki yatay kesitlerde haritaladık. Güneybatı Türkiye altındaki makaslama dalgası hız dağılımını da yaklaşık 250 km derinliğe kadar saptayabilmek için bir dizi terz cözüm uyguladık. Üç boyutlu makaslama dalgası hız modelinin belirlenmesi, Afrika-Anadolu yitim mekanizmasının karmaşık levha geometrisi ile ilgili önemli hususlara ışık tuttu. Yüksek ve düşük hız anomalileri, bize yitim zonlarının doğasını oluşturan levha kopması, levha yırtılması, astenosferik malzeme yükselimi ve volkanizma hakkında faydalı fikirler verdi. Sağlıklı yorumlar yapılabilmesi amacı ile, bu çalışmanın sonuçları güncel ve daha eski çalışmalarla karşılaştırıldı.

TABLE OF CONTENTS

LIST OF FIGURES

LIST OF TABLES

LIST OF SYMBOLS

C_o	Isotropic Phase Velocity Component
H	Layer Thickness
J_c	Critical Angle
N	Number of Grid Points
S	Average Phase slowness
SH_I	Incoming SH Wave
SH_R	Reflected SH Wave
SH_T	Transmitted SH Wave
SV_I	Incoming SV Wave
SV_R	Reflected SV Wave
U	Displacement vector
V	Poisson Ratio
W	Weighting Parameter
c	Phase Velocity
f	Frequency
k	Wavenumber
α	P-wave Velocity
λ	Wavelength
β	Shear Wave Velocity
μ	Density
ψ	Back Azimuth
ϕ	Phase
w	Angular frequency
τ	Travel Time
υ	Angular Deviation

LIST OF ACRONYMS/ABBREVIATIONS

1-D	One Dimensional
2-D	Two Dimensional
3-D	Three Dimensional
AB	Antalya Bay
AEP	Aegean Extensional Province
AKT	Aksu- Kyrennia Thrust
AM	Anaximander Mountains
AP	Anatolian Plate
BAP	Boğaziçi Research Fund
BB	Broad Band
BS	Bitlis Suture
CB	Cilica Basin
CI	Crete Island
DSTFZ	Dead Sea Transform Fault Zone
EAFZ	East Anatolian Fault Zone
EAP	East Anatolian Plateau
ESM	Erastothenes Sea Mount
E-W	East – West
FBFZ	Fethiye Burdur Fault Zone
FR	Florence Rise
Hz	Hertz
IA	Isparta Angle
IRIS	Incorporated Research Institutes for Seismology
JWKB	Jeffreys-Wentzel–Kramers–Brillouin
KOERI	Kandilli Observatory and Earthquake Research Institute
MM	Menderes Massif
MS	Marmara Sea
NAFZ	North Anatolian Fault Zone
NEMC	National Earthquake Monitoring Center
N-S	North - South

PF	Paphos Fault
PREM	Preliminary Reference Earth Model
PT	Pliny Trench
RB	Rhodes Basin
RI	Rhodes Island
RMS	Root Mean Square
SDU	Süleyman Demirel University
SF	Sultandagi Fault
ST	Strabo Trench
WAEP	Western Anatolia Extensional Province.
Vp	P-wave velocity
Vs	S-wave velocity

1. INTRODUCTION

In solid earth sciences, substantial knowledge of the earth's interior is highly required in order to understand the complicated processes occurring at the surface such as seismicity, volcanism, plate movements and perturbations in the geomagnetic field. Focusing solely on seismology, one of the major challenges is to establish a coherent relationship between mantle dynamics and its main surface expression, plate tectonics. To accomplish this goal, earth scientists have adopted numerous seismological techniques and extracted valuable information from the earth's crust, mantle and core with the use of indirect observations (Thurber, 1993). In this sense, a quite popular seismic imaging technique referred to as "seismic tomography" has emerged in the last couple of decades. Seismic tomography can be defined as the reconstruction of a field from knowledge of linear path integrals through that specific field (Clayton, 1984). The word "tomo" comes from the Greek language which means "slice". If we take a slice from a three dimensional (3-D) object, we obtain a two dimensional (2-D) section. By combining these 2–D slices, a 3-D image can be reconstructed. This method was originally called the "3-D" inversion in the seismological community until the early 1980's. In latter stages, seismic tomography has become a very powerful tool to map the present state of seismic velocity variations within the earth's interior on a variety of scales as seismic wave propagation is influenced by the materials located along the waves' path through the earth. Furthermore, with the use of imaging techniques borrowed from medicine and tremendous advances in computing together with graphics, seismic tomography has achieved breakthrough advances from global scale earth processes to meter-scale resource exploration (Hirahara, 1993).

Fundamentally, seismic tomography benefits from the usage of seismic body waves (P & S waves), surface waves (Rayleigh & Love waves) and seismic noise. Velocity information can be retrieved either from P and S wave arrival times or from surface wave dispersion in various scales as stated by numerous authors (e.g. Spakman et al., 1988, Zhou, 1996; Grand et al., 1997; Van Der Hilst et al., 1997; Bijwaard et al., 1998; Kennett et al., 1998; Ritzwoller and Levshin, 1998; Bijwaard and Spakman, 2000; Boschi and Dziewonski, 2000; Pasyanos et al., 2001; Karason and Van Der Hilst, 2001; Zhao, 2001; rand, 2002; Pasyanos and Walter, 2002; Ritzwoller et al., 2002; Piramallo and Morelli, 2003; Li et al., 2003; Kennett and Gorbatov, 2004; Pasyanos, 2005; Shapiro et al. 2005;

Lei and Zhao, 2006; Moschetti et al. 2007; Yang et al. 2007; Van Hinsbergen et al., 2010; Cambaz and Karabulut, 2010; Biryol et al., 2011; Ceylan et al., 2012; Salaün et al., 2012).

The sensitivity of surface waves to crustal and upper mantle accounts for the extensive use of surface waves (both Rayleigh & Love waves including group and phase velocity measurements) to map the three-dimensional shear wave velocity structure beneath the Earth, referred to as "Surface Wave Tomography". Throughout the last couple of decades, dispersion estimations from topographic inversions have been commonplace with new methods and various approaches being implemented both on regional and global scales. Tomographic techniques differ in geometry (i.e Cartesian versus spherical), model parameterization (regular vs irregular grids/nodes), certain theoretical assumptions (ray/wave paths and scattering), smoothing parameters and whether azimuthal anisotropy can be estimated simultaneously with the isotropic velocities. Traditional surface-wave tomography is based upon JWKB ray theory, which is valid only if the lateral length scales of the heterogeneities are larger than the characteristic wavelength of the seismic waves. Recent publications on surface wave tomography have focused on finite frequency effects (Spetzler et al., 2002; Yoshizawa and Kennett, 2002; Zhou et al., 2004) and one specifically in the case of group velocities (Ritzwoller et al., 2002). These finite frequency methods each take slightly different approaches to move beyond ray theory and more closely approximate the true sensitivity kernels. As a result of the long wavelength nature of surface waves, surface wave tomography is more appropriate for the global or large-scale regional studies. Even though body waves have higher spatial resolution due to the shorter wavelengths, sparse and uneven coverage of networks restricts the resolution.

In this research, our primary objective is to provide valuable insights on the 3-D lithospheric structure of Anatolian – African Subduction zone and the surroundings which includes a significant tectonic element, the Isparta Angle (IA). Determination of reliable dispersion characteristics and phase velocities will also lead us to put accurate constraints on the shear wave velocity structure beneath southwestern Turkey and eastern Mediterranean. We have chosen to investigate the lithospheric structure of IA and the surroundings because this area is located at the junction two subduction zones (Hellenic and Cyprus arcs) with different geometries and subduction characteristics. This triangle shaped region plays an enigmatic role in neotectonic development of the Eastern

Mediterranean region and needs to be considered as a whole since the nature and timing of the active deformation within the Anatolian continental lithosphere has not been well documented. In this respect, we adopted a Rayleigh wave phase velocity inversion technique (Forsyth et all., 1998, Forsyth and Li, 2003, Yang and Forsyth, 2006) which has been effectively used to model both phase velocity and amplitude variations across an array of broadband sensors. Since phase velocities can only bring us integrated information about crust and the mantle, direct information at various depths can be revealed by inverting for shear wave velocities. This is succeeded by another inversion algorithm from Saito, (1988).

In chapter two, an extensive overview tectonics and previous seismological studies will be presented. The present-day geodynamics of Turkey, the tectonic processes occurring in the African-Anatolian subduction system and the seismicity of the region will be explained in detail.

Chapter three consists of basic surface wave definitions, their generation and propagation characteristics, group/phase velocity measurements and relevant studies. This part will be followed by the description of Rayleigh wave data set and teleseismic event analysis. Then, the details of surface wave tomography method, the results of one/two dimensional isotropic phase velocity inversions together with the resolution assessment will be presented.

Chapter four includes the construction of a three-dimensional (3-D) shear wave velocity model from 1-D/2-D phase velocity inversion results. Determination of an initial shear velocity model and the subsequent inversions for a 3-D velocity structure will be explained. We are also going to evaluate the resolution of model parameters and their relation with depth.

In chapter five, vertical cross sections of shear wave velocity variations along the tectonically significant features beneath the African-Anatolian subduction system will be displayed. The geometry of the subducting African lithosphere and the current state of this subduction process will be emphasized. In addition, we will attempt to correlate the overall results with the most recent seismic tomography studies.

2. AN OVERVIEW OF TECTONICS & SEISMOLOGICAL STUDIES

The present-day geodynamics of Turkey is governed by tectonic interactions between three major plates; Africa, Eurasia, Arabia and the ongoing internal deformation along their boundaries (Figure 2.1). These interactions impose a large variety of complex tectonic processes such as collision, subduction, back-arc extension, strike slip faulting and rotation of different blocks and micro-plates within a relatively small geographical area.
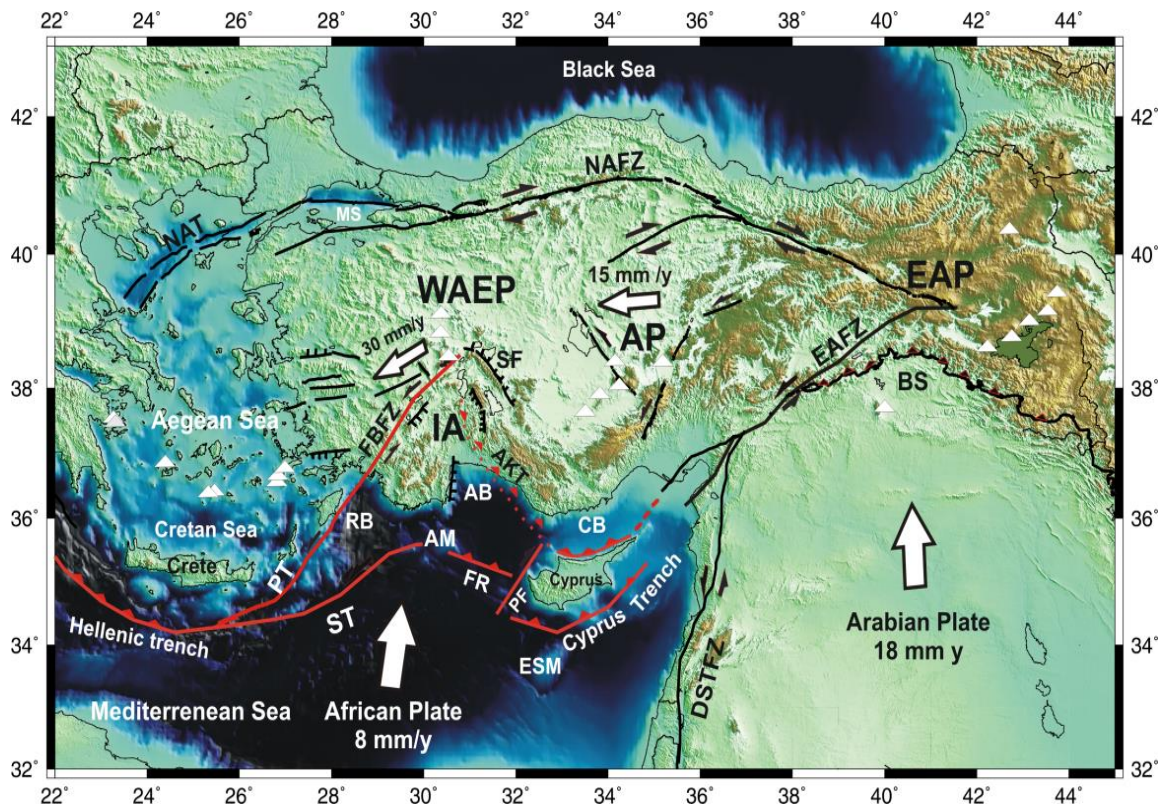
Figure 2.1. A simplified tectonic map of Turkey and the surroundings. Plate motions and are shown by white arrows. AB: Antalya Basin, AKT: Aksu- Kyrennia Thrust, AM: Anaximander mountains, AP: Anatolian Plate, BS: Bitlis Suture, CB: Cilica Basin, DSTFZ: Dead Sea Transform Fault Zone, EAFZ: East Anatolian Fault Zone, EAP: East Anatolian Plateau, ESM: Erastothenes Sea Mount, FBFZ: Fethiye Burdur Fault Zone, FR: Florence Rise, IA: Isparta Angle, MS: Marmara Sea, NAFZ: North Anatolian Fault Zone, PF: Paphos Fault, PT: Pliny Trench, RB: Rhodes Basin, SF: Sultandagi Fault, ST: Strabo Trench, WAEP: Western Anatolia Extensional Province.

African and Arabian plates converge towards Eurasia with northeastward and northward motion, respectively. Within this concept, two key factors play an essential role in understanding the major tectonic features in the region (Anatolia): 1) Continental collision of Arabia and Eurasia plates across the Bitlis-Zagros suture zone since middle Miocene (Mckenzie, 1978), 2) Subduction of African plate beneath the Aegean-Anatolian microplate along the Hellenic and the Cyprian arcs (trenches) since the late Cretaceous (Westaway, 1994). Recent Global Positioning System (GPS) measurements indicate differential plate motions of Africa (< 10mm / year) and Arabia (~ 18 mm / year) in a Eurasia fixed reference frame (Reilinger et al. 1997, McClusky et al., 2000, 2003). This velocity difference induces major strike-slip faulting along Dead Sea Transform Fault Zone (DSTFZ) leading to westward extrusion of Anatolian plate where its movement is partitioned along North Anatolian Fault Zone (NAFZ) to the north and East Anatolian Fault Zone (EAFZ) to the south (Reilinger et al., 1997; Armijo et al., 2003). To further west, southern Aegean margin is moving coherently towards the Hellenic arc at a larger speed than the central Anatolia block (30 mm/yr vs. 15 mm/yr). These blocks are indeed separated in western Anatolia by a ~N–S stretching area. The overall geometry suggests that the extra-relative speed of central Aegean with respect to Eurasia is mostly due to the pull resulting from the Hellenic subduction zone (Kahle et al., 1999; McClusky et al., 2003, Nyst and Thatcher, 2004; Faccenna, 2006).

Numerous seismological studies have been extensively performed in order to provide valuable insights on the lithospheric structure beneath Eastern Turkey. Tomographic velocity models (both regional and teleseismic), seismic anisotropy, P & S wave receiver functions, seismic wave propagation and attenuation (Pn, Sn and Lg phases) studies all together revealed the lack of mantle lithosphere, crustal thickness values ranging between 40 and 45 km, low Pn-Love wave velocity anomalies and wide zones of Sn wave blockage (Sandvol et al.. 2003; Al-Lazki et al., 2003; Gök et al.,2000, 2003, 2007; Zor et al., 2003, 2007; Türkelli et al., 2003; Angus et al., 2006; Maggi and Priestley 2005; Özacar et al., 2008; Gans et al., 2009; Cambaz and Karabulut 2010; Biryol et al., 2011, Warren et al; 2013). Based on these observations, lack of mantle lithosphere suggested the detachment of northward subducting Arabian slab giving ways to slab steepening and break-off. A teleseismic tomography study by Zor (2008) mapped the detached slab at ~600 km depth. Consequently, upwelling of hot asthenosphere beneath this subduction-accretion complex

lead to extensive melting and widespread volcanism across the entire East Anatolian plateau (Sengör 2003; Keskin 2003). The extent of this hot, buoyant low velocity body is thought to be supporting the relatively thinner crust of this ~2km high plateau (Sengör 2003; Özacar et al., 2003; Zor et al., 2003).

Eastern Mediterranean region has been shaped by the compression, extension and rotation of different lithospheric blocks and micro-plates (Figure 2.1). Western Anatolia Extensional Province (WAEP) comprises the Aegean domain and lies within the convergence zone of African and Eurasian plates. This plate boundary is characterized by subduction tectonics and is in the initial stages of collision driven orogenic buildup (Dilek, 2006). Aegean region is one of the most seismically active (Figure 2.2) and rapidly deforming domains of the Alpine-Himalayan mountain belt. Since the late Cretaceous, the ongoing subduction of African plate beneath Eurasia has been occurring along two separate arcs: the Hellenic and the Cyprian (Westaway, 1994; Kremer et al., 2003; van Hinsbergen et al., 2005 and the references therein). The Hellenic arc is characterized by a relatively steep retreating subduction (due to slab rollback), whereas the Cyprian Arc seems to involve a shallow subduction with two major seamounts impinging on the trench (Kempler and Abraham 1987; Zitter et al., 2003). Subduction rollback along Hellenic trench has resulted in N-S upper plate extension in western Anatolia and the gravitational collapse of the Tethyan orogenic crust since early Miocene (Seyitoglu et al., 1992; Jolivet et al., 1994; Jolivet and Faccenna 2000, Bozkurt 2001; Faccenna et al., 2003; Dilek and Altunkaynak, 2008). N-S extension is accommodated by a system of well-developed E-W trending grabens in western Anatolia. Backarc extension in the Aegean region appears to have started long before the onset of southwestward displacement of the Anatolian plate in the late Miocene (Barka and Reilinger 1997; Jolivet and Faccenna 2000). The extensional tectonic regime has also been expressed by crustal thinning and normal faulting outlined by numerous papers on P & S wave receiver functions (Saunders et al., 1998; Bohnhof et al., 2001; Horasan et al., 2002; Li et al., 2003, Meijde et al., 2003; Karagianni et al., 2005; Sodoudi et al., 2006; Zhu et al., 2006; Akyol et al., 2006; Tezel et al., 2010, Vanacore et al., 2013), inversions with gravity data (Tiberi et al., 2001; Tirel et al., 2004), magnetotelluric profiles (Bayrak and Nalbant 2001; Gürer et al., 2004; Ulugerli et al., 2007) and focal mechanisms (Kiratzi and Papazachos 1995; Papazachos and Kiratzi, 1996; Koçyiğit et al., 2000, Taymaz and Tan, 2001; Taymaz et al., 2002; Kiratzi and

Louvari, 2003, Shaw and Jackson, 2010). Present kinematics together with a detailed moho- topography of the overriding Aegean and the subducting African lithosphere is discussed by Sodoudi et al., (2006) and the references therein.

Seismic anisotropy patterns in the eastern Mediterranean were investigated in several studies mostly indicating NE-SW anisotropy/asthenospheric flow (Hatzfeld et al., 2001; Sandvol et al., 2003; Schmid et al., 2004; Sapaş and Güney, 2009; Biryol et al., 2010; Endrun et al., 2011; Faccenna et al., 2013). Biryol et al. (2010) suggested that the SW rollback of Hellenic slab could account for the consistent NE-SW pattern of flow underneath the central-west Anatolia and according to Le Pichon and Kreemer (2010); the circular pattern of present day motion in the Eastern Mediterranean is enforced by a counterclockwise asthenospheric flow from Levantine Basin to Arabia, Anatolia and the Aegean. Furthermore, a very recent study from Paul et al., (2014) emphasized that slab rollback related trench normal flow is an evidence of a slab window causing an exception of NW-SE fast polarization directions beneath southwestern Anatolia.

Subduction along the Hellenic arc has been clearly mapped by relatively higher seismic velocities with respect to adjacent plates (Papazachos and Nolet, 1997; Spakman et al., 1998; Piromallo and Morelli,. 1998, 2003; Wortel and Spakman 2000; Faccenna et al., 2006; Dilek and Sandvol 2009; Hinsbergen et al., 2010; Biryol et al., 2011) and a single slab more than 1500 km long is present (Jolivet et al., 2003, Jolivet and Brun., 2010 and the references therein). High velocity anomalies extend to depths exceeding the intermediate depth seismicity in the region (Figure 2.2). The long-lived Hellenic subduction is more matured and the slab is probably partly anchored in the lower mantle (Jolivet and Brun, 2010). Seismicity along the Hellenic arc is typical of subduction zones with deeper events toward the back-arc region (Figure 2.1). Seismicity zone terminates at a depth of about 180 km (Papazachos et al., 2000). Intermediate depth events (depth: 60-150 km) are mainly located in the inner part of the arc and in Antalya Basin along the Aksu Thrust (AT). Shallow events are widespread along the Hellenic Arc, Greece-Turkey mainlands and the Aegean Sea. Considering the state of the upper mantle; Sn phase is attenuated along the volcanic arc towards the north of Crete and parallel to Hellenic arc (Gök et al., 2000, 2003). In northern Aegean Sea, there is also a partially attenuating Sn zone with low upper mantle Pn velocities (Al-Lazki et al., 2003). Partial attenuation might

be linked to active extensional deformation in the back-arc setting (Dilek and Sandvol, 2009).

In contrast, the image of the Cyprian slab is much weaker in most tomographic models and vertically discontinuous (Widiyantoro et al., 2004; Faccenna et al., 2006), possibly complicated by the collision of Eratosthenes Seamount with Cyprus (Ben-Avraham et al., 1995; Robertson 1998; Glover and Robertson 1998) and the westward lateral escape of Anatolia (Şengör et al., 1985; Reilinger et al., 1997; Le Pichon et al. 1995). Moreover, the blockage of the subduction process along the central and eastward segments of the Cyprian arc was also depicted by many researchers (Ben-Avraham et al., 1995; Kempler and Garfunkel 1994) on the basis of seismic reflection data as well as seismicity observations. The plate boundary along the western segment of Cyprian Arc is often inferred to join the Florance Rise (FR) and the eastern extremity of the Strabo Trench (ST), through the south of Anaximander mountains (Figure 2.1). Sn wave propagates efficiently along the Cyprian arc consistent with a relatively high velocity Pn zone (Gök et al., 2003; Al-Lazki el at., 2004) and S-wave velocities (Diluccio and Pasyanos, 2007). A study by Dilek and Sandvol (2009) point out that the shallow slab of the Cyprian subduction zone may not be in direct contact with the Anatolian lithosphere and extend almost to the NAFZ, based on several teleseismic velocity models. Cyprian Arc is less active in terms of seismicity compared to Hellenic arc (Enghdal 1998; Wdowinski et al., 2006); majority of the earthquakes are located below Anaximander Mountains as well as below the Florence Rise (Figure 2.2). There are no indications for a Benioff zone in the eastern Cyprus arc that forms the plate boundary between the Anatolian plate in the north and the Sinai plate in the south (Segev et al., 2006; Wdowinski et al., 2006).

Hellenic and Cyprian arcs intersect at a sharp bend, named as the Isparta Angle (IA-Blumenthal, 1963). This triangular region plays an enigmatic role in neotectonic development of the Eastern Mediterranean and needs to be considered as a whole. IA separates areas of different relative plate motion in Turkey; from westward motion to the east of IA, to more southwestward motion to the west. It is also emphasized that this zone behaves as an obstacle to the westward motion of Anatolia (15 mm /year) based on the slower motion of IA (10 mm /year) with respect to Eurasia (Barka and Reilinger, 2007). McClusky et al., (2003) suggested that the lithosphere within the IA is moving

independently, decoupled from the rest of the Anatolian Plate and might be attached to the African Plate instead also supported by a recent- study from Tiryakioğlu et al., (2013). Paleomagnetic studies found very little rotation of the IA in the last 10 million years (Tatar et al., 2002).

Figure 2.2. Seismicity from 1975 to 2012. Event information ware gathered from several catalogues including IRIS, USGS-NEIC and ISC. Abbreviations; AB: Antalya Basin, AM: Anixamander Mountains, AP: Anatolian Plate, ES: Eratosthenes Seamount, FR: Florence Rise.

IA records a history of tectonic phases such as compression, strike-slip faulting and extension (Robertson, 1993; Robertson et al., 2003, 2009). It underwent compression and transpression during the late Miocene related to the emplacement of Lycian and Hoyran-Beyşehir Nappes from west to east, respectively. The latest extensional phase throughout the Aegean-West Anatolian region lead to the formation of grabens and half-grabens as well as a series of N-S trending normal faults and transtensional faults of various sizes

(Glover and Robertson, 1998; Ten Veen et al., 2004; Alçiçek et al., 2005). IA is bounded by NE-SW trending Fethiye-Burdur Fault Zone (FBFZ) to the west and NW-SE trending Sultandağı Fault (SF) to the east (Figure 1.a). Even though the type of deformation along FBFZ had been debatable, it is considered to be a continuation of the NE trending left lateral system of Pliny/Strabo trenches (Yağmurlu et al., 1997; Price and Scot 1994), verified by GPS measurements (Barka and Reilinger, 1997; Tiryakioğlu et al., 2013). Towards east, SF is well documented as a normal fault in recent observations (Koçyiğit et al., 2000; Taymaz et al., 2002; Kiratzi and Louvari, 2003, Koçyiğit and Özacar, 2003). In addition, the presence of Aksu-Kyrenia thrust and the normal Kırkkavak fault complicate the panorama inside the IA (Dumont and Kerey, 1975; Poisson et al., 2003). The offshore part of IA is bordered by Anaximander Mountains to the south where the Aegean and Cyprus arcs meet. The geometry of this region is partially shaped by opposite rotations of
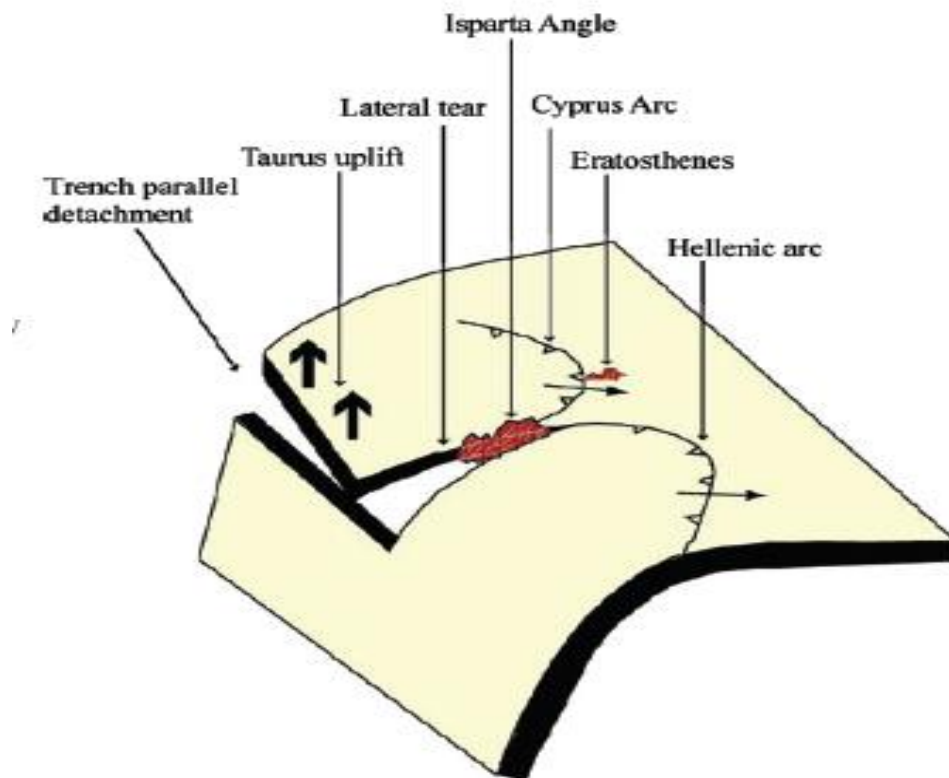
Figure 2.3. A cartoon illustrating the development of a slab tear or subduction transform edge propagator (STEP) fault beneath the Tauride block and the positions of subducting African lithosphere along the Cyprean and Hellenic arcs (after Barka & Reilinger, 1997).

both sides of the angle, i.e 30° counterclockwise rotation of the western limb during the Miocene (Kissel and Poisson, 1986) and a 40° clockwise rotation of the eastern limb since the Eocene (Kissel et al., 1990) whereas the core of IA does not indicate any detectable rotation (Kissel and Poisson 1986; Zitter et al., 2003).

As mentioned earlier, different slab geometries and the differential plate motions between Hellenic Arc (relatively steep retreating subduction) and Cyprus Arc (static-shallower subduction) might be indicating a vertical/sub-vertical tear or gap in the subducting African Lithosphere beneath western Anatolia as shown in Figure 2.3 which is responsible for the active deformation (De Boorder et al., 1998, Agostini et al., 2007; Dilek and Altunkaynak, 2009, Dilek and Sandvol, 2009; Biryol et al., 2011). This condition though is to have allowed the fast southward retreat of the Hellenic slab during the Miocene (de Boorder et al., 1998; Govers and Wortel 2005, Jolivet et al., 2013). Left Lateral Fethiye − Burdur Fault Zone might be seen as the continuation of Strabo-Pliny trenches and the surface expression for a lateral tear (Barka et al., 1995). Lithospheric tear induces asthenospheric upwelling leading to linearly distributed alkaline magmatism younging in the N-S direction of tear propagation (Dilek and Altunkaynak, 2008; Dilek and Sandvol, 2009; Biryol et al., 2011 and the references therein). Pn-Sn tomographic maps indicate high attenuation beneath this region (Gök et al., 2000, Al-Lazki et al., 2004; Şahin, 2008; Şahin et al., 2009) and surface wave tomography studies (both event and ambient noise based) reveal anomalously slow Love and shear wave velocity anomalies (Cambaz and Karabulut, 2010; Salaün et al., 2012, Delph et al., 2015) underlying the IA.

3. SURFACE WAVES: DATA & TOMOGRAPHY METHODS

3.1. An Overview & Surface wave Definitions

Surface waves compose the longest and the largest amplitude parts of broadband seismic waveforms generated both by explosions and shallow earthquakes. Additionally, they contain most of the low frequency information emitted by seismic sources. Surface waves are usually a prominent feature on seismograms; especially when large earthquakes occur, the surface waves can propagate and encircle the Earth several times. Their lower frequency content (f ~< 0.1 Hz) enables us to map the deeper structures in the upper mantle. Fundamentally, surface wave measurements have been crucial for determining crustal and upper mantle velocity structure beneath the Earth. Furthermore, broadband surface wave dispersion provides valuable insights for estimating the 3-D seismic models of the crust and uppermost mantle which are considerably valuable in calculating accurate locations of small events for which only limited regional data may be available. The success of these applications mainly depends on obtaining reliable dispersion measurements and representing them in a useful form, mostly as group or phase velocities.

In an inhomogeneous medium like Earth; seismic wavefield is fundamentally influenced by the existence of a free surface in addition to other wave phenomena such as refraction, wave conversion, diffraction and scattering that highly contribute to body wave complexity. Since all seismic wave measurements are performed at or near the free surface, it is extremely important to take into account the free surface effects. The special stress boundary condition expressed by the vanishing of surface tractions gives rise to the effective propagation of surface waves along the free surface. The mathematical treatment of surface wave propagation is complex (Aki and Richards, 1980) and boundary conditions together with derivation of surface wave displacement equations are beyond the scope of this dissertation.

The interaction of coupled, inhomogeneous P-SV waves (satisfying the boundary condition for post-critical incidence angles) at the free surface generates an interference

wave travelling along the surface as a Rayleigh wave (Figure 3.1) with a velocity lower than shear wave velocity (β). Their amplitudes decay with depth and the amplitude decrease is two-dimensional (proportional to $1/r^{1/2}$) from the source compared to three-dimensional decay of body waves.
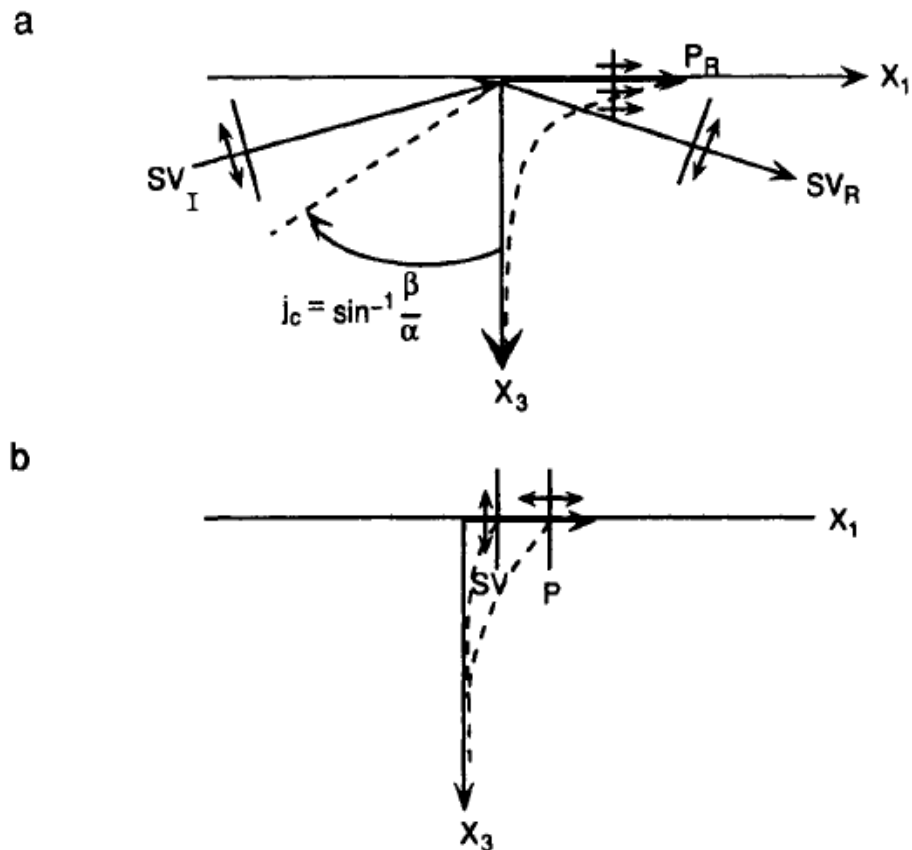
Figure 3.1. (a) Post critical SV wave incident on a free surface gives rise to an evanescent P wave (P_R) propagating along the boundary as well as to a phase-shifted SV reflection (SV_R), J_c is the critical angle. (b) Simultaneous existence of evanescent P- and SV-wave energy traveling horizontally along a free surface (taken from Lay and Wallace, 1995). β and α denote the S and P wave velocity, respectively.

The particle motion is elliptical because of the 90° phase shift between the displacements in x_1 and x_3 directions. Rayleigh wave motion is confined in the vertical plane (in x_1-x_3 planes) with no tangential displacement (u_2). They are strongly observed in vertical and radial components of a seismogram and tend to be the largest arrivals on long-period or broadband seismograms. Sources near the surface tend to generate strong surface

waves, whereas sources deep in the Earth excite only weak surface waves. For typical values of Poisson's ratio $(0.2 < V < 0.4)$, the Rayleigh-wave velocity is within the interval of 0.9β to 0.95β. Rayleigh waves only require a free surface to be a viable solution of the equations of motion except a half-space which can produce an undispersed Rayleigh pulse. Dispersion concept will be discussed in more detail in the preceding chapters.
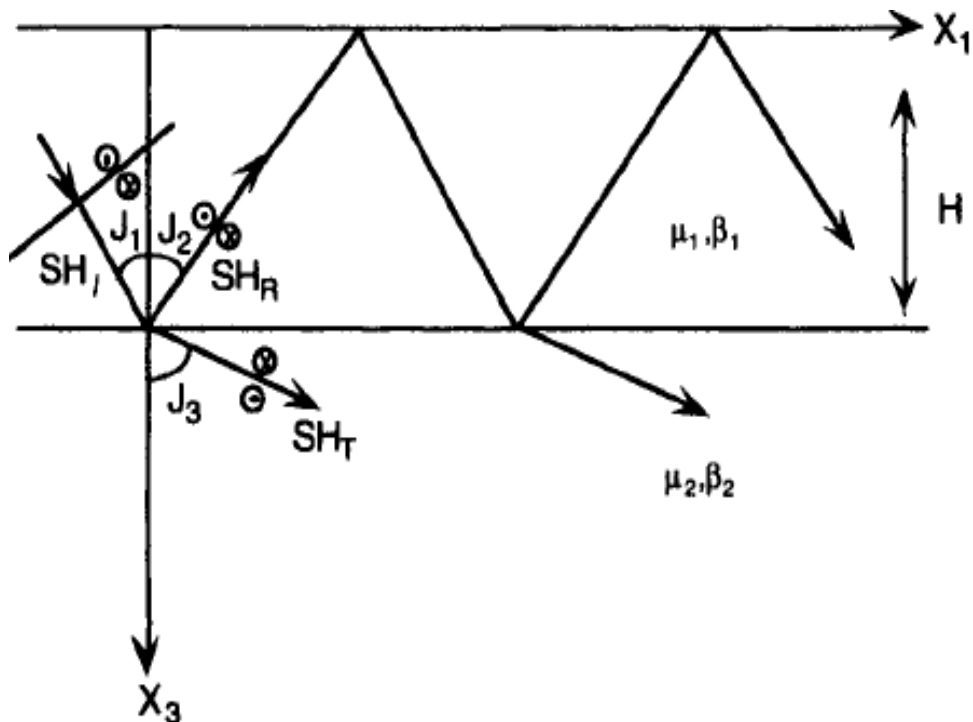
Figure 3.2. SH waves those repeatedly reflect in a layer over a half-space. $X_3=0$ is a free surface, and the layer thickness is H. Interactions with the boundary of $X_3=H$ involve incident (SH_I), reflected (SH_R,) and transmitted (SH_T) waves (from Lay and Wallace, 1995). For $\beta_1 < \beta_2$, a critical angle $j_c=\sin^{-1}(\beta_2/\beta_1)$ will exist beyond which SH reverberations will be totally trapped in the layer (Lay and Wallace, 1995; Aki and Richards, 1980).

On the other hand, total reflections of the incoming SH wave from the free surface combined with the internal layering of the earth (where β is increasing with depth) trap the SH waves between the free surface and the reflecting layer boundary (a low velocity layer over a half space) at post-critical incidences (Figure 3.2). In this case, an additional

boundary condition exists which is defined as the continuity of stress and displacement along the boundary (Z=H). The trapped SH reverberations in a layer over half space will generate the second type of surface waves called the Love waves. Love waves propagate horizontally and the particle motion is parallel to the free surface which is completely different from the Rayleigh waves. They travel faster than Rayleigh waves and mostly observed in the transverse component of a seismogram. Love waves are always dispersive since they require at least a low-velocity layer over a half-space to exist.

3.2. Surface Wave Dispersion: Group & Phase Velocity Measurements

Except Rayleigh waves in an isotropic half space, all surface waves exhibit dispersion meaning that velocity is a function of frequency even though shear wave velocity has no frequency dependence. Dispersion clearly alters the appearance of a seismic record since waves with lower frequency components will predominantly arrive earlier. Thus, surface waves as seen on seismograms are not compact wavelets like body waves, but appear as long wave trains in which the period slowly decreases. With the increasing period, surface waves will sample the deeper structures beneath the earth. Surface waves are used to retrieve a general image of Earth structure through the analysis of their dispersion. Since different regions of the Earth have different distributions of velocity with depth, each region can be characterized by different dispersion curves. Dispersion curves are obtained from the previously mentioned continuous band of periods both for Rayleigh and Love waves (Figures 3.4 and 3.5). These curves can be effectively used to determine the crustal and upper mantle structure of the target medium. One drawback is that the velocity value will be calculated as the average along the entire ray path. Due to their generation mechanism, Love waves are a bit more sensitive to shallower structures such as the Earth's crust at the corresponding frequency bands. Two types of velocities are associated with the propagation of surface waves. If we consider a natural or human-made seismic source with a continuous spectrum of frequencies, each individual frequency component is going to travel with a velocity, c(w), called the phase velocity. In this case, the total ground motion will contain both constructive and destructive disturbance patterns. Group velocity, U(w), is defined as the velocity of these constructive patterns that behave as wave packets (Figure 3.3).
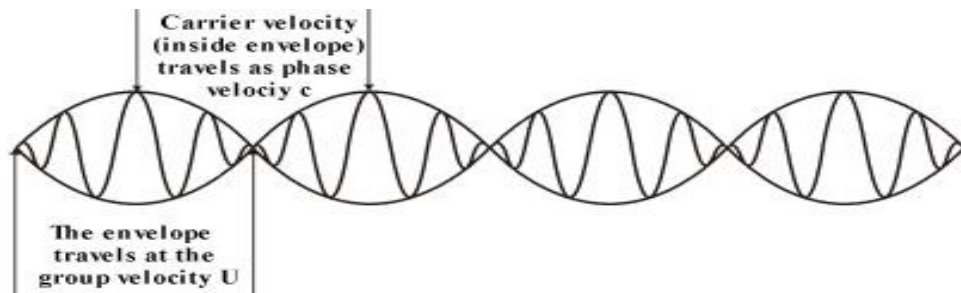
Figure 3.3. Schematic Description of Group and Phase velocities (Principles of Seismology)

Group and phase velocities are related to each other by the following equations:

$$c = w / k , \quad U = dw / dk = c + k. \, dc / dk = c - \lambda \, dc / d\lambda ; \qquad (3.1)$$

where **w** is the angular frequency (rad), **k** is the wavenumber, λ is the wavelength (m) of the seismic wave. Since the phase velocities in the Earth decrease with frequency (or increases with the wavelength), group velocities will always be lower than the phase velocities ($dc / d\lambda > 0$). If we determine c (w) across a certain frequency range, group velocity can then be calculated directly from the phase velocity by the equation given below (Udias, Principles of Seismology);

$$U = c / [(w/c) \, (dc/dw) - 1]. \qquad (3.2)$$
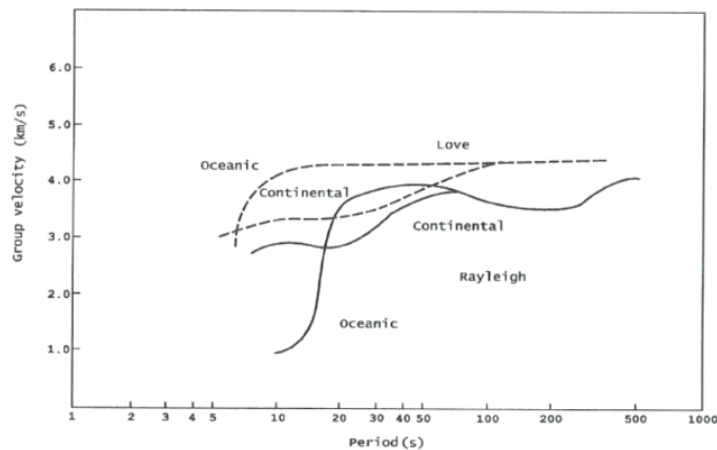
Figure 3.4. Variation of group velocity in the earth (Modified from Bullen and Bolt, 1985)

As seen in the figures 3.4 and 3.5, phase velocity curves tend to be monotonic, whereas group velocity curves often exhibit a local minimum. Existence of a local minimum suggests that a significant amount of energy will arrive at almost the same time producing an amplification and interference effect referred to as the airy phase (from Modern Global Seismology, Lay and Wallace, 1995). Airy phase occurs at 20 sec period for continental paths and 200 sec period for oceanic paths (Figure 3.4).
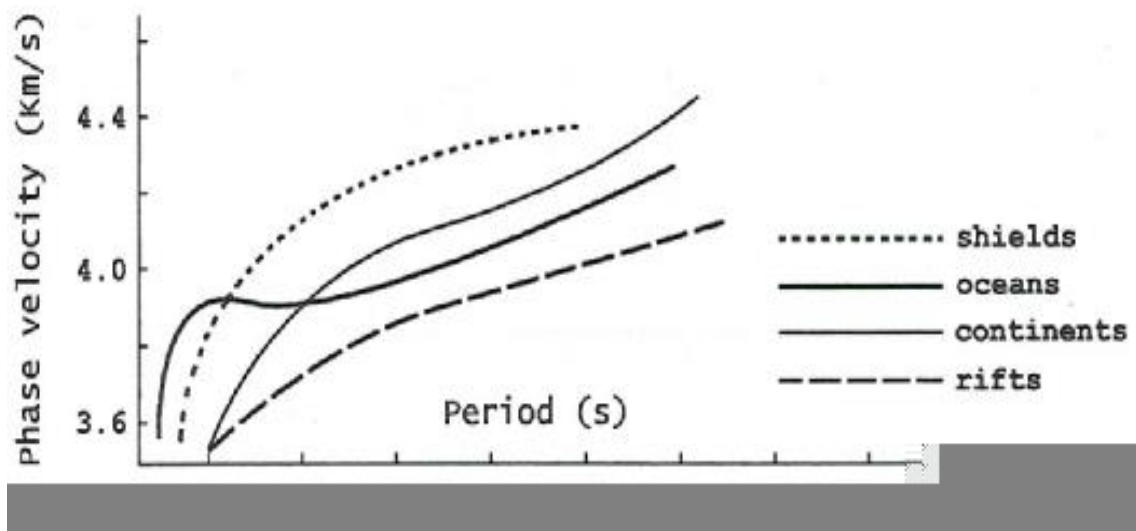
Figure 3.5. Variation of phase velocities in the earth (Mean curves modified from Knopoff, 1972)

Basically, several single and two-station methods are used to measure surface wave group velocities. Narrowband filtering of a seismogram isolates the wave packet (corresponding to the central frequency of the filter) and the group velocity of that narrow frequency interval can then be calculated by dividing the path length by the travel time. These methods require accurate knowledge of source location and origin time; and one of the major assumptions is that the rays must propagate along the same great-circle path. In two-station methods, the group velocity dispersion can be determined by measuring the difference in arrival times of filtered wave packets. The measurements of Rayleigh and Love wave group velocities are performed on the wave packet envelope and can be accurately determined across a wide frequency range (e.g., Dziewonski et al., 1969; Levhsin et al., 1992; Ritzwoller et al., 1995; Pasyanos et al., 2001; Pasyanos and Walter, 2002; Pasyanos, 2005).

Phase velocity measurements are typically obtained by waveform fitting (e.g Woodhouse and Dziewonski, 1984) by differentiating the phase spectra obtained at adjacent stations or from nearby events. However, absolute phase velocity measurements are strongly affected by the initial source phase (Muyzert and Snieder, 1996, Ekstrom et al., 1997; Erduran et al., 2008) which may be poorly known for small events. Secondly, phase velocities are difficult to measure unambiguously below 30 second period. In this sense, group velocities have been considered more useful for nuclear explosion monitoring purposes than phase velocities.

3.2.1. Surface Wave Tomography

The sensitivity of surface waves to crustal and upper mantle has massively contributed to the extensive use of both Rayleigh and Love waves to map the three-dimensional shear wave velocity structure beneath the Earth, referred to as "Surface Wave Tomography". Throughout the last couple of decades, the estimation of dispersion by tomographic inversions has been widely used, new methods and numerous approaches have emerged both on regional and global scales. Tomographic techniques differ in geometry (i.e Cartesian versus spherical), model parameterization (regular vs irregular grids/nodes), certain theoretical assumptions (ray/wave paths and scattering), smoothing parameters and whether azimuthal and radial anisotropy can be estimated simultaneously with the isotropic velocities.

Fundamental mode surface wave dispersion studies (S-wave velocity structure derived from both phase and group velocities) have been also performed for a number of broad regions including Africa-Arabia-Eurasia (Pasyanos et al., 2001; Pasyanos and Walter, 2002; Payanos, 2005), Antarctica (Ritzwoller et al., 2001), Asia (Yanovskaya and Kozhevnikov, 2003), Australia (Debayle and Kennett, 2000), China (Huang et al., 2003), Eurasia (Ritzwoller and Levshin, 1998), Turkish-Iranian Plateau (Maggi and Priestley, 2005), Turkey and the surroundings (Cambaz and Karabulut, 2010) as well as globally (Ritzwoller et al., 2002). Regarding the phase velocity tomography in particular; Bruneton et al, (2002) have investigated Baltic Shield, Forsyth et al., (1998), have studied the East Pacific Rise, Li et al., (2003) have focused on the shear wave velocities and azimuthal anisotropy in North America, Godey et al., (2003) have constructed phase velocity maps

for the Caribbean region and most recently Bakırcı et al., (2012) has determined the 3-D S-wave structure of the upper mantle beneath Turkey using a conventional two-station method.

Traditional surface-wave tomography is based upon JWKB ray theory, which is valid only if the lateral scales of the heterogeneities are larger than the characteristic wavelength of the seismic waves. Several recent publications on surface wave tomography have focused on finite frequency effects (Spetzler et al., 2002; Yoshizawa and Kennett, 2002; Zhou et al., 2004) and one in the case of group velocities in particular (Ritzwoller et al., 2002). These methods take slightly different approaches to go beyond the ray theory and more precisely approximate the true sensitivity kernels. Due to the long wavelength nature of surface waves, surface wave tomography is more appropriate for global or large-scale regional studies. Even though body waves have higher spatial resolution due to the shorter wavelengths; sparse and uneven coverage of networks restricts the resolution. Teleseismic surface wave tomography suffers from the following principal difficulties: (1) the wavefields impinging on the station array usually exhibit considerable amplitude variations on small spatial scales which are caused by interference of multipath arrivals generated by heterogeneities in crust and upper mantle along the raypath. (2) Because of the non-planar wavefields propagating across the array, estimates of phase velocities from phase differences between stations deviate from the true phase velocity (Friederich, 1999; Forsyth and Li, 2003).

A recent and an intriguing approach with possible numerous applications, is to extract surface waves by cross-correlating long sequences of seismic ambient noise. This approach has yielded a substantial number of group-velocity measurements on inter-station paths. Empirical Green's functions (EGFs) between pairs of seismographs can be estimated from the time derivative of the long-time cross-correlation of ambient seismic noise. These EGFs reveal velocity dispersion at relatively short periods, which can be used to resolve structures especially in the crust much more efficiently than traditional surface-wave tomography.

The first attempts to use ambient noise for surface wave tomography were applied to stations in Southern California (Shapiro et al., 2005; Sabra et al., 2005, Moschetti et al.,

2007). These studies resulted in group speed maps at short periods (7.5–15 s) that displayed a striking correlation with the principal geological units in California. Recent applications have arisen across all of California and the Pacific Northwest (Moschetti et al., 2007), in South Korea (Cho et al., 2006), in Tibet (Yao et al., 2006), in Europe (Yang et al., 2007), New Zealand (Lin et al., 2007), Northeastern Tibetan Pleteau (Li et al., 2014) and most recently across southwestern Turkey – Central Anatolia (Delph et al., 2015).

3.3. Data & Rayleigh Wave Observations

In order to provide valuable insights on the complex lithospheric structure beneath IA and the surroundings, a temporary seismic network consisting of 11 three-component broadband stations (seven Nanometrics–Trilliums and four Güralp CMG-3T sensors was installed in August 2006 and operated until August 2007 with support from University of Missouri. In March 2007, nine additional broadband stations (three Güralp CMG-3TD and six Güralp CMG-6TD sensors) were deployed and operated until September 2009 with support from Boğaziçi University Research Fund (BAP, project no: 07T203) and National Earthquake Monitoring Center (NEMC-BDTİM). An essential part of the data set was provided by Kandilli Observatory and Earthquake Research Institute (KOERI-NEMC) with 21 permanent BB stations. In addition, two permanent stations of Süleyman Demirel University (SDU) and five stations of IRIS-Geofon Network (120 sec STS2 sensors) were also included to extend the station coverage (Figure 3.6). Data was recorded at 40 Hz. Each sensor had a response up to approximately 140 seconds period, except the Güralp CMG6T sensors which had a flat velocity response up to nearly 50 seconds.

Relatively shallow teleseismic earthquakes (depth < 50 km) recorded by at least 14 stations within a distance range of $30^{o} – 120^{o}$ and with body wave magnitudes larger than 5.5 were selected for further processing. Signal to noise ratio, azimuthal coverage of events, and coherence from station to station were also taken into account during event selection. Out of 240, 80 events provided high-quality data (Figure 3.7). The distribution of events shows a substantial azimuthal coverage, which is important for resolving both lateral heterogeneity and azimuthal anisotropy. After the removal of mean, trend and the instrument responses; the data was decimated to 1 Hertz.
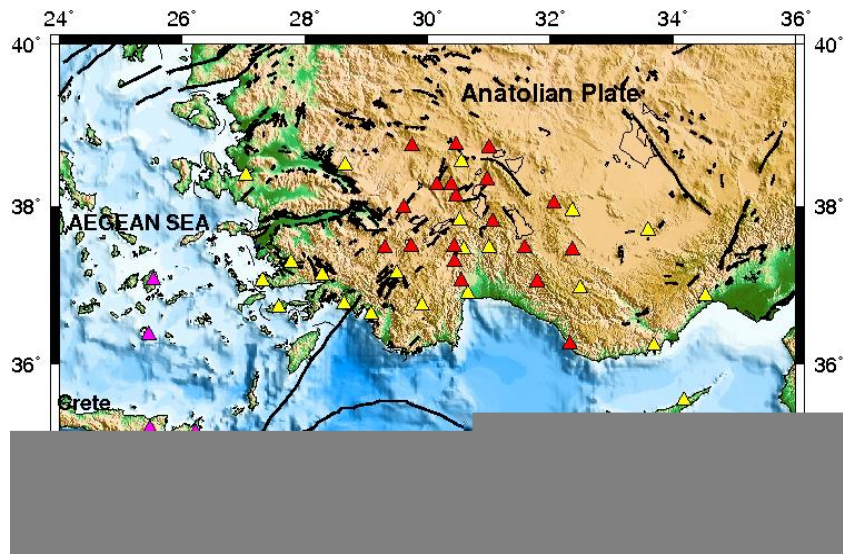
Figure 3.6. Station distribution. Red and yellow triangles represent the temporary and the permanent deployments, respectively. Purple triangles represent the IRIS-Geofon stations. Faults are shown with gray lines.
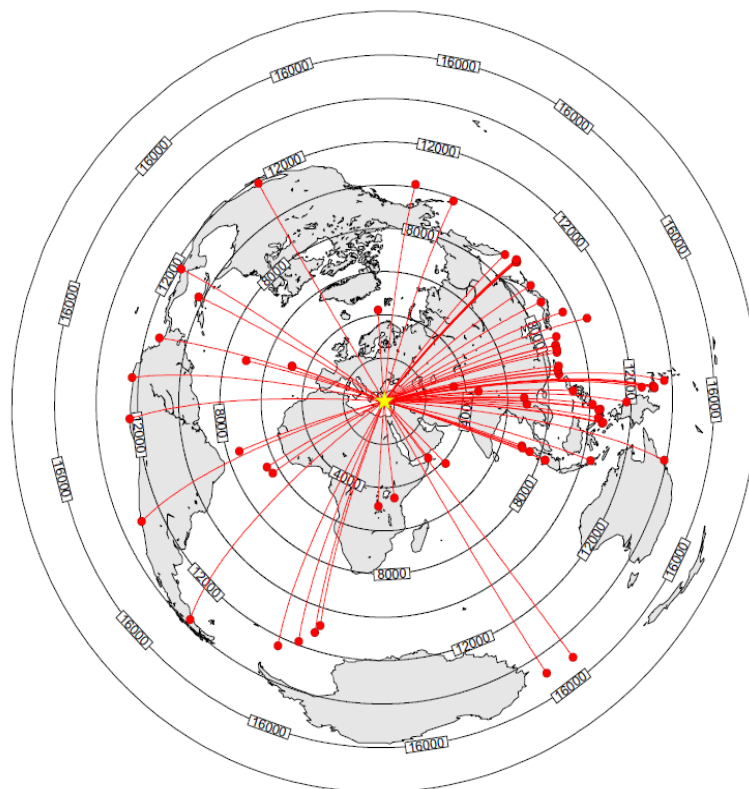
Figure 3.7. Earthquake distribution. The image is centered on the middle of the array from azimuthal equidistant projection (the yellow star). The red circles indicate the event locations.

12 different narrow band-pass filters centered at periods ranging from 25 to 142 seconds were applied to the vertical component seismograms. Each filter was a zero phase shift, 10-mHz wide, forth order double pass Butterworth filter. Fundamental mode Rayleigh waves were obtained and isolated from other seismic phases with a rectangular window with cosine tapers at both ends. Frequency dependent windowing effectively isolates the dispersed fundamental mode from higher modes and minimizes the effect of noise. The amplitude of fundamental mode is much stronger than that of higher modes for the shallow earthquakes. Window length was based on the epicentral distance and dispersion characteristics. It might be different for each period, but the same window length was applied to all seismograms for a given event. For each pass band, maximum amplitudes were manually picked on the waveforms for each event. Rayleigh wave phase and amplitude were measured using a positive Fourier transform of the filtered/windowed seismograms. Normalized amplitudes (with respect to a selected reference station) were then corrected for geometric spreading, attenuation and site effects. We neglected the source radiation pattern because the aperture of the array is quite small compared to the distance between sources and receivers.

Most of the data at short periods (below 33 seconds) indicate incoherence, multipathing and scattering effects reflecting a complicated incoming wavefield. Rayleigh waves that propagated through fewer tectonic boundaries have clean records; however, some events exhibit spectral holes due to the excitation function at the source. Passbands near these holes were discarded, or, if retained, be poorly fit and down weighted in the inversion process as described in the following paragraphs. At longer periods, Rayleigh waves records become simpler and cleaner, but the signal to noise ratio decreases because of reduced amplitudes and poor long-period response at some stations. An example from one event – station pair is given in Figure 3.5. As expected from the distribution of events, the ray coverage is excellent. The crossing ray paths at 50 seconds are denser within the area marked by the blue open box in Figure 3.6. Ray density slightly decreases with increasing period.
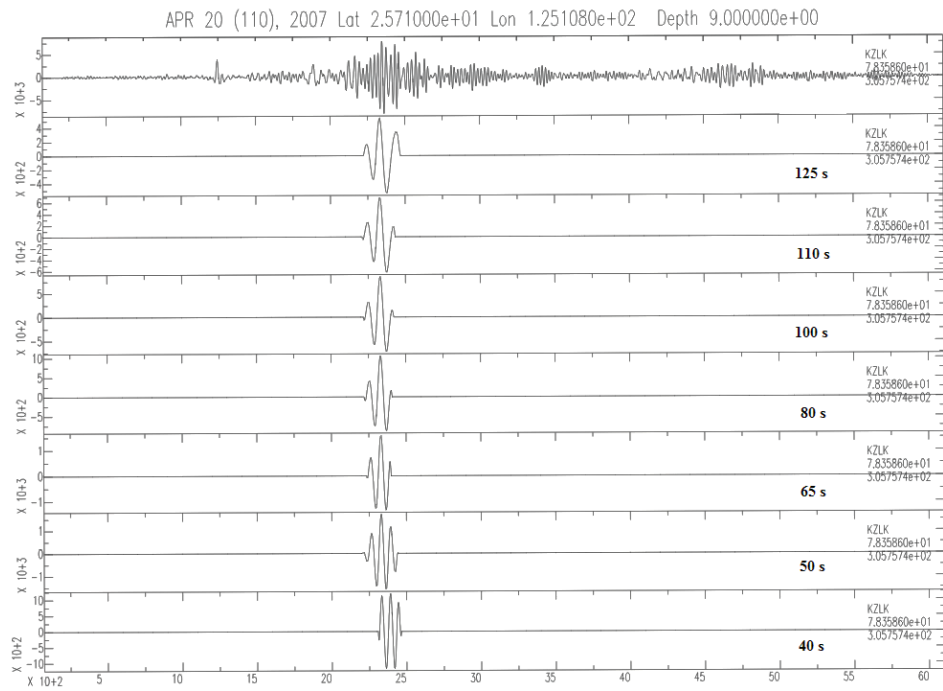
Figure 3.8. Sample seismograms for a single station. Unfiltered seismogram is shown at the top. Filtered, windowed and isolated seismograms across various periods are also shown.
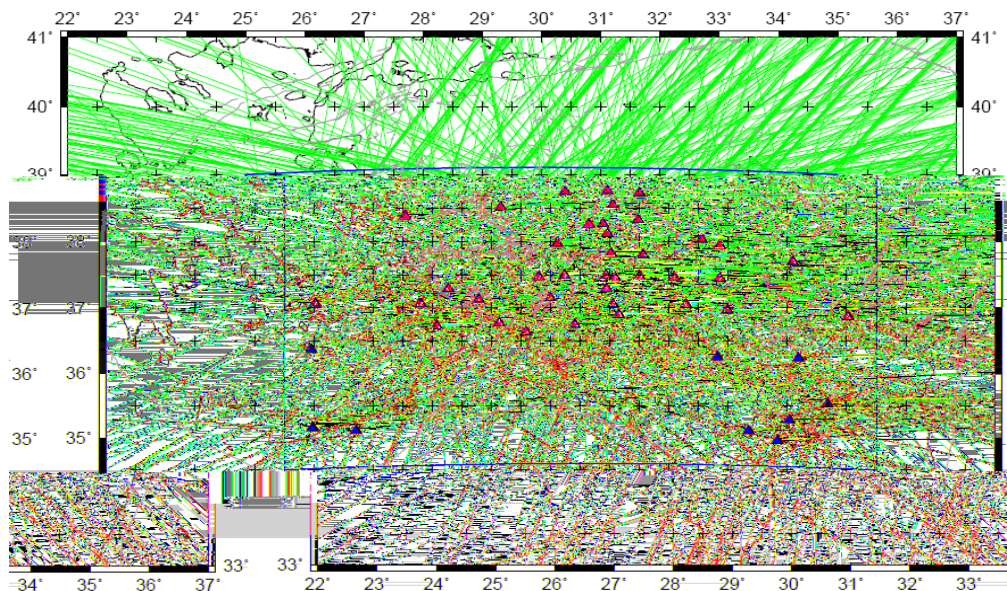
Figure 3.9. Great circle paths in the vicinity of the array at a period of 50 seconds. Red triangles represent the stations. Crosses denote the grid nodes.

3.4. Surface Wave Tomography Method

The measurement of fundamental mode surface wave phase velocities beneath an array of sensors is a powerful way to detect variations in lithospheric and asthenospheric structure. The main challenge in surface wave tomography applications is to appropriately represent the incoming complex wavefield. Conventional surface wave tomography regards the incoming waves as plane waves propagating along great circle paths and uses phase differences between station pairs to determine average velocities along the path connecting the stations (e.g Woodhouse and Dziewonski, 1984; Laske et al., 2008). By combining many crossing paths, a phase velocity map is obtained for selected frequencies. These maps are inverted in a second step for 3-D-shear wave velocity. Traditional methods also solve for slowness and apparent direction of propagation assuming the incoming wave is planar (Ritzwoller et al., 2001; Spetzler et al., 2002). However, these approaches mentioned above have been proven to yield unreliable results if the wavefields strongly deviate from plane waves since surface waves encounter lateral heterogeneities along their path. These heterogeneities distort the wavefields leading to deviations from great-circle azimuths, incoherent scattering and multipathing effects. Due to non-planar wavefields propagating across the array, estimates of phase velocities will be biased (Friederich, 1999; Forsyth and Li, 2003). Hence, non-planar energy can also dominate the signals for Rayleigh waves at periods less than 50 seconds (Wielandt, 1993; Forsyth and Li, 2003). Another drawback is that absolute phase velocity measurements are strongly affected by the initial source phase (Muyzert and Snieder, 1996; Ekstrom et al., 1997) which may be poorly known for smaller events.

We adopted a two-plane-wave inversion technique (Forsyth et al., 1998) to simultaneously solve for the incoming wave field and phase velocity. Since its introduction by Forsyth et al., (1998), this method has been successfully applied in a variety of tectonic settings, including continental collision (Zhang et al., 2011, Ceylan et al., 2012), subduction zones (Calixto et al., 2013), cratons (Li, 2011), and mid-ocean ridges (Forsyth 1998; Forsyth and Li, 2005). The wave field is represented by the sum of two plane waves with initially unknown phase, amplitude and propagation direction with a total of six parameters for each event. It has been precisely documented that; although this is a simpler representation of a more complex wavefield in many cases, it accounts for the amplitude

variation patterns more effectively (Li et all, 2003; Li and Burke, 2006; Yang and Forsyth, 2006). This approach avoids the damping necessary for stability when a series of orthogonal polynomials are employed to represent the plane waves (Friederich and Wielandt, 1995; Friederich, 1999; Pollitz, 1999) and help us further understand the trade-off between lateral heterogeneity and azimuthal anisotropy.

Surface wave phase velocities in a slightly anisotropic media can be expressed by the following equation (Smith and Dahlen, 1973):

$$c(\omega,\psi) = C_0(\omega) + A(\omega)\cos(2\psi) + B(\omega)\sin(2\psi)$$
$$+ D(\omega)\sin(4\psi) + E(\omega)\sin(4\psi) \tag{3.3}$$

where $c(w, \psi)$ is the phase velocity, w is frequency and ψ is back azimuth. $C_0(w)$ is the isotropic phase velocity, A and B denote the azimuthally averaged phase velocities containing the phase and amplitude data at each node. The anisotropic terms including 4ψ are discarded because they are expected to be small for Rayleigh waves (Montagner and Nataf, 1986).

Following Forsyth and Li (2005), slowness at every point (x,y) in the grid is given as:

$$_iS = \sum_{j=i}^{N} \frac{_iW_j}{_iV_j} \Big/ \sum_{j=i}^{N} {_iW_j} \tag{3.4}$$

where N is the number of grid points, and $_iV_j$ corresponds to the phase velocity at the j_{th} point. The weights are expressed by,

$$_iW_j = exp\left[-\frac{(x - {_ix_j})^2 + (y - {_iy_j})^2}{L_w^2} \right] \tag{3.5}$$

and $({_ix_j}, {_iy_j})$ is the location of the jth point in the coordinate system of the ith event. Weighting function contains the "L_w" parameter which acts as the smoothing factor of this

controlling the- scale length for variations in velocity. The significance parameter will be discussed further in assessing the resolution of phase velocity tomograms.

For the phase velocity inversion, we formed an unevenly spaced grid consisting of 210 nodes shown in Figure 3.10**.** The density of grid nodes is higher at the center of the region with a spacing of 0.5° and coarser towards the edge of the model with nodes at 1° apart both in latitude and longitude. Grid spacing at the edges is larger than where phase velocities are better resolved by crossing ray paths because phase velocities towards the edge of the model can absorb some of the phase effects of more complex wavefields which cannot be adequately represented by two plane waves (Li et al., 2003). Resolution assessment would be easier if the grid points were spaced regularly, but by using a sparser grid at the edges of the model, total number of variables in the inversion will be reduced. In order to model the variations of phase velocity across the array, we used a continuous function that is a weighted average of velocities at neighboring grid points (Forsyth and Li, 2005).
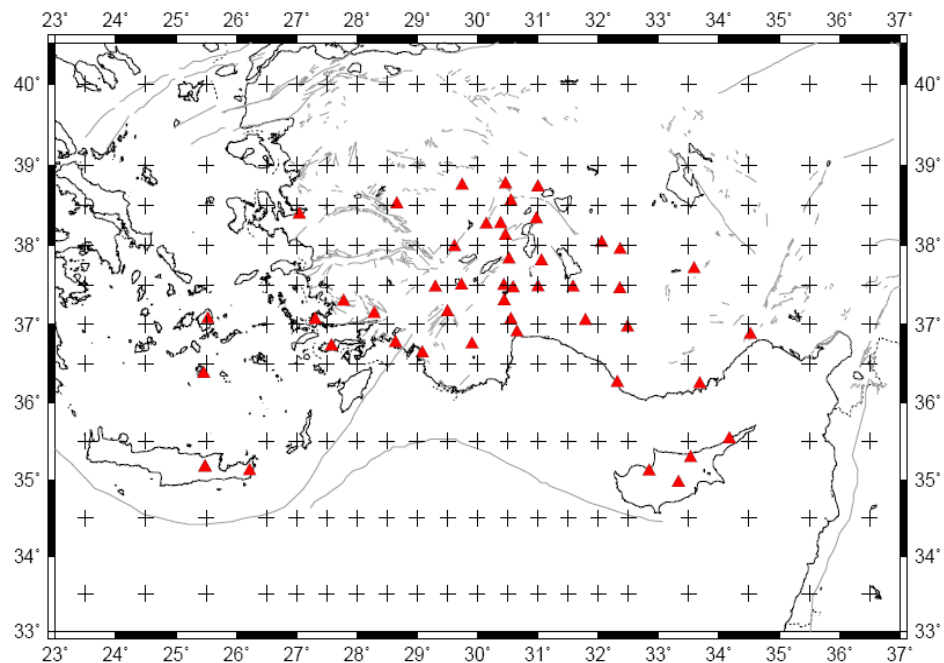
Figure 3.10. Grid nodes used in phase velocity inversion. Red triangles denote the stations and black crosses denote the grid node locations. Faults are shown by gray lines.

Vertical displacement of an incoming plane wave is expressed in Equation 3.6 as the interference of two horizontally propagating plane waves, where **k** is the horizontal wavenumber and **x** is the position vector.

$$U_2(\omega) = A_1(\omega)exp[-i(k_1 \cdot x - \omega t)] + A_2(\omega)exp[-i(k_2 \cdot x - \omega t)] \tag{3.6}$$

Position within the array is described relative to a selected reference station and a common reference origin time for all records of a single event. The reference station is determined using the highest amplitude and/or lowest root mean square error of amplitudes with respect to the mean value. Hence, the predicted displacement at the kth station for the ith event at each frequency is defined as,

$$_i^kU = {}_iA_1\,exp\left(-i{}_i^k\varnothing_1\right) + {}_iA_2\,exp\left(-i{}_i^k\varnothing_1\right) \tag{3.7}$$

where

$$_i^k\varnothing_1 = {}_i^0\varnothing_1\,\overline{_i^kS\omega}\left\{{}_i^kr\cos\left({}_i^k\psi - {}_i\vartheta_1\right) - {}_i^kx\right\} + \omega({}_i^k\tau - {}_i^0\tau) \tag{3.8}$$

and

$$_i^k\varnothing_2 = {}_i^0\varnothing_2\,\overline{_i^kS\omega}\left\{{}_i^kr\cos\left({}_i^k\psi - {}_i\vartheta_2\right) - {}_i^kx\right\} + \omega({}_i^k\tau - {}_i^0\tau) \tag{3.9}$$

$_i{}^0\varnothing_1$ and $_i{}^0\varnothing_2$ point the phases of the first and second plane waves for the reference station, $_i^k\tau$ and $_i^0\tau$ are the travel times along the great circle path from the edge of the study area to the kth and reference stations, $_i\upsilon_1$ and $_i\upsilon_2$ are the angular deviations from the great circle path of the first and second waves and $_i^kS$ is defined as the average slowness. The station coordinates are also described in terms of polar coordinates (r, ψ) centered on the reference station and adjusted in terms of great circle path. The travel times are obtained by integrating along the great circle path from the edges of the grid to each station in Equation 3.10. Thus,

$$_i^k\tau = \int_{_ix_{edge}}^{_i^kx} {}_iSdx \tag{3.10}$$

The average slowness in equation 3.10 is given as,

$$\overline{_i^kS} = \left[{}_i^k\tau/\left({}_i^kx - {}_ix_{edge}\right) + {}_i^0\tau/\left({}_i^0x - {}_ix_{edge}\right)\right]/2 \tag{3.11}$$

Travel times and average slowness parameters are dependent on velocity coefficients at all grid points as defined by the Gaussian averaging functions. On the other hand, the grid points which are closest to the great circle path are most heavily weighted.

3.4.1. Inverse Problem

With the use of two-plane wave approach, we are able to model both phase and amplitude variations. The inversion basically has two steps: (1) Solving for initial plane wave parameters (Press et al., 1992). (2) Mapping dispersion and phase velocities by inverting Rayleigh wave amplitude and phase data over a grid of nodes (Tarantola and Valette, 1982). To begin with, a reference station with the largest observed amplitude is assigned because two plane waves will most likely be in phase at that station. Amplitudes at other stations are normalized with respect to the amplitude and phase at this reference station. The initial phases of the two plane waves are set to zero but not fixed during the inversion. Since the wavefields for each event at each frequency are described by six unknown parameters with two pieces observed information per station (amplitude and phase or real and imaginary components), a minimum of four stations is needed to put constraints of the phase velocity structure. Quite frankly, a much more reliable solution can be found by increasing the number of stations.

Firstly, the velocity model is fixed and best fitting plane wave parameters (amplitude, phase and propagation direction for two plane waves) are determined in a least squares sense by simulated annealing (Press et al., 1992). This method works efficiently in cases of ambiguity when two incoming plane waves have similar azimuths and standard inversion techniques fail to achieve the global minimization. Simulated annealing search is performed separately at each iteration and for each independent event by keeping the velocity model fixed. A total number of six plane wave parameters are calculated at the end of each iteration.

During the second stage of each iteration; phase velocities and azimuthal anisotropy at every grid point together with the wave parameters for each event were simultaneously solved by a linearized least square inversion technique (Tarantola and Valette, 1982). The solution to the nonlinear, least squares inversion is given by:

$$\Delta m = (G^T C_{nn}^{-1} G + C_{mm}^{-1})^{-1} (G^T C_{nn}^{-1} \Delta d - C_{mm}^{-1}[m - m_0]) \qquad (3.12)$$

where **m** is the current model including the velocity and wave parameters, $\mathbf{m_0}$ is the starting model, $\mathbf{\Delta m}$ is the change to the current model, $\mathbf{\Delta d}$ is the difference between the predicted and observed data, **G** is the partial derivative/sensitivity matrix, $\mathbf{C_{nn}}$ is the a priori data covariance matrix, and $\mathbf{C_{mm}}$ is the a priori model covariance matrix. Initially, $\mathbf{C_{nn}}$ is assumed to have only diagonal terms. The observed data are the real and imaginary components at an independent frequency (we invert each frequency independently) for each of the filtered and windowed vertical seismograms. We assigned a priori error of 0.1 to real and imaginary data based on the a posteriori standard deviations found for each earthquake after the first stage of iterations explained in the previous paragraphs. Therefore, eliminating one or two events with large residuals will have a small effect on the velocity model (Forsyth and Li, 2005).

In this case, the nature of this non-linear inverse problem leads to underdetermined model solutions due to the number of observations being greater than the number of model parameters. For instance, at 50 seconds period we have 712 seismograms or 1424 observations from 52 events. Three velocity parameters (B_0, B_1 and B_2) at each of 210 grid points and 312 wave parameters from 52 events add up to a number of 942 unknowns which is smaller than the number of observables. To regularize the problem, off-diagonal terms are introduced into $\mathbf{C_{mm}^{-1}}$ to smooth the solution. Standard deviations per each event and frequency band were calculated after 10 iterations and assigned as the new error for the following iterations. The main source of variance is the deviations from planar wavefronts. The data which are not properly represented by two plane waves were down weighted. Furthermore, the variance of the outer nodes was assigned much higher (by a factor of 10) in order to protect the interior area from large travel time deviations.

3.5. Inversion Results

3.5.1. Model Resolution & Checkerboard Tests

As stated in all kinds of tomography studies or inverse problems, a significant trade off exist between model variance and model resolution which can be treated by the

covariance matrix. In this case, we define the limits of resolution by two parameters. The first one is the rank parameter which is described as the sum of diagonal terms in the resolution matrix. Rank is a measure of the number of independent pieces of information about the model. The second one is the standard error (square root of variance at a given map point). Since the phase slowness at every point is represented by a weighted function of surrounding nodes with a characteristic scale length L_w (in km), selection of an appropriate frequency dependent smoothing value plays an important role in balancing model variance/resolution (Li et al., 2003) and accounting for the frequency dependent scattering in the wavefield (Spetzler and Snieder, 2001). With the use of a proper value, the region of sensitivity broadens about the great circle path as the wavelength increases. At a shorter scale length, the rank and the resolution are higher and the misfit is smaller, but the standard deviation increases. On the other hand, if L_w is set too big, we get a very smoothed solution with small variance but poor resolution. Selection of L_w depends on the grid size, the number of crossing raypaths, the width of the Fresnel zone and the station distribution. A detailed explanation on Fresnel zones and the selection of L_w is given in Weeraratne et al, (2003). This parameter was determined by testing several values and chosen as 80 in this case (Table 3.1).

Table 3.1. Ranks and standard errors for velocity models with different smoothing lengths. Values in bold indicate the selected smoothing length and the corresponding values.

Smoothing Length (L_w) km	Total Rank	Velocity Rank	Standard Error at at 31°, 38° (m/sn)
100	443.6	75	15.17
80	**482.8**	**91**	**17.03**
60	496.7	100.5	19.12

In order to further assess the resolving power of the data set, we generated a synthetic checkerboard pattern of velocities given in Figure 3.11. The wavelength of the synthetic anomalies (velocities and travel times) is roughly between 200 and 250 km. The

resulting recovered models are shown in the bottom panels for different periods. We have added Gaussian distributed noise to both normalized amplitudes (0-1) and phases (0-2π). We used the same scale length ($L_w = 80$) that was applied in the analysis of actual data. The input model alternates %5 faster and %5 slower velocities with respect to the average starting values extracted from the 1-D dispersion curve given in the next section.
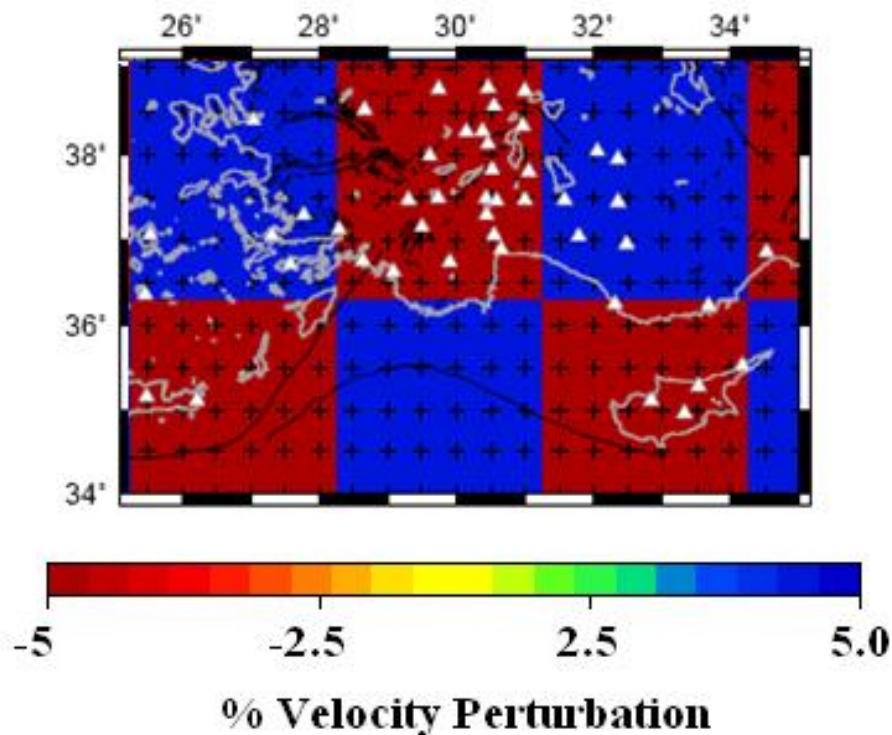
Figure 3.11. The synthetic input velocity model used for resolution tests. White triangles and black crosses denote the stations and the grid points, respectively. Black lines represent the faults.

The pattern of small-intermediate scale anomalies were largely recovered up to almost 130 seconds, however, the strength of the anomalies were slightly reduced despite they were well retrieved. We start to observe smearing at higher periods (Figure 3.12 a-c). This effect might be caused by higher travel time errors at longer periods as wavefronts propagate at large distances through major tectonic boundaries such as continents or oceans.
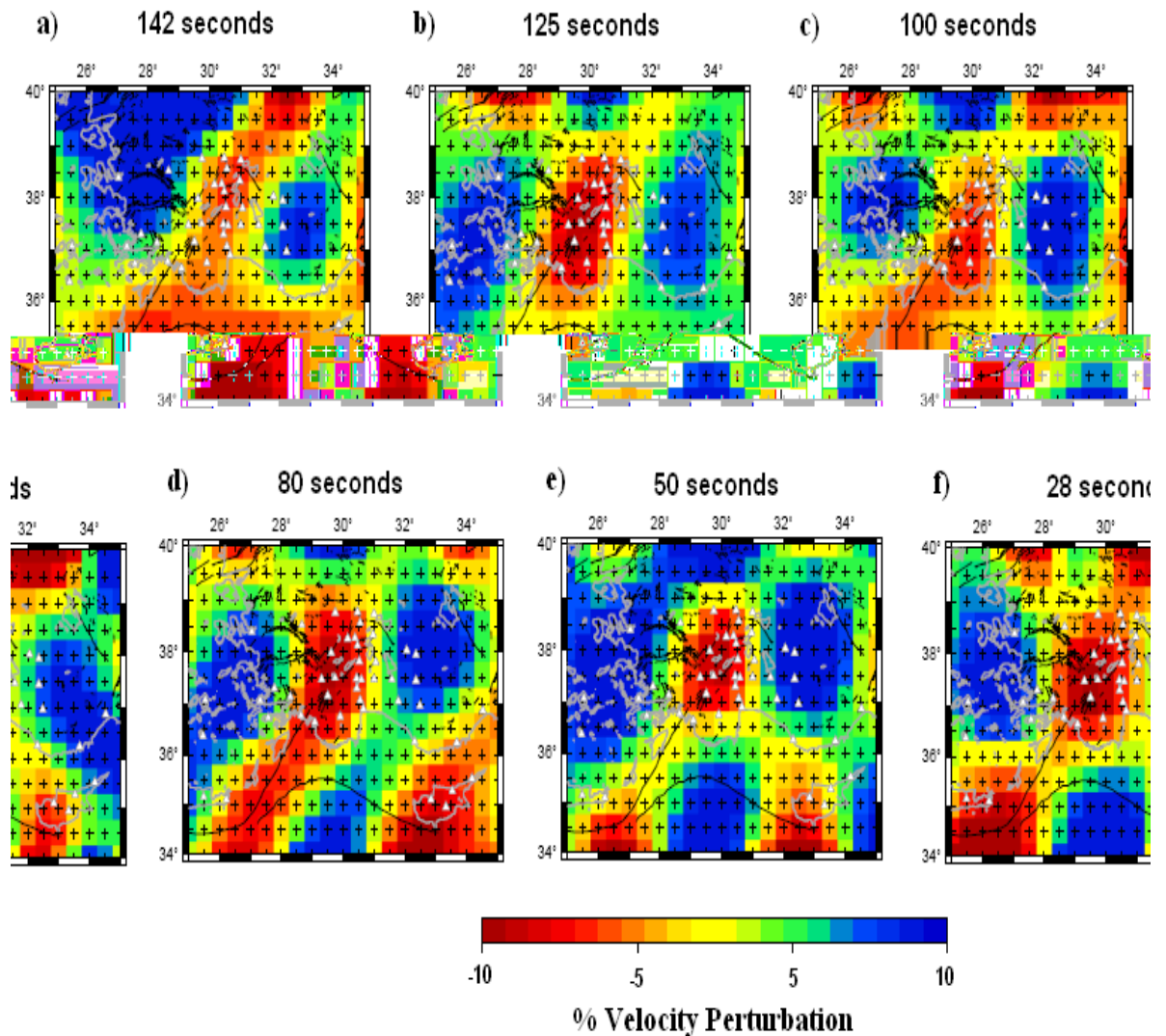
Figure 3.12. Checkerboard test results. Corresponding recovered anomalies at various periods are based on the input model shown in Figure 3.11. White triangles and black crosses denote the stations and the grid points, respectively. Black lines represent the faults.

The anomalies cannot be adequately resolved above 130 seconds; they are smeared together or averaged out in the solution. Moreover, finite frequency effect is partially reducing the lateral resolution at higher periods combining with the insufficient station responses. This problem might be minimized in future studies by applying an improved two-plane wave technique with finite frequency kernels (Yang and Forsyth, 2006b). Resolution is definitely much higher in areas where the stations are densely distributed

such as Isparta Angle and the surroundings. As expected, errors are smaller around the center of the array where resolution decreases towards the edges of the model and the resolution tend to decrease with the increasing depth for 3-D structure. The lateral resolution is about 150-200 km at short periods and 300-400 km at longer periods.

3.5.2. One Plane-Wave versus Two-Plane Wave

The major factors contributing to the complexity of surface wave records have been discussed in the previous chapters. In this section, we take a further step to investigate whether the two-plane wave assumption works better than the one-plane wave assumption or not. To address this question, we inverted for phase velocities by representing each incoming wavefield as a single plane wave. Figure 3.13 shows the comparison of results from each approach at 50 seconds period. As seen in figure 3.13, two-plane wave approach has definitely improved the fit to both amplitude and phase. Variance of phase has also reduced of about %24. We also found that the rank of velocity under the two-plane wave assumption is 91 which is higher than 79 from the one-plane wave assumption. In other words, an increase in rank for velocity parameters will be observed only if the improvement in the model with the two-plane wave parameters is significant at the %99 confidence level (Li et al., 2003). The comparisons in Figure 3.13 support the idea that the two-plane wave assumption, although simple, not only treats the non-planarity of the incoming wavefield effectively but also increases the resolution of phase velocities.

3.5.3. 1-D Average Phase Velocities

In both inversions for average (1-D) and 2-D phase velocities, we employed the same two-plane-wave inversion technique (Forsyth et al., 1994, Forsyth and Li, 2003) to simultaneously solve for the incoming wave field and phase velocity. To begin with, we performed a 1-D inversion to measure the average isotropic phase velocities and obtain the corresponding dispersion curve (Figure 3.14). This step was necessary since the area of interest comprises distinctive tectonic features such as the ongoing subduction of the African plate and a possible lithospheric tear beneath Isparta Angle and its vicinity. A reasonable average phase velocity model will be useful in determining the lateral variations of phase velocities.
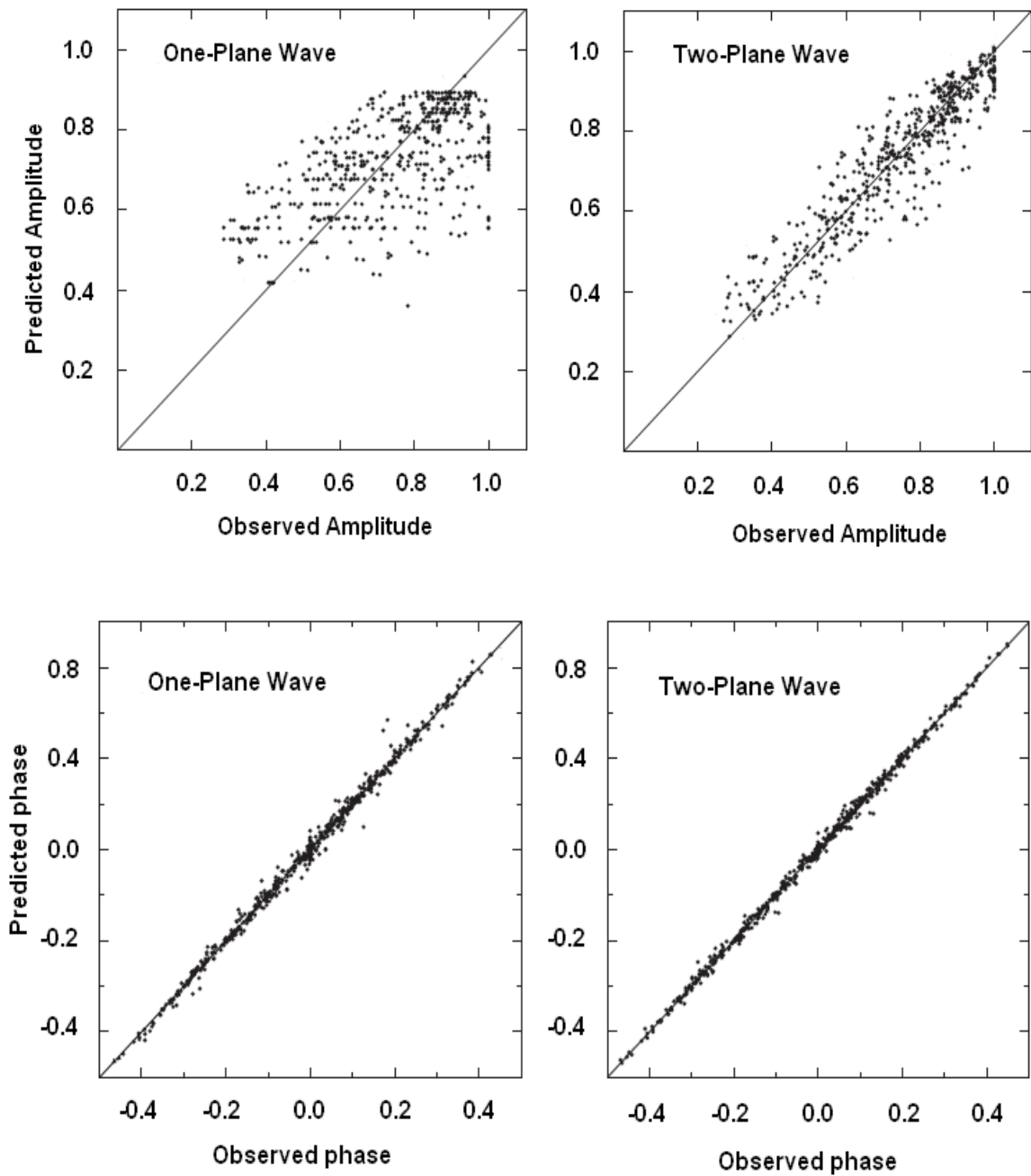
Figure 3.13. Scatter plots for predicted and observed Rayleigh wave amplitudes (top) and phases (bottom) under one-plane and two-plane wave assumptions.

In Figure 3.14, phase velocities gradually increase from 3.37 km/sec at 25 seconds to 3.96 km/sec at 142 seconds period. Phase velocities below 25 seconds are not going to be reliable because the number of observations is not sufficient to extract any information from the upper crust. Error above 125 seconds is also slightly high due to relatively low

signal to noise ratio and lack of station response. At all other periods, phase velocities are mostly well constrained with standard deviations from 0,0069 to 0.015 km/sec as seen from the error bars in Figure 3.14 and table 3.2. Regarding each event and frequency band, amplitude errors (data standard deviation) did not exceed 0.15 and phase misfits are quite reasonable.
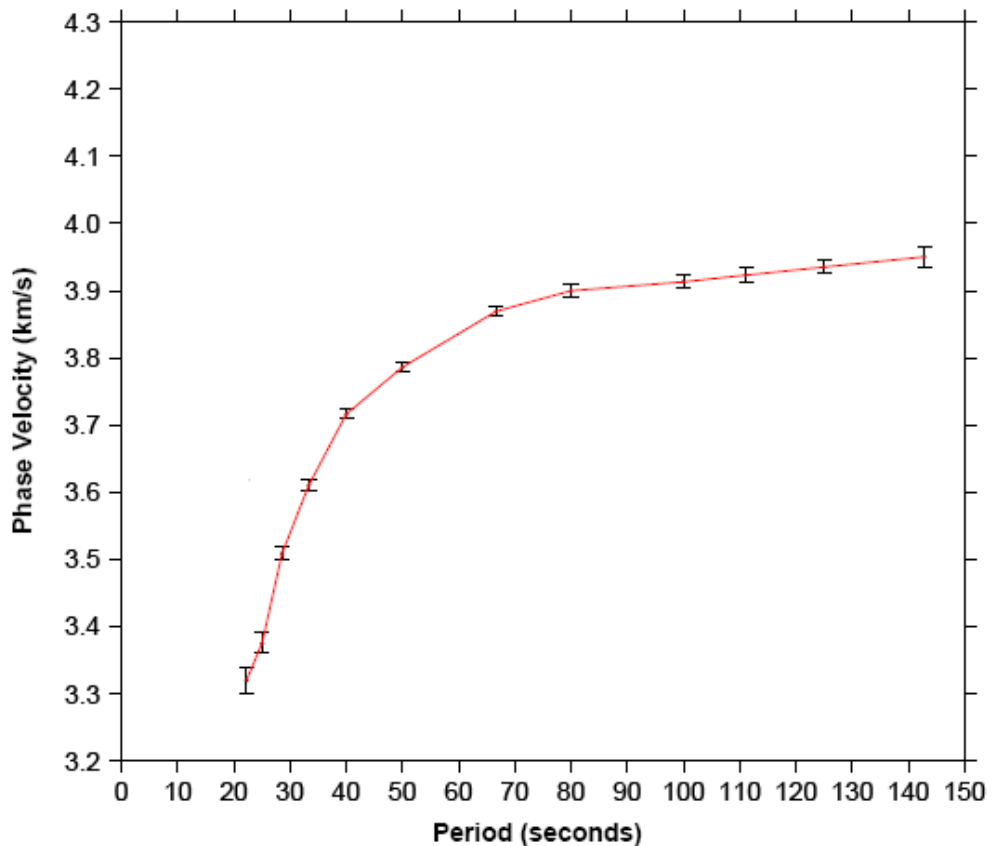
Figure 3.14. 1-D Average Rayleigh wave phase velocities and the corresponding dispersion curve (red line). Error bars are also presented with solid black bars.

A change in slope of the dispersion curve at around 40 seconds probably indicates a shift from crustal sensitivity to mantle sensitivity of Rayleigh waves. We especially observe significantly low phase velocities above 50 seconds compared to typical velocities from Knopoff (1972), Erduran (2008), which is an early sign of an influenced low velocity anomalies beneath Southwestern Turkey. These low velocities are in accord with the dispersion curve obtained by a recent study from Bakırcı et al., (2012) despite their higher error estimates. In general, phase velocities are more sensitive to deeper structures than

group velocities. These initial values suggest that we will likely get a good resolution for phase velocities below ~25 km down to nearly 230 km depending on the lateral extents and wavelength of the anomalies.

3.5.4. 2-D Isotropic Phase Velocity Variations

2-D lateral variations of phase velocities at each period are obtained using the average phase velocities from the 1-D inversion as the starting model, allowing the phase velocity coefficients at each node to vary with a light damping. The coefficients at these nodes are used to generate maps of lateral phase velocity variations on finer grids (0.1° by 0.1°) by averaging the values at neighboring nodes using a Gaussian weighting function with a characteristic length of 80 km. Mean reference velocities are taken from the dispersion curve in Figure 3.14 and listed in Table 3.2. Sample dispersion curves from different locations of the final phase velocity model are also presented in Appendix A.

To better picture the Rayleigh wave sensitivity versus depth, we first computed the fundamental mode Rayleigh depth sensitivity kernels as a function of depth at a set of different periods (Figure 3.15). The partial derivatives of group velocity with respect to shear velocity are computed in a layered flat model corrected for Earth flattening that approximates the radially anisotropic model Preliminary Reference Earth Model (PREM).

Each Rayleigh wave phase velocity provides integrated information about velocity structure over a broad depth range. Sensitivity kernels presented in the inset of Figure 3.15 show that total sensitivity to changes in shear velocity is distributed over a broad depth range but peak sensitivity occurs at a depth of approximately one third of the wavelength.

The maps of phase velocity perturbations at a period range of 28-142 seconds are shown in Figures 3.16-3.18. Taking into account the sensitivity kernels given in Figure 3.15, Rayleigh waves at 28-33 period range mainly reflect the variations in lower crust and upper mantle structure which is influenced by Moho depth in particular (Figure 3.16). The error estimates for 50 and 100 seconds are also given in Figure 3.16.

Table 3.2. Reference phase velocity values for each period to serve as an input for the upcoming tomographic inversion.

Period (sec.)	Mean Phase Velocity (km/sec)	Standard Deviation (km/sec)
142	3.9663	0.0155
125	3.9354	0,0101
111	3.9230	0,0108
100	3.9133	0.0095
85	3.8995	0.0091
66	3.8692	0.0071
50	3.7858	0.0069
40	3.7163	0.0075
33	3.6104	0.0083
28	3.5087	0.0101

In this sense, negative phase velocity anomalies will likely correspond to a thicker crust, whereas positive anomalies will be related to a relatively thinner crust. We mostly found low phase velocities beneath the Isparta Angle (IA), Antalya Basin, Cyprus Island and Rhodes Basin at 28-33 seconds. These findings are in agreement with low P_n velocities (Al Lazki et al., 2004; Gans et al., 2009), low Love wave group velocities (Cambaz and Karabulut, 2010) and low Rayleigh wave phase velocities (Bakırcı et al., 2012; Delph et al., 2015).

A significant transition to positive phase velocity anomalies was observed towards the western part of the study area beneath the South Aegean Sea (including Rhodes Basin, Santorini and Naxos Islands) also observed by Delph et al., (2015). These anomalies are well resolved, indicated by resolution tests shown in Figure 3.12f.
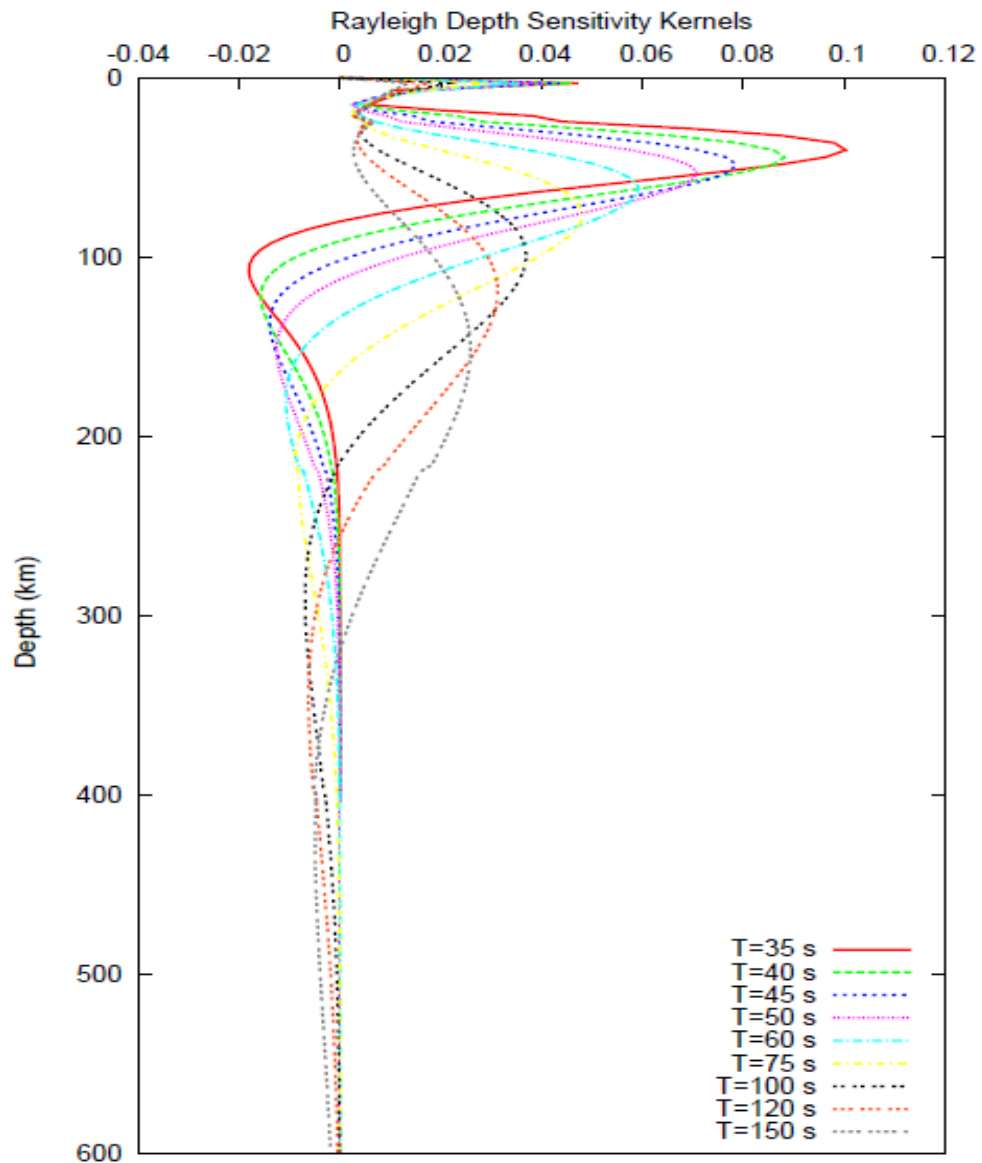
Figure 3.15. Rayleigh wave depth sensitivity kernels for various periods.

This velocity pattern is mostly consistent with extensional regime related crustal thinning beneath Western Anatolia and Aegean Sea together with crustal thickening towards IA domain and Central Anatolia as reported by numerous studies (Bohnhoff et al., 2001; Wigner, 2002; Kiratzi and Louvari, 2003; Liu et al., 2003; Sodoudi et al., 2006; Karagianni et al, 2005; Zhu et al., 2006; Diluccio and Pasyanos, 2007; Erduran, 2008; Tezel et al., 2010). Liu et al., (2003) also suggested an anisotropic crustal structure beneath the Santorini Island. A map of crustal thickness in the Aegean constructed by Tirel et al., (2004) also reveals a pronounced NE–SW trending of crustal thinning in the northern
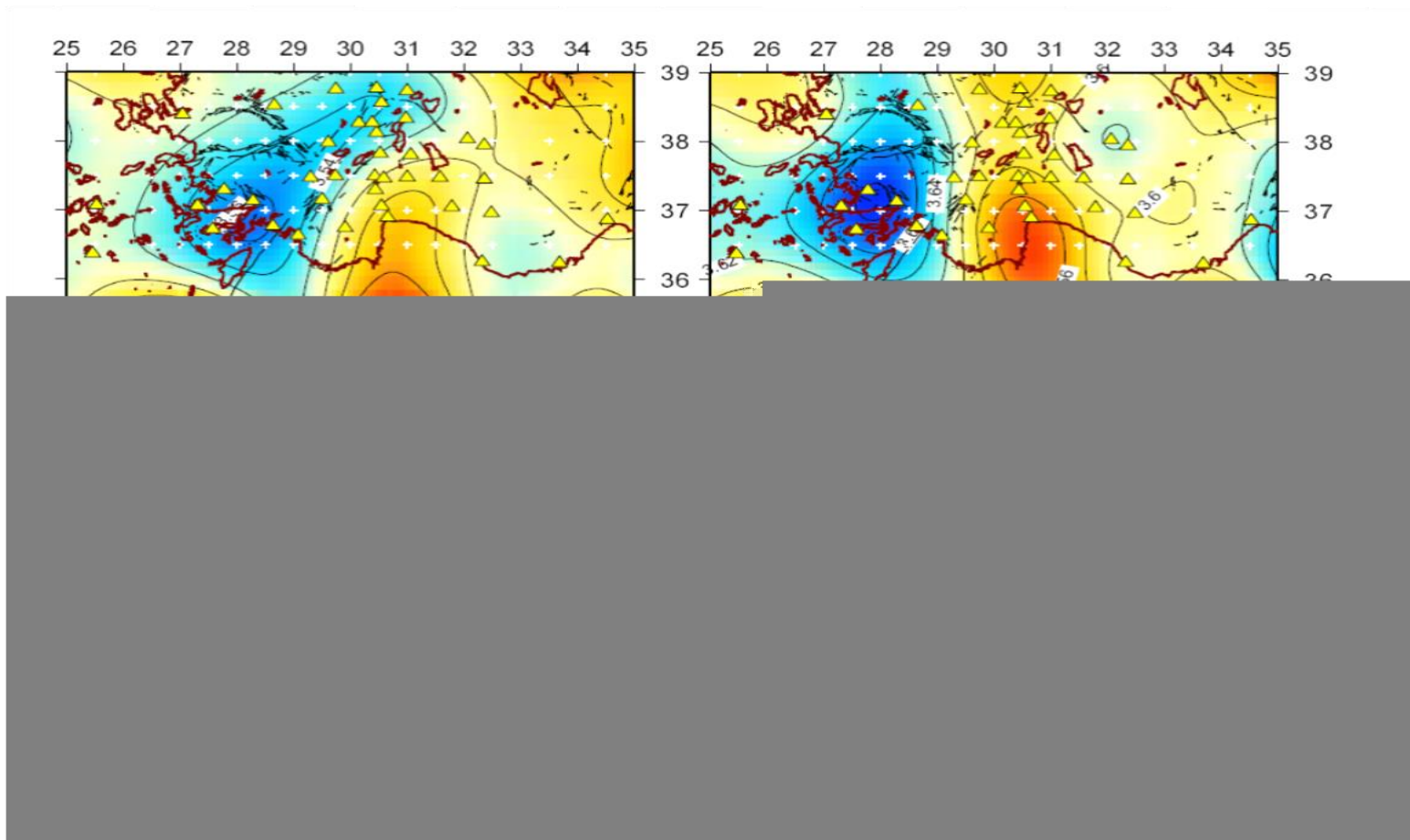
Figure 3.16. Phase velocity variations (%) at 28-33 seconds together with errors at 50 and 100 seconds. Yellow triangles and the black lines represent the stations and faults, respectively. Velocities are contoured in every 0.02 km/sec intervals.

Aegean probably due to a presence of several basins. Regarding the complex Moho topography beneath Cyprian Arc and its vicinity, Koulakov and Sobolev, (2005) found a relative crustal thickening up to 33 km in Cyprus and 27 km below the Eratosthenes Seamount in good agreement with the results from Diluccio and Pasyanos, (2007). They also obtained low velocities in the lower crust and underneath the Moho suggesting that the crust has a continental nature. Gravity data show a higher Bouguer anomaly in Cyprus with respect to the Eratosthenes seamount (Khair and Tsokas, 1999) together with seismic and magnetic data (Makris et al., 1983; Ben-Avraham et al., 2002). Resolution at this depth range is better compared to a recent P-wave tomography study by Biryol et al., (2011) due to the frequency content and propagation characteristics of surface waves. Therefore, resolution towards the edges of the model degrades due to insufficient number of stations.

At periods between 40 and 65 seconds (Figures 3.16 and 3.17) where the Rayleigh waves penetrate deeper in the upper mantle, the striking features are the two positive velocity anomalies (with a ~+%2 velocity perturbation) which are interpreted as the subducting segments of the African oceanic lithosphere along Cyprian and Hellenic Arcs (Spakman et al., 1988; De Boorder et al., 1998; Piromallo and Morelli, 2003; Bourova et al., 2005; Faccenna et al., 2006; Amaru, 2007; Chang et al., 2010; Biryol et al., 2011, Bakırcı et al., 2012). Our 40 seconds phase velocity map also correlates well with the most recent phase velocity results of Bakırcı et al., (2012) and Delph et al., (2015) obtained from Rayleigh wave and ambient noise tomography, respectively. The eastern segment of Hellenic arc is not covered by our stations. A slight separation between these two distinctive anomalies can be seen at 40 and 50 seconds, however, they merge at 65 and at 80 seconds. This is in contrast with the P-wave tomograms from Biryol et al., (2011), where the separation is much more obvious.Moreover, Bakırcı et al., (2012) mostly observed high phase velocities beneath IA at 65 seconds which does not correlate well with our findings. The common feature in Figures 3.16 and 3.17 is the low velocity anomaly beneath Menderes Massif, IA and its vicinity comprising Kula and Afyon-Kirka volcanics which is in line with the results by Yagmurlu et al., (1997), Savascin & Oyman, (1998), Dilek and Altunkaynak, (2009), Dilek and Sandvol, (2009), Biryol et al., (2011) and Salaün et al., (2012). In Figue 3.17, the amplitude of Cyprian arc anomaly is still clear at 80 seconds but becomes weaker compared to Hellenic Arc which does not match the results of Salaün et al., (2012) where this distinctive high velocity feature does not exist.
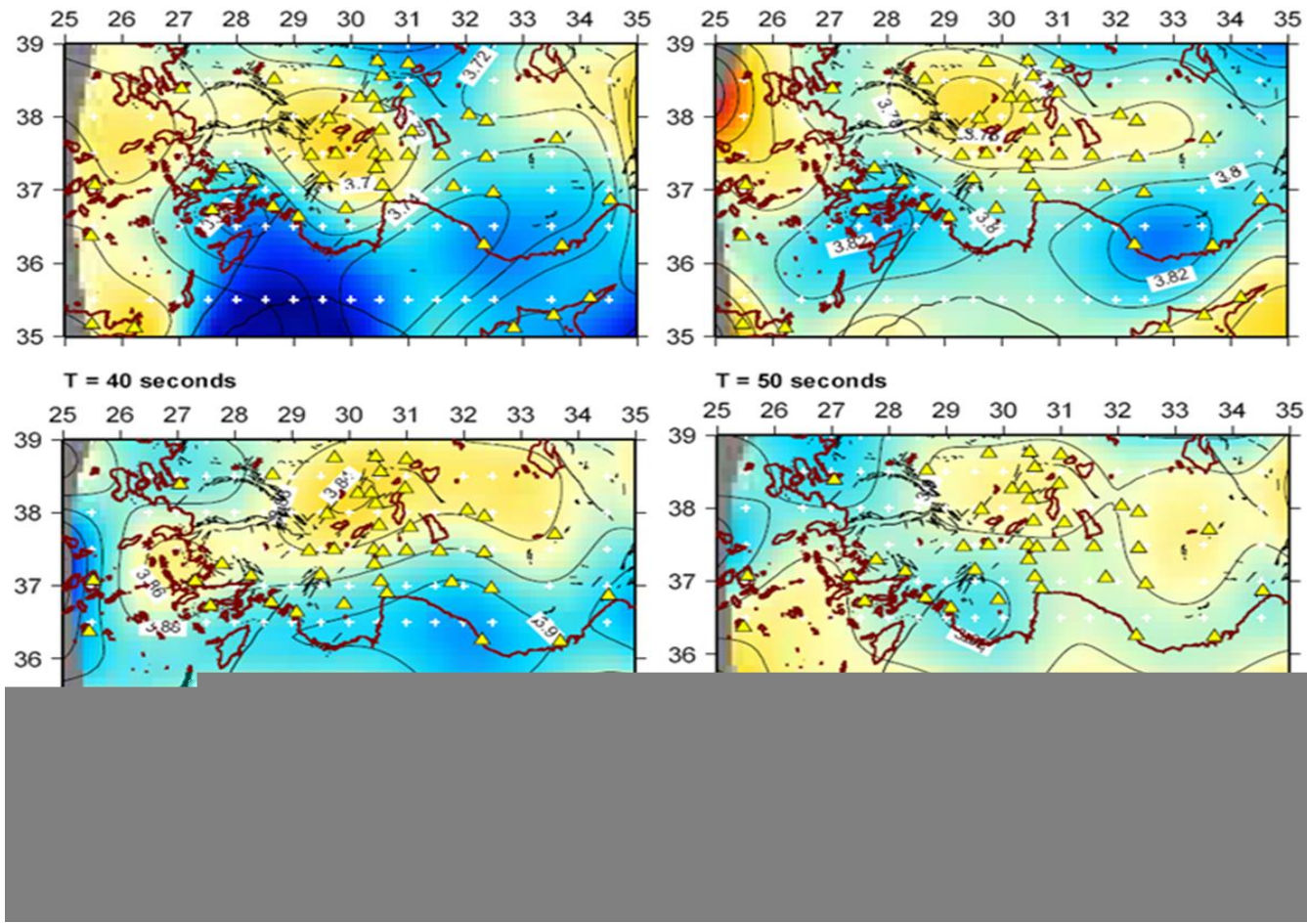
Figure 3.17. Phase velocity variations (%) at 40-80 seconds. Yellow triangles and the black lines represent the stations and faults, respectively. Velocities are contoured in every 0.02 km/sec intervals.

On the other hand, their calculated phase velocities were found to be relatively higher at almost all period ranges up to 200 seconds.

Figure 3.18 illustrates the phase velocity variations between 100 and 142 seconds. At this period range, Rayleigh waves sample the deeper parts of the upper mantle between ~130 and 230 km. Cyprian anomaly is still well detected at 100-110 seconds period range, partially in accord with the results from Bakırcı et al., (2012) where their slab anomaly slightly shifts north. Another common observation is a wide zone of low phase velocities occupying almost the entire southwestern Anatolia. Hellenic slab fast anomaly beneath the Aegean Sea is now replaced with low velocities with a slight shift towards Menderes Massif to the north. This observation is not in accord with the results of Biryol et al, (2011) and Salaün et al., (2012) where they still observe consistently high velocities. We suggest that Hellenic subduction is not continuous beneath the South Aegean Sea and might be detached from the subducting lithosphere giving rise to asthenospheric upwelling through a slab window. A recent teleseismic P-wave tomography study from Amaru, (2007) supports this idea. Ongoing roll-back of the retreating slab might also play a role in slab detachment. On the contrary, Hellenic slab anomaly was clearly mapped by Bourova et al, (2005) and Biryol et al, (2011). Despite the slightly degrading resolution at the highest periods, a low velocity corridor is clearly mapped from the northern tip of IA to further southwest extending to Rhodes Basin and South Aegean Sea where the subduction roll-back is taking place. The locations of Anaximander Mountains and the junction of Hellenic and Cyprus arcs are marked by high phase velocities.
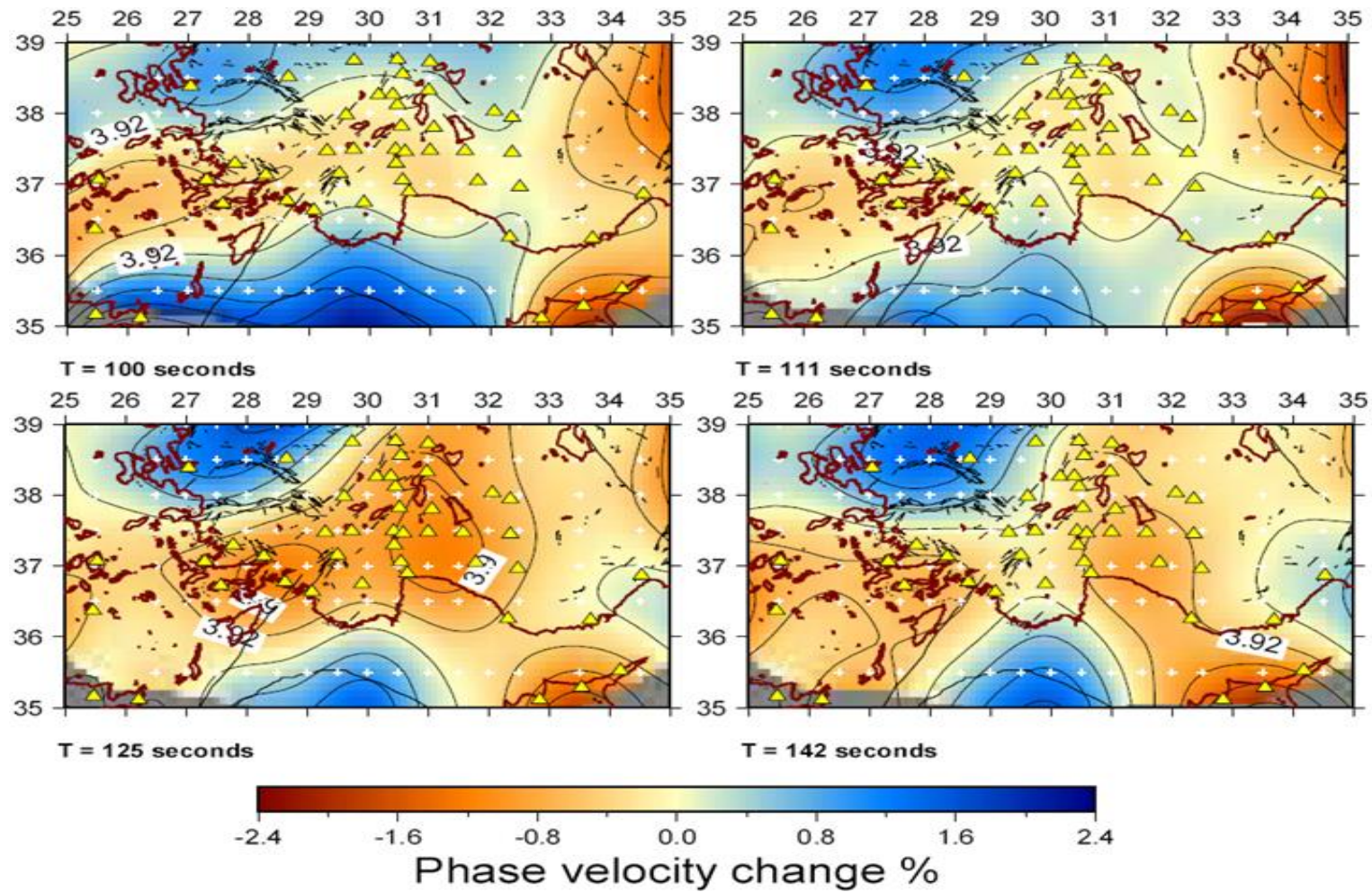
Figure 3.18. Phase velocity variations (%) at 100-142 seconds. Yellow triangles and the black lines represent the stations and faults, respectively. Velocities are contoured in every 0.02 km/sec intervals.

4. DETERMINATION OF 3-D SHEAR WAVE VELOCITY STRUCTURE

4.1. 1-D Average Shear Wave Velocity Structure beneath Southwestern Turkey

Phase velocities can only provide us integrated information about the upper mantle. In order to retrieve direct information at various depths, phase velocities should be inverted for shear wave velocities. Rayleigh wave phase velocities are primarily dependent on S-wave velocities (with the maximum sensitivity depth at ~1/3 of a given wavelength), less on density and P-wave velocity. Rayleigh wave sensitivity to P-wave structure is confined to very shallow depths (primarily the crust) even at longer periods. Therefore, we only solve for S-wave velocities by linking P-wave velocities to S-wave velocities with a constant Poisson's ratio, which is a reasonable approximation for crust and uppermost mantle (Weeraratne et al., 2003; Yang and Forsyth, 2006).

In order to obtain an appropriate 1-D reference model for the entire region, we first performed an inversion with the previously calculated average phase velocities (represented in Table 3.2) and used the AK135 model from Kenneth et all, (1995) as the starting model. We adopted the method of Saito (1988) to calculate the derivatives of phase velocities with respect to model parameters (derivatives with respect to the change in P and S wave velocities) at each layer, which can be written as:

$$dc/d\beta = \partial c/\partial\beta + (\partial c/\partial\alpha)(\partial\alpha/\partial\beta) = \partial c/\partial\beta + 3^{1/2}(\partial c/\partial\alpha) \tag{4.1}$$

We slightly damped the model parameters by assigning a priori standard deviations of 0.2 km/s to the diagonal elements of the model covariance matrix and a correlation coefficient of 0.3 between the adjacent layers to smooth the model. A Vp/Vs ratio of $3^{1/2}$ is also applied in order to calculate the total derivatives and P wave velocity models. It is challenging to determine an appropriate Vp/Vs ratio for a mantle structure; but at greater depths, sensitivity to P-wave velocity is negligible. The crustal thickness is fixed at 33 km, which is the average crustal thickness in southwestern Turkey constrained from the most recent receiver function studies for the Aegean region (Li et al; 2003; Sodoudi, 2006;

Tezel, 2010). In this reference model, velocity is allowed to vary to a depth of 350 km, because the standard deviations of the average phase velocities are much smaller than the uncertainties associated with lateral variations, providing better depth resolution (Yang and Forsyth, 2006). The Resulting 1-D Shear wave velocity model is given in Figure 4.1.
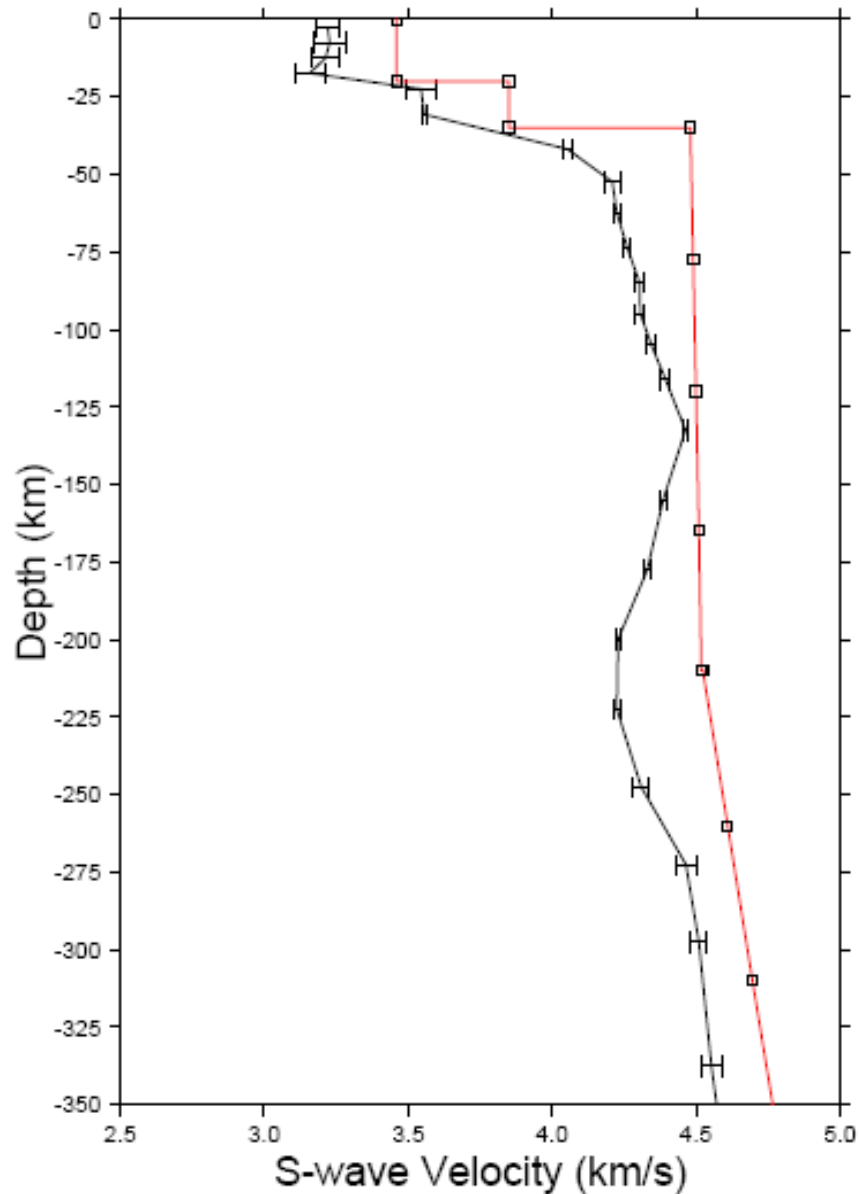
Figure 4.1. The resulting 1-D shear wave velocity model (thick black line) with the standard deviations (horizontal bars). Ak135 model is represented by the red line.

The errors at crustal depths are relatively higher due to the lack of Rayleigh wave sensitivity to upper and mid crust (periods < 30 seconds). Overall, shear wave velocities are found significantly lower than the AK135 model. A gradual velocity increase is observed with increasing depth with an exception of a negative velocity anomaly (down to a velocity of 4.25 km/sec) located at a depth range of ~130–230 km. The starting depth of this negative velocity gradient can be interpreted as the best estimate of the base of the lithosphere (Humpreys and Clayton, 1990; Humpreys and Hager, 1990). Below 230 km, shear wave velocities tend to coincide with the AK135 model. In this study, our lithospheric thickness estimate is tentatively at around 130 km taking into account the negative gradient in Figure 4.2 which exceeds the value of ~80 km obtained for Eastern Anatolia from S-wave receiver functions (Angus et al., 2006). The increasing velocity pattern of shear waves probably suggests the presence of the subducting oceanic African lithosphere. This observation is in accord with a previous study from Meier et al., (2004), where the S-wave velocities down to approximately 200 km are derived from 1-D phase velocity inversions between several station paths (using a two-station method) along a SW–NE profile that extends from northern Africa via the Libyan Sea, Crete and Santorini towards central Turkey. They also found anomalously low upper mantle velocities along a path from Santorini Island (SANT) to Central Anatolia consistent with another S-wave tomography model from Marone et al., (2003).

S-wave velocities are widely used to discriminate between cooled oceanic lithosphere of that age and continental mantle lithosphere. Velocities larger than 4.5 km/sec are inferred for cold oceanic lithosphere (Stein and Stein, 2006; Erduran et al., 2008). For comparison, in case of such an old oceanic lithosphere, Rayleigh wave inversions yield typical lithosphere velocities of 4.6 to 4.7 km/sec in the upper mantle (van der Lee, 2002; Rychert et al., 2005, Yang and Forsyth, 2006). Also a fairly recent study of Erduran et al., (2008) emphasized the discrimination between the remnants of oceanic African lithosphere and the continental lithosphere along several paths between station pairs from Cyprus to Crete beneath and Cyprus to Isparta Angle. They found slightly higher velocities between the path between ISP and the CSS stations located in Cyprus revealing the existence of an oceanic lithosphere.

Temperature variations also play an important role in velocity perturbations; for instance a ~0,3 km/sec or 6,5% decrease in velocity of the lid can be compensated by an increase in temperature of ~750 °C if retrieved purely through elastic effects (Stixrude and Lithgow-Bertelloni, 2005). The large velocity drops obtained in this study might indicate nonsteady state temperature variations at the base of the lithosphere due to cooling of the lower continental lithosphere during African slab subduction, currently replaced by asthenosphere analogous to the ancient subducted Farallon slab beneath northwest California (Humpreys and Hager, 1990). It is difficult to explain the shear wave velocities in this study as low as 4.2 km/sec in the upper mantle without the existence of partial melt as observed beneath Eastern Anatolia region (Sandvol et all, 2003; Gök et all, 2003 and the references therein). This is also consistent with the findings of Diluccio and Pasyanos, (2007) since they also obtained low upper mantle shear wave velocities and suggested that in the Eastern Mediterranean basin, the presence of partially molten material as well as the presence of serpentinite could explain the observation of slow seismic velocities. The results of the subsequent shear wave inversions will be displayed both in map views and vertical cross sections in the following chapters.

4.2. Model Resolution

We also need to evaluate the resolution of model parameters, which will tell us how well shear velocities at different depths are resolved. The elements of the resolution matrix provides useful measurements of resolution (Yang and Forsyth, 2006a; Li et al., 2003). The rank of the resolution matrix provides an overall measurement of resolution, which describes the number of pieces of independent information about the model parameters provided by the data, i.e., the number of linearly independent combinations of model parameters that can be resolved. The resolution to shear wave velocity decreases with depth in general. As shown in Figure 4.3, peak values in the model resolution matrix become smaller at greater depths. Although velocities in each layer cannot be perfectly resolved, the average velocity can be well determined at the depth ranges of 50 km, 100 km, 150 km and ~250 km from the shallow to the lower upper mantle.
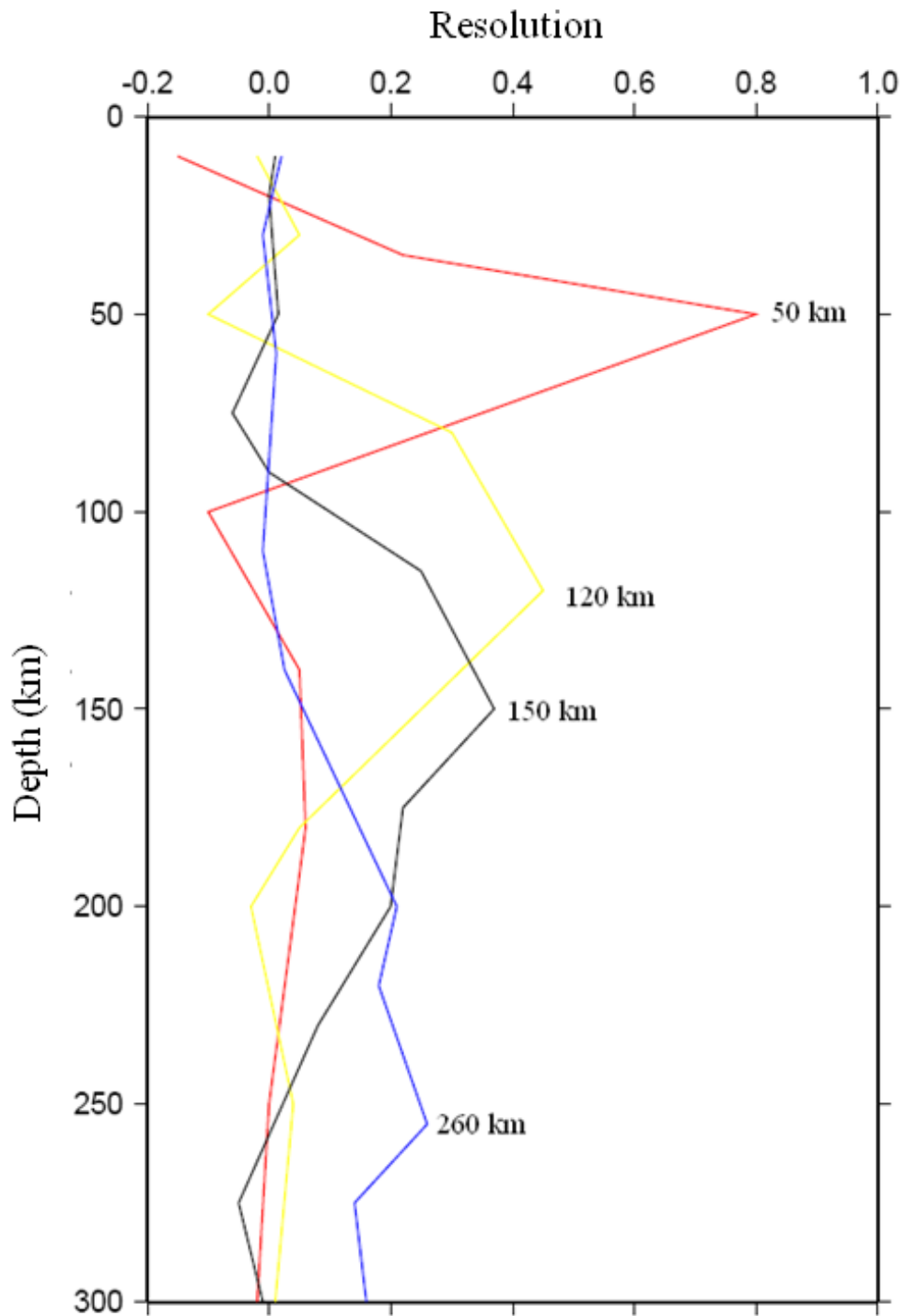
Figure 4.2. Rows of the resolution matrix corresponding to four layers with median depths at 50, 120, 150, and 260 km. A peak value at the corresponding depth indicates good resolution. The sharper the peak is, the higher the resolution for that layer.

4.3. Shear Wave Velocity Structure

In order to map the shear wave velocities beneath the southwestern Anatolia, we applied the same inversion technique from Saito (1988) to each map point in the Rayleigh wave inversion grid. The crustal thicknesses were fixed at each map point and the values are estimated by interpolating them from a combination of recent studies (Sodoudi et al., 2006; Zhu et al., 2006; Akyol et al., 2006; Erduran, 2008; Tezel et al., 2010). Thus, there is a large trade-off between crustal thickness and velocity of lower crust and uppermost mantle. For instance, a 5-km change of Moho depth with a 0.7 km/sec shear velocity shift across the Moho approximately corresponds to 0.1 km/sec phase velocity change over a depth range of 20 -55km (Yang and Forsyth, 2006). Uncertainties in crustal thickness values can bias the results in the lower crust and the uppermost mantle but their influence below ~60 km is negligible. Overall, errors in the shear wave velocities were mostly found below 0.1 km /sec within the array and gradually decreased towards the less sampled parts of the model (Figure 4.6).

Horizontal depth slices of the tomographic model at various depths between 60 and 250 km are presented in figures 4.3-4.5. High velocity anomalies up to 4% (with respect to AK135 Model) located to the north of Cyprus-Hellenic trenches and beneath the West Anatolian Extensional Province might hereafter be interpreted as the segments of the subducting African Lithosphere, namely the Aegean and Cyprian Slabs. Figure 4.3 shows the map views of the model at 60 and 80 km depth. A north-south trending low velocity anomaly extending from IA to Anaximander Mountains separates the Aegean slab fast anomaly to the west (occupying the South Aegean cost and the Rhodes Island) and the remnant Cyprian slab beneath the eastern limb of IA and further east. Despite the degrading resolution, low shear wave velocities are observed beneath the Crete and Cyprus Islands whereas Menderes Massif exhibits relatively high velocities. The fast anomalies associated with the Aegean and Cyprian slabs become clearer at 80 km (Figure 4.3b). This is also in agreement with the corresponding phase velocity maps of 40-80 seconds period given in Figure 3.17. Previous tomography studies from Spakman et al, (1998), Piromallo and Morelli (2003) and Chang et al, (2010) also detected the Aegean slab fast anomaly; however, those studies were not able to clearly image the Cyprus slab.
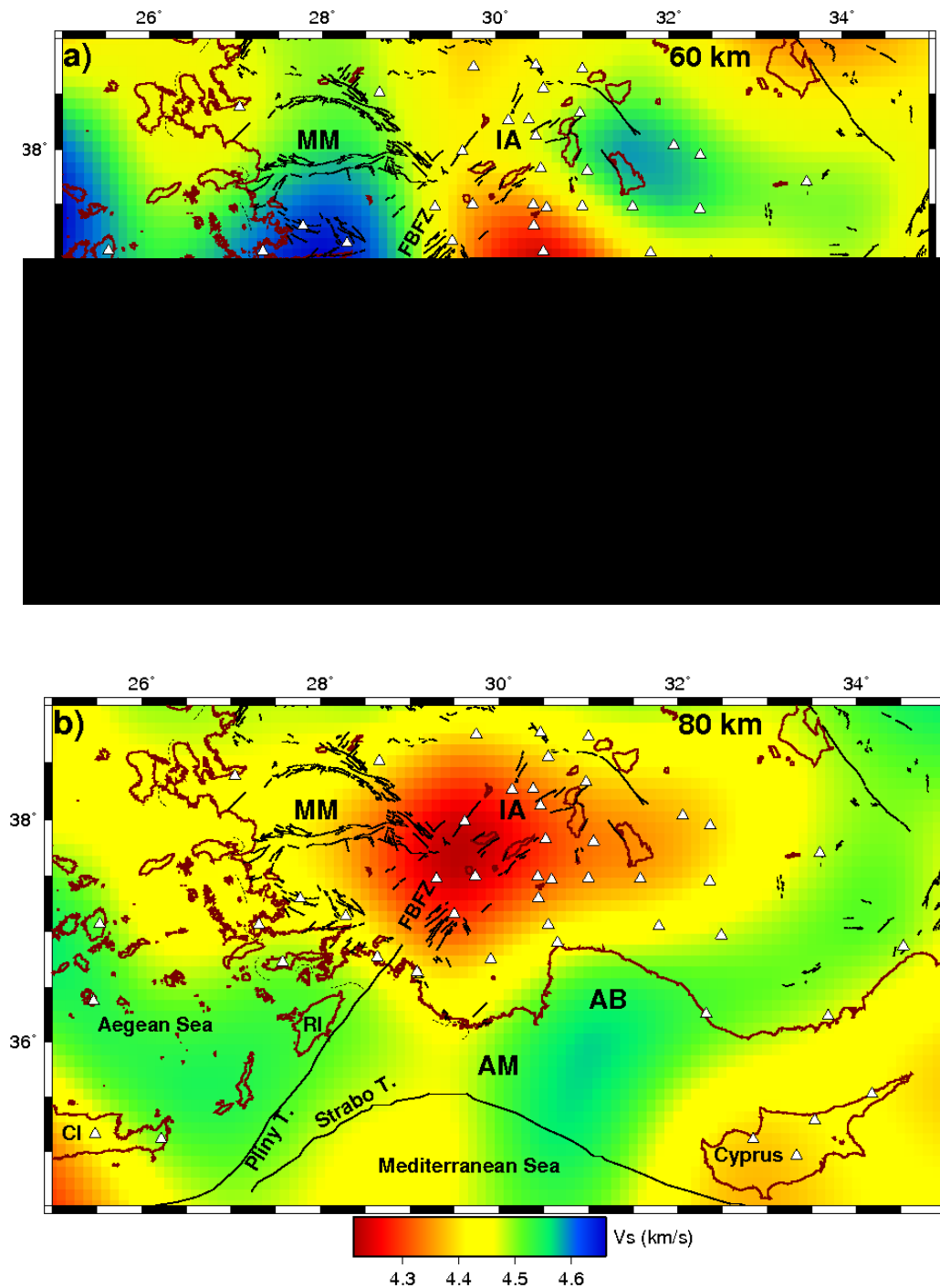
Figure 4.3. Map views of the shear wave velocity model a) at 60km and b) at 80 km. Faults are shown by black lines. Stations are shown with white triangles Abbreviations: AB: Antalya Bay, AM: Anaximander Mountains, CI: Crete Island, FBFZ: Fethiye-Burdur Fault Zone, IA: Isparta Angle, MM: Menderes Massif, RI: Rhodes Island, Pliny T: Pliny Trench, and Strabo T: Strabo Trench.

A recent teleseismic P-wave tomography study from Biryol et al, (2011) mapped the Cyprus slab as a subvertical anomaly in their vertical cross sections. Another striking feature is the significantly slow velocities (at the order of ~4% with respect to AK135 Model corresponding to ~4.25 km/sec) beneath almost the entire IA region including the Kula Volcanic Field (KVF) and extending towards Menderes Massif (MM). This results correlates well with the results of recent surface wave tomography studies from Salaün et al., (2012) and Bakırcı et al., (2012).

The effect of both Aegean and Cyprian slabs become much more evident at 120 km where the anomalies are slightly shifting north and merging towards Antalya Bay and the southern portion of the IA (Figure 4.4a). Similar to Bakırcı et al., (2012), Cyprian slab anomaly gets even stronger beneath Antalya Bay where several intermediate depth earthquakes were previously reported (Papazachos et al., 2000; Wdowinski, 2006). We also note that the Aegean slab anomaly slightly weakens and is less pronounced compared to the Cyprian slab. This geometry is in contrast with Salaün et all, (2012) since they have not detected this pattern completely. They observed a low velocity structure beneath the entire western Anatolia with no presence of Cyprian slab fast anomaly. On the other hand, this structure partially correlates with Biryol et all, (2011) where they again observe a N-S trending corridor of slow P-wave velocity pattern. In our study, slow shear wave velocities occupy the entire width of IA and Menderes Massif. At 160 km, South Aegean Sea, Cyprus Island, Antalya Bay, Pliny-Strabo trenches display low velocities. Hellenic slab does not seem to be continuous beneath the South Aegean Sea and Cyprian slab anomaly moved slightly towards north beneath IA extending to Menderes Massif. Salaün et al, (2012) were not able to map these high velocity bodies; instead they observed a slow velocity distribution.

Velocity structure at 200-250 km depth range displays similar velocity patterns as shown in Figure 4.5. The most prominent features are the continuous east-west trending fast and slow velocities across the model. Aegean and Cyprian slab anomalies tend to merge beneath IA and Menderes Massif, whereas the slow velocities dominate the South Aegean Sea, Antalya Bay, Pliny and Strabo Trenches. Slab anomalies shifted slightly north compared to the map view at 160 km which is an indication of a northward dipping African lithosphere.
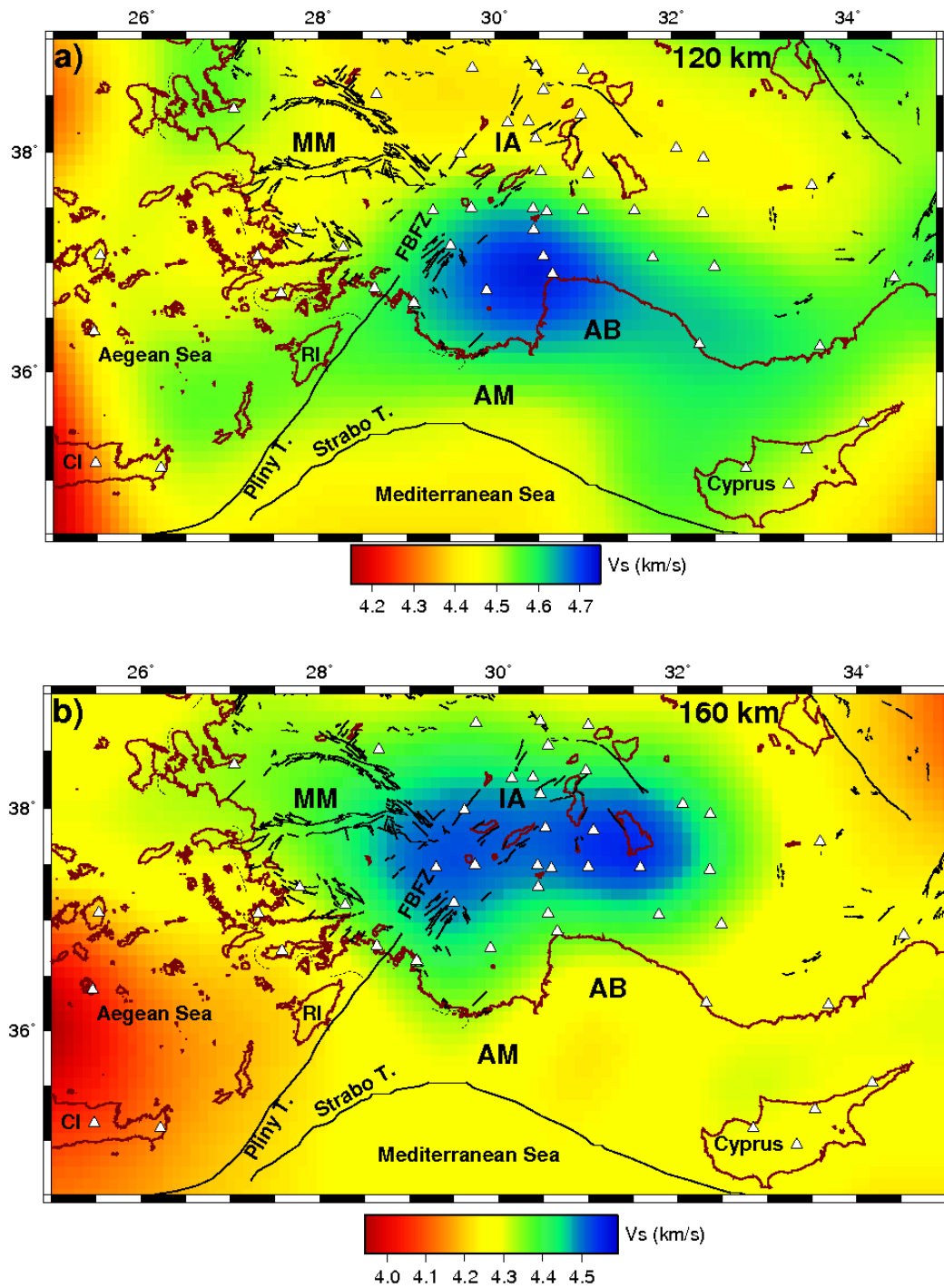
Figure 4.4. Map views of the shear wave velocity model a) at 120km and b) at 160 km. Faults are shown by black lines. Stations are shown with white triangles. Abbreviations: AB: Antalya Bay, AM: Anaximander Mountains, CI: Crete Island, FBFZ: Fethiye-Burdur Fault Zone, IA: Isparta Angle, MM: Menderes Massif, RI: Rhodes Island, Pliny T: Pliny Trench, and Strabo T: Strabo Trench.
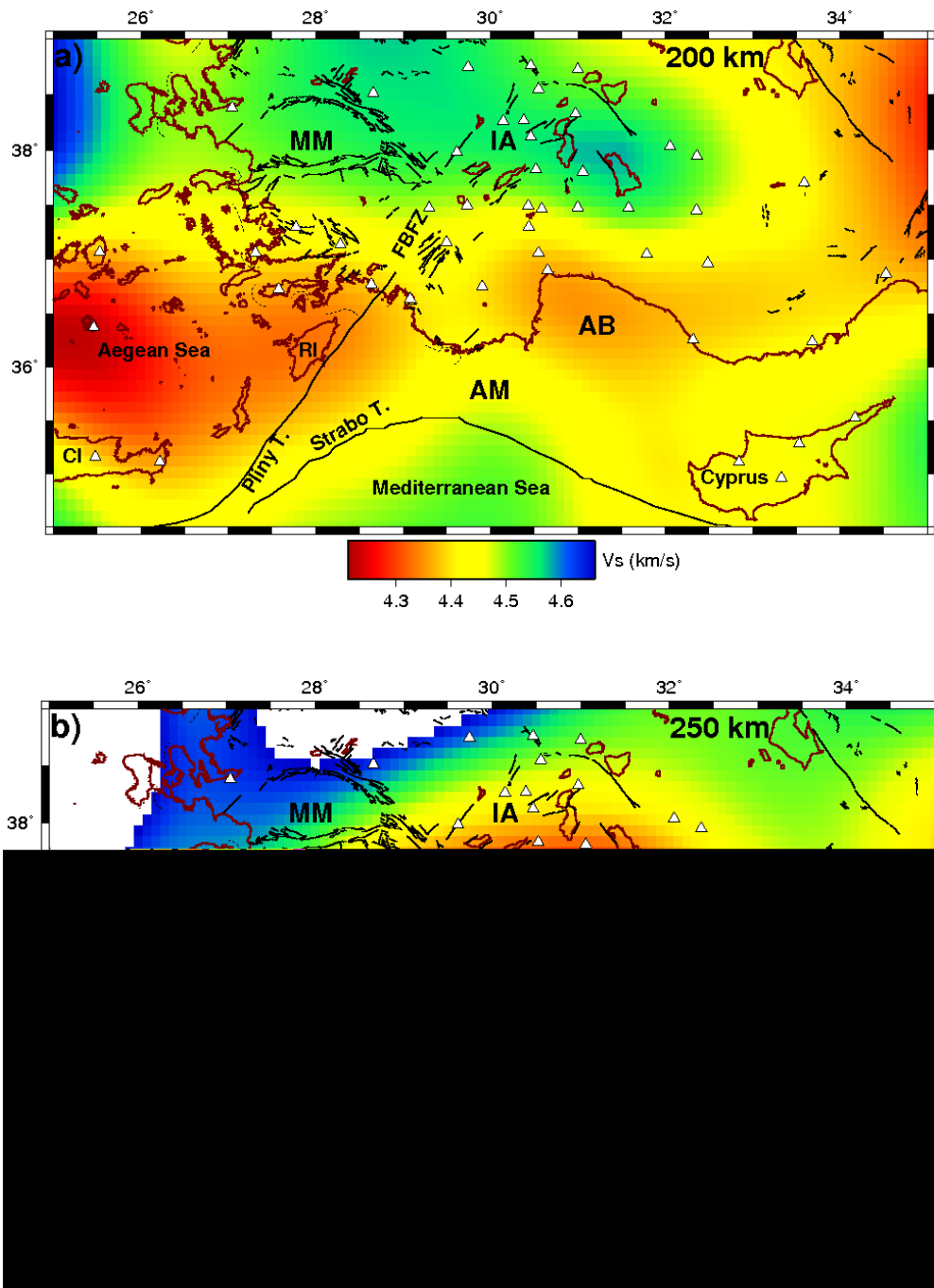
Figure 4.5. Map views of the shear wave velocity model a) at 200 km and b) at 250 km. Faults are shown by black lines. Stations are shown with white triangles. Abbreviations: AB: Antalya Bay, AM: Anaximander Mountains, CI: Crete Island, FBFZ: Fethiye-Burdur Fault Zone, IA: Isparta Angle, MM: Menderes Massif, RI: Rhodes Island, Pliny T: Pliny Trench, and Strabo T: Strabo Trench.

On the contrary, Biryol et al., (2011) identified the Cyprus slab as subvertical at depths shallower than 200 km. Our findings are more or less in agreement with Salaün et al., (2012) with just a few differences in lateral extents of the observed anomalies. The offshore Anaximander Mountains which is an important link between both arcs acts as a transition from low to high velocities from the south of IA towards the Cyprian arc.
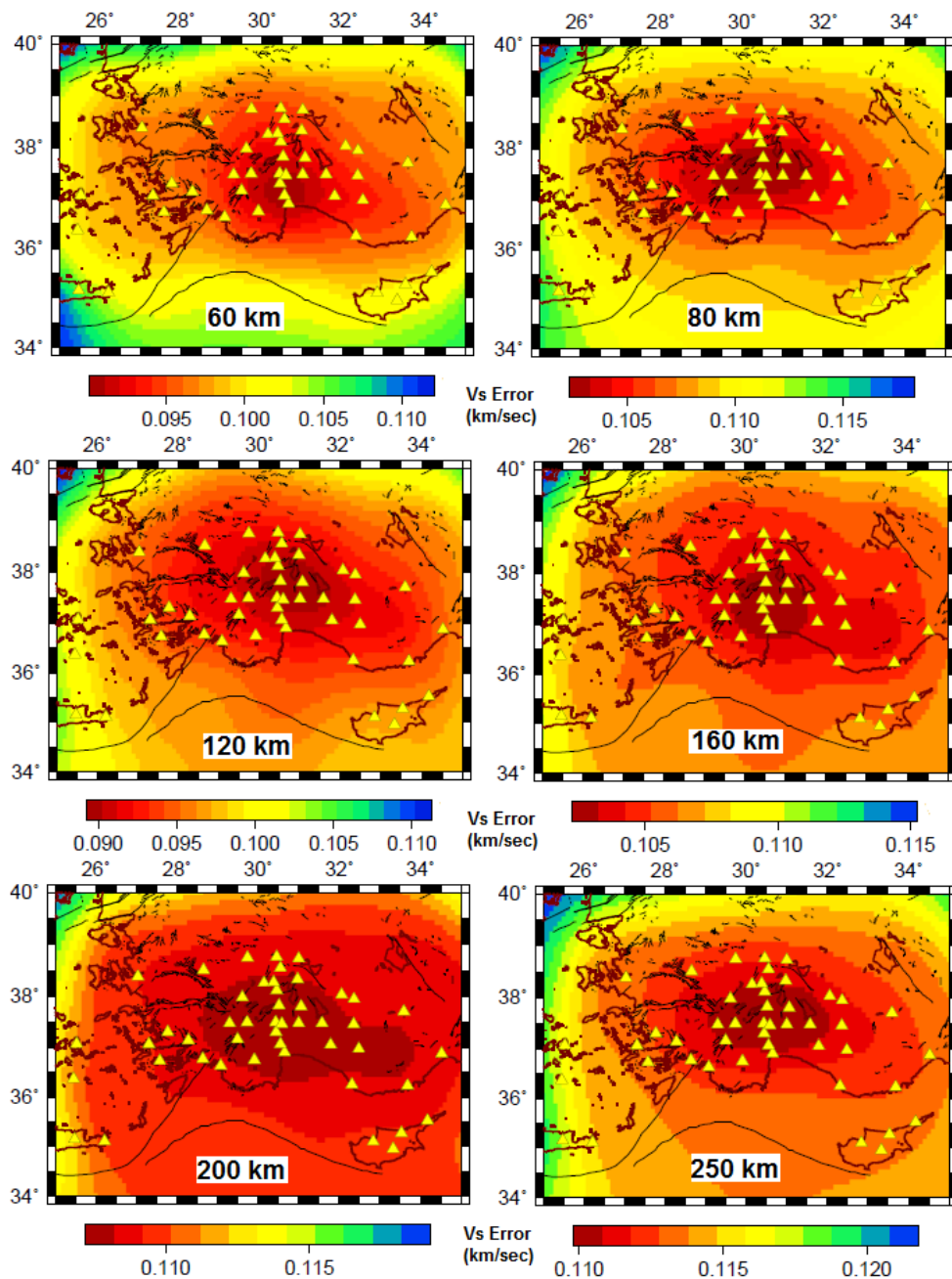
Figure 4.6. Maps of errors in shear wave velocities at corresponding depths. Stations are denoted by yellow triangles. Faults are shown by black lines.

5. CONLUSIONS AND DISCUSSION

In this section, S-wave velocity variations obtained from surface wave tomography results will be presented in several vertical cross sections in order to put accurate constraints on the lithospheric structure and slab geometry beneath the African-Anatolian plate boundary down to ~250 km depth. The structures located below this range km are beyond the resolution capability of highest period Rayleigh waves used in this study.

Three N-S vertical cross sections along the Hellenic arc are presented in Figure 5.1. The fast and continuous velocity anomaly of the Hellenic subduction (at the order of ~4%) is well imaged along longitude 29°E. The slab dips towards north with a shallow angle and starts to flatten out at around 150 km depth nearly beneath the western limb of IA. Hellenic slab anomaly was therefore mapped by various previous studies (Spakman et al., 1988; Bijward et al., 1998; Piramallo and Morelli, 2003; Amaru, 2007, Chang et al., 2010, Salaün et al., 2012). The apparent slab thickness is approximately 100 km smaller than the value (~150 km) obtained by Salaün et al., (2012). We observe similar patterns along longitude 27.5°E, a northward dipping slab with an angle of ~30° below 100 km but the fast anomaly associated with it becomes weaker. In addition, seismicity across this profile more or less aligns with the Hellenic slab fast anomaly (Enghdal, 1988; Wdowinski et al., 2006). This observation partially correlates with the P-wave tomograms from Biryol et al, (2011) since they emphasize that the slab is nearly subvertical down to 200 km depth. The most striking feature is mapped along another vertical slice along longitude 26°E (Figure 5.1, profile no: 6). Keeping in mind that the southwestern part of the model volume is relatively less sampled, we might tentatively suggest that the Hellenic slab is not continuous anymore and might have detached from the African lithosphere at around 125 km depth at a location close Cretan sea and the volcanic island arc. This situation might be linked with the presence of a low velocity zone beneath the volcanic chain in that region and might have also occurred due to slab pull forces acting on the retreating Hellenic trench. The geometry of the Aegean subduction also appears to be in agreement with the consistent NE-SW pattern of anisotropy underneath Western Anatolia Extensional Province (Hatzfeld et al, 2001; Sapaş and Güney, 2009; Biryol et al., 2010).
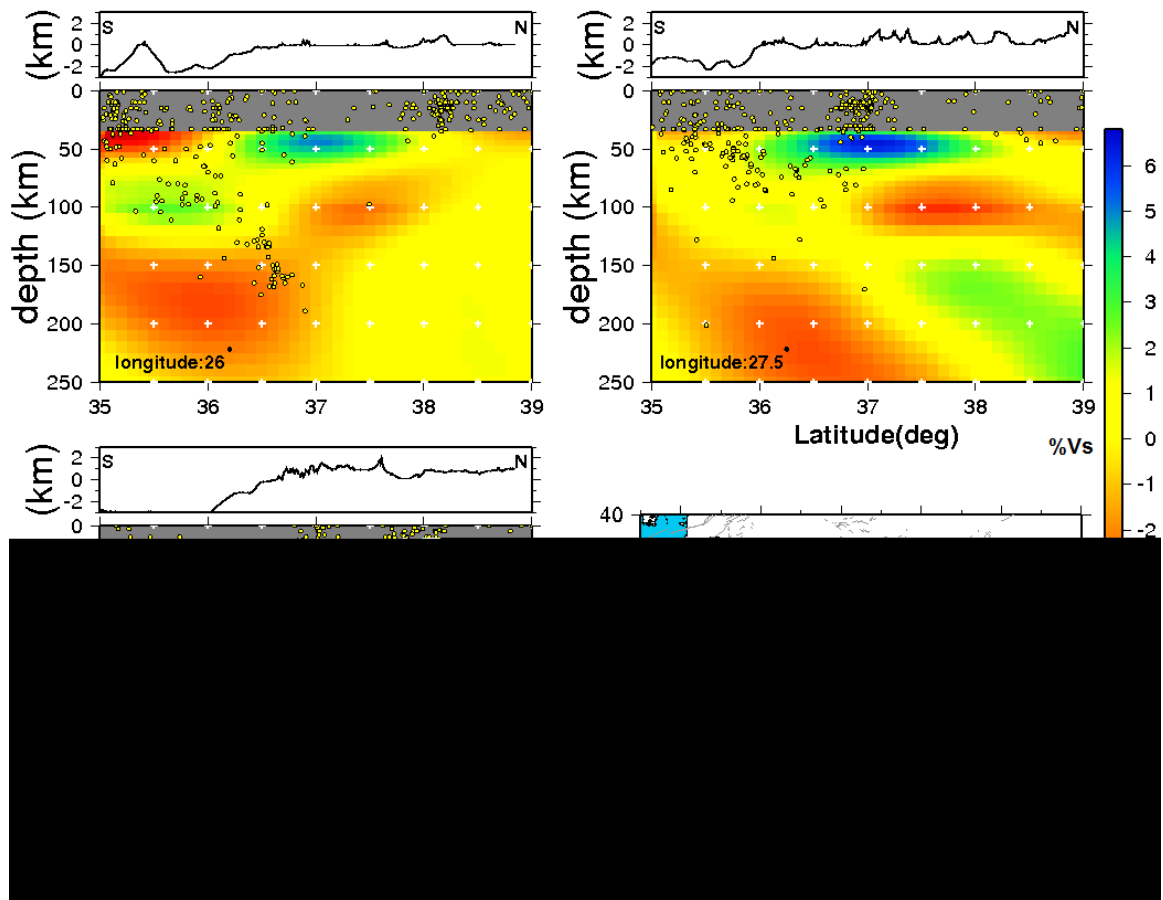
Figure 5.1. Shear wave velocity variations (%) across three vertical profiles across the Hellenic arc. The locations of the profiles are given in the map. Yellow circles indicate the earthquake locations. Topography data is also provided above each profile.

Figure 5.2 illustrates three vertical cross sections along the Cyprian segment of African subduction and IA. Velocity patterns across 30-31° longitudes display very similar features. Analogous to Hellenic subduction, the slab beneath Cyprus is clearly identified by northward dipping fast velocity perturbations at the order of ~5% and intermediate depth seismicity. Cyprian Arc is less active in terms of seismicity compared to Hellenic arc (Enghdal 1998; Wdowinski et al., 2006); majority of the earthquakes are located below Anaximander Mountains as well as below the Florence Rise (Figure 2.2). The apparent slab thickness is approximately 100 km; however the horizontal and vertical smoothing makes it impossible to give a precise estimate. This anomaly has also been clearly resolved by the most recent teleseismic tomography studies (Biryol et al., 2011; Salaün et al., 2012; Bakırcı et al., 2012), however, the trace of Cyprus subduction could not be sufficiently

followed by various earlier studies (Spakman et al, 1988 and 1993; Piramallo and Morelli, 2003; Marone et al, 2003; Faccenna et al, 2006). Our findings suggest that Cyprian slab dips with an angle close to 45° but begins to flatten out at around 125-200 km depth range beneath the northern tip of IA. This result is not in agreement with the study from Biryol et al., (2011) given the fact that they described the Cyprian slab as a subvertical fast anomaly at depths shallower than 200 km. Furthermore, Salaün et al., (2012) could not trace the Cyprian slab above 200 km; they were only able to image the Cyprian slab as a north dipping continuous feature below 200 km depth with quite high S-wave perturbations up to ~10%. Similar subduction behavior was observed across the profile mapped along longitude 32°E (with slightly reduced amplitudes) where the slab dips and starts to flatten-
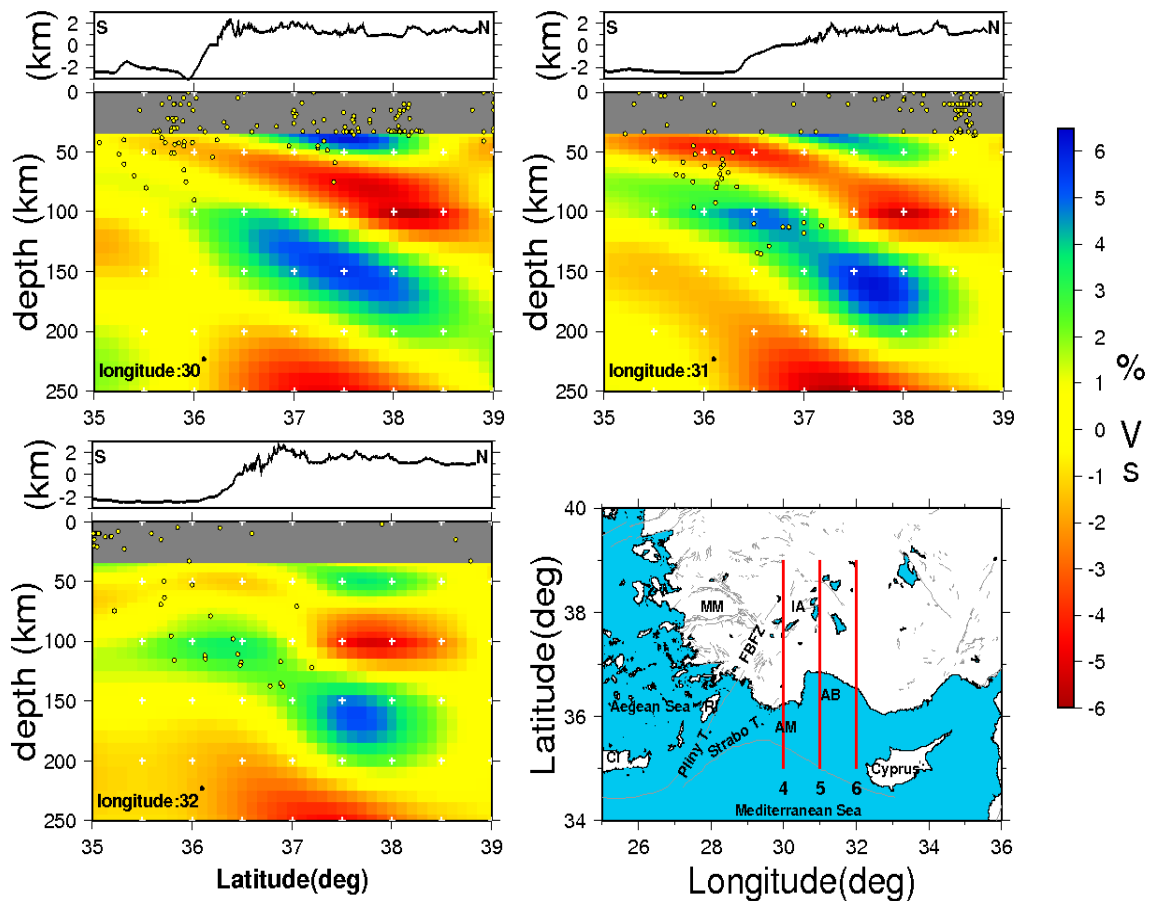
Figure 5.2. Shear wave velocity variations (%) along three vertical profiles across the Cyrus arc. The locations of the profiles are given in the map with numbers and red lines. Yellow circles indicate the earthquake locations. Topography data is also provided above each profile.
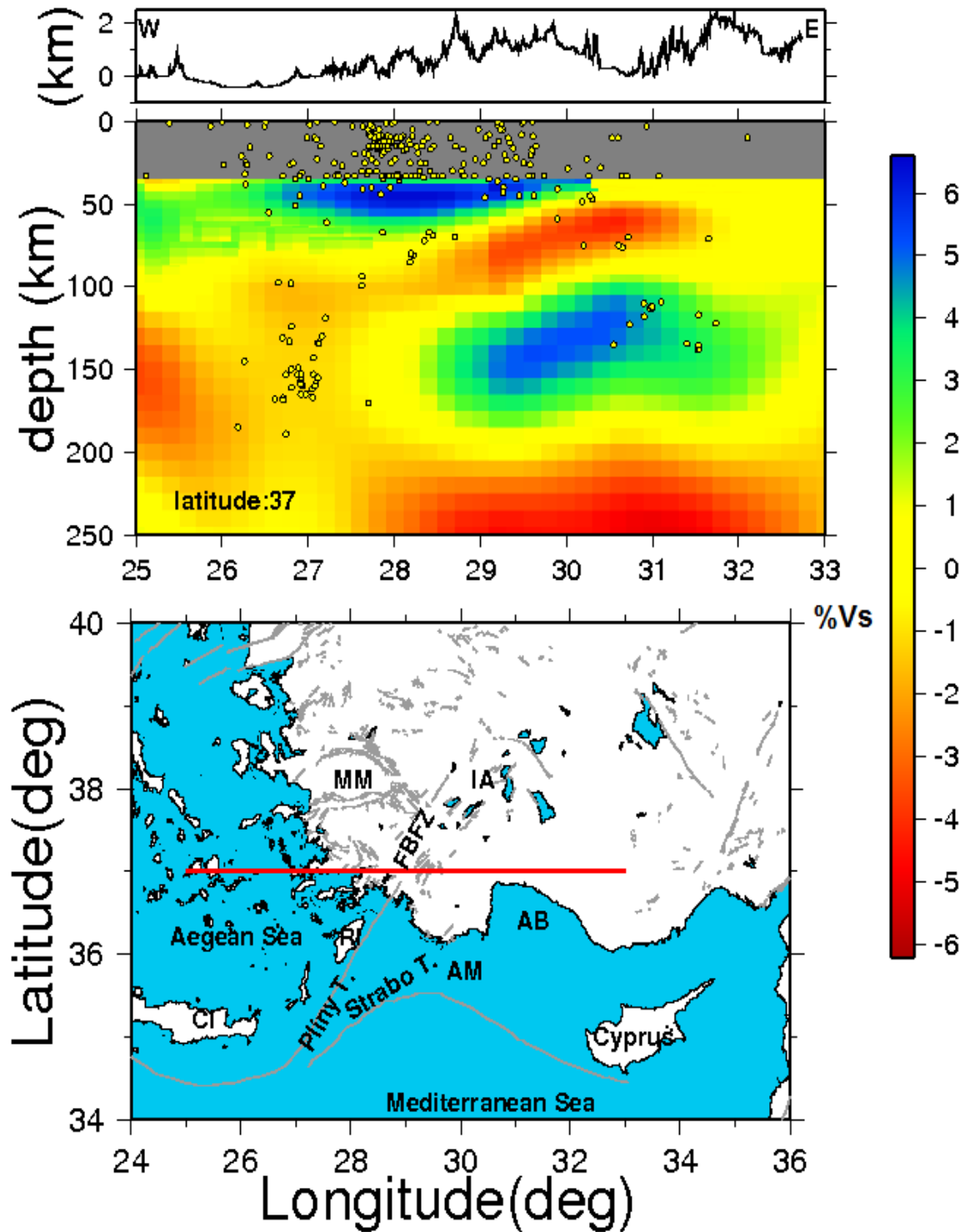
Figure 5.3. Shear wave velocity variations (%) along a vertical profile across latitude 37°
N. The location of the profile is shown in the lower panel by a red line. Yellow circles
indicate the earthquake locations. Topography data is also provided above the profile.

out at 150-200 km depth range (Figure 5.2, profile number 6). This result might support the idea that Cyprus subduction is relatively shallow compared to Hellenic subduction imaged along Crete to central Aegean Sea (profiles in Figure 5.1) as suggested by Faccenna et al, (2006). Our findings suggest that western extension of the Cyprus slab was clearly mapped beneath southern IA and Antalya Basin and its fast anomaly merges with the Hellenic slab anomaly at 120-150 km depth range (Figure 4.4) also supported by Bakırcı et al., (2012). The geometry of eastern part of the Cyprus slab is beyond our resolving power due to insufficient number of ray paths beneath the southeastern extremity of our model. Furthermore, Bakırcı et al., (2012) emphasized the existence of a relatively minor tear within the Cyprus slab located approximately at 37°N-34°E within 60-100 km depth range that terminates beneath the quaternary volcanoes, in agreement with the tomographic model of Biryol et al., (2011).

As discussed earlier, several authors pointed out that Isparta Angle is defined with a vertical tear in the northward subducting African Plate (Barka and Relinger, 1997; Bijwaard et, 1998; Wortel and Spakman, 2000; Piramallo and Morelli, 2003; Dilek and Sandvol, 2009; Biryol et al, 2011). Our findings seem to be supporting this interpretation. Figure 5.3 illustrates a vertical profile taken from western edge of the model to east along latitude 37°N. As mentioned earlier, the gap in the African lithosphere beneath southwestern Anatolia (spanning the entire IA in particular) which is currently occupied by low velocities is also evident at ~50-130 km depth range. This situation is fairly in agreement with the tomograms across the same latitude from Biryol et al, (2011), and Salaün et al., (2012). Conversely, they were able to image this low velocity zone with sufficient resolution down to 300 km depth. The surface expression of this gap/tear might be the left lateral Pliny and Strabo trenches in agreement with Hinsbergen et al, (2010). These studies also stated that Hellenic and Cyprus slabs merge at a depth of ~500 km and forms a flat-lying broad anomaly associated with the 660 km discontinuity. On the other hand, our model seems to be in agreement with the interpretation of Bakırcı et al., (2012) stating that the tear might have closed based on the merged slab anomalies of both Hellenic and Cyprus slabs beneath the IA. Consequently, upwelling of hot asthenospheric material gives rise to low velocities beneath the volcanic regions in Isparta Angle and the surroundings such as Kula and Afyon-Isparta volcanics. This idea is supported by geochemical studies by Gülen, (1990) and Tokçaer et al, (2005). Similarly, Afyon-Isparta

volcanic field is associated with alkaline volcanism younging in the direction from north to south (Dilek and Altunkaynak, 2009 and the references therein).

One major difference we observed is the non-continuous subduction of the Hellenic slab (Figure 5.1, profile no: 1 and Figures 4.4-4.5) that might tentatively be associated with a slab detachment process. Hinsbergen et al, (2010) suggests that there is present gap in the slab between 400 km depth and the surface, and the ongoing Africa–Europe convergence after slab break-off is accommodated by shortening in the overriding plate. Slab detachment had been a consequence of partial subduction of buoyant continental edges, as the denser leading edge of the relatively cold oceanic lithosphere broke off and sank into the lower mantle. Slab tearing might have occurred along the intersection of strongly arcuate subduction zones such as the Cyprian and Hellenic arcs having different convergence rates and directions (Dilek, 2006; Dilek and Sandvol, 2010). Both slab detachment and slab tearing might trigger slab roll-back and jointly play a crucial role in asthenospheric upwelling and partial melt. This condition gave rise to crustal collapse further leading to extension in the upper plate and formation of post-collisional alkaline magmas in the region such as Kula and Afyon-Kirka Volcanics.

APPENDIX A: DISPERSION CURVES
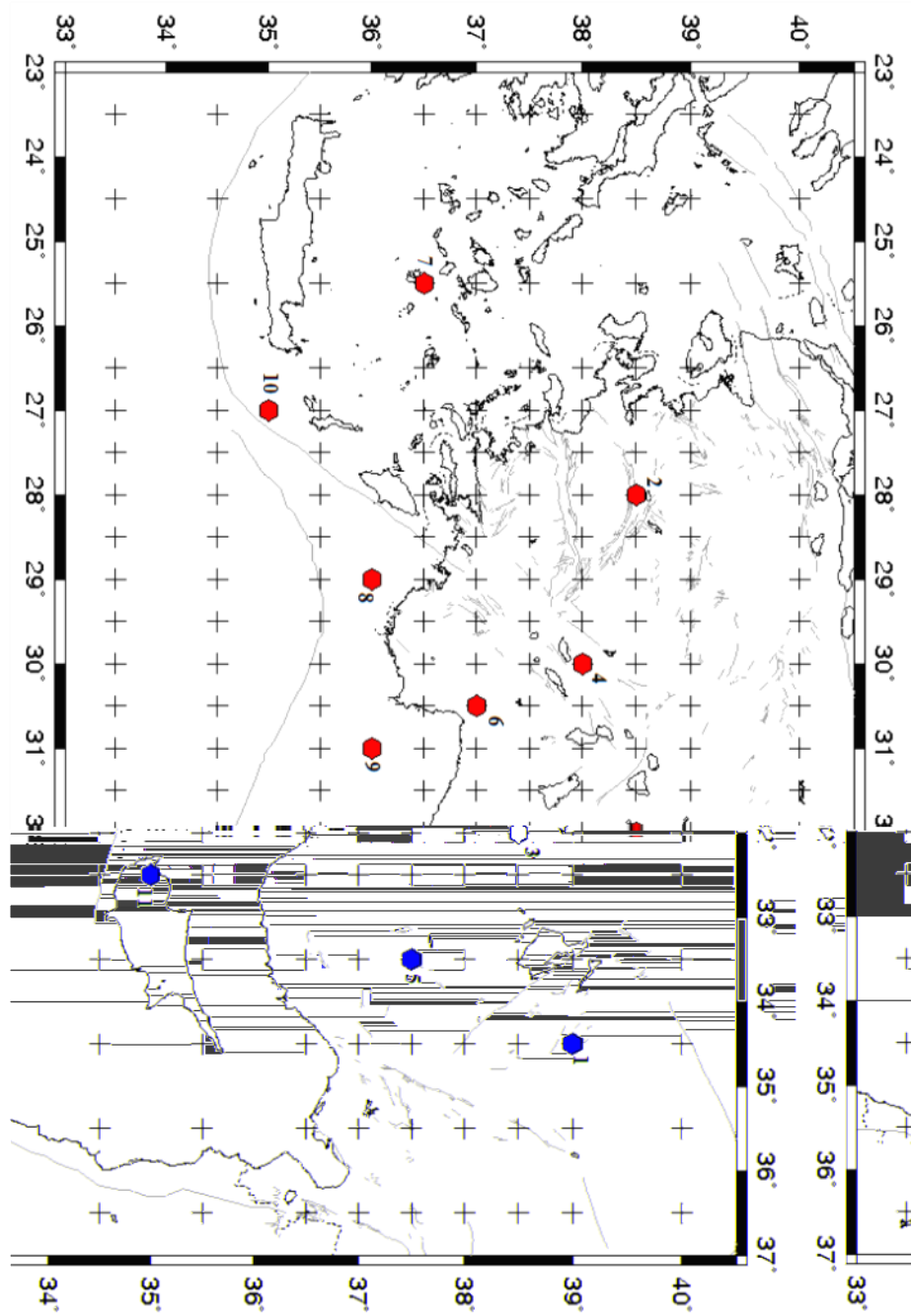
Figure A.1. The locations of dispersion curves (red hexagons) presented in Figure A.2 with the corresponding numbers.
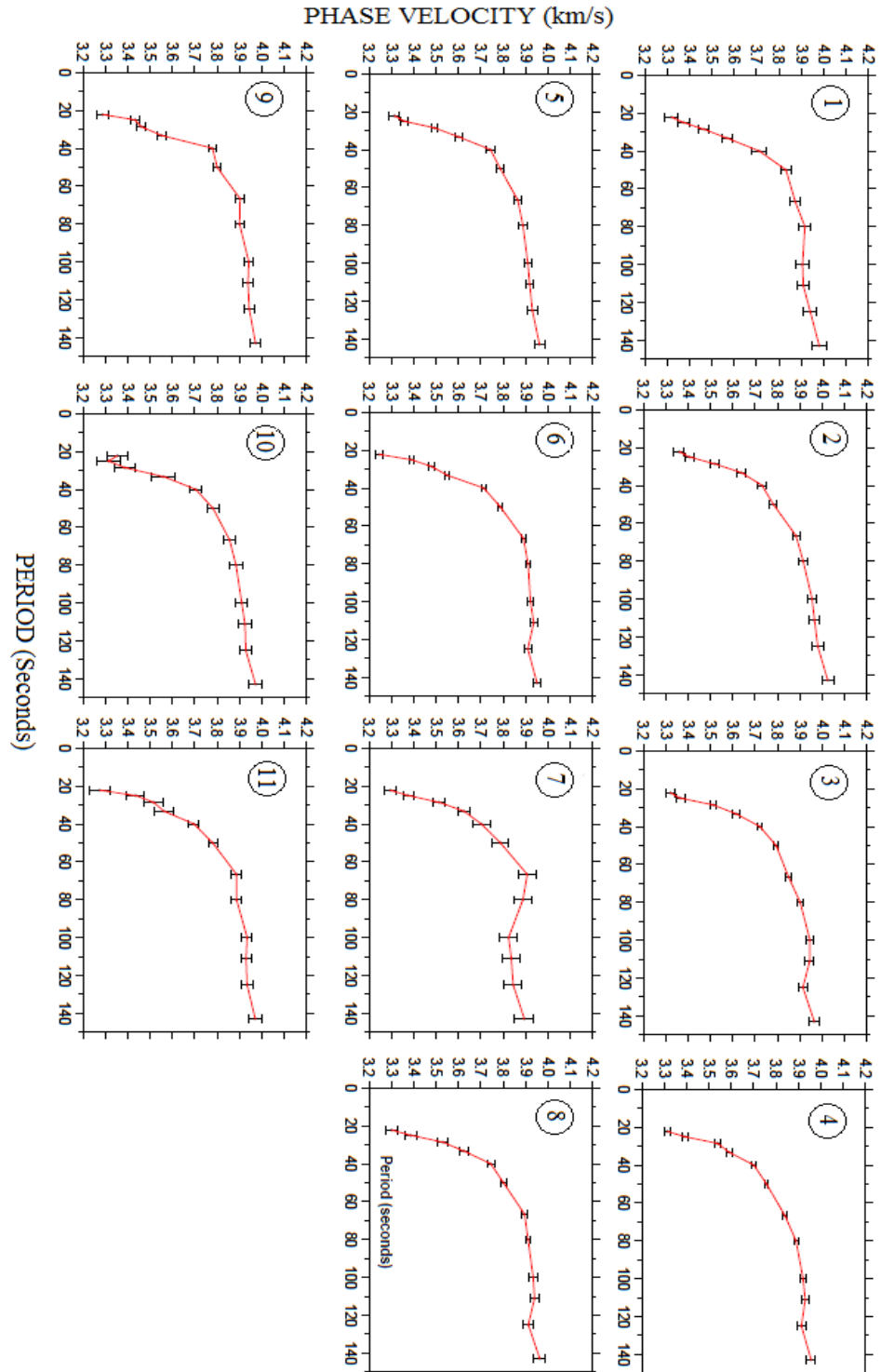
Figure A.2. Dispersion curves which were extracted from different parts of the final velocity model shown as red hexagons with the corresponding numbers in Figure A.1. Errors are shown with solid bars

REFERENCES

Agostini, S., C. Doglioni, F. Innocenti, P. Manetti, S. Tonarini, M.Y. Savasçın, "The transition from subduction-related to intraplate Neogen magmatism in the Western Anatolia and Aegean area. In: Beccaluva, L., Bianchini, G., Wilson, M. (eds) Cenozoic Volcanism in the Mediterranean Area", *Geological Society of America Special Paper*, Vol. 418, pp. 1–16, 2007.

Aki, K., P.G. Richards, "   , University Science Books, Sausalito, CA, 2002.

Akyol, N., L. Zhu, B.J. Mitchell, H. Sözbilir and K. Kekovalı, "Crustal structure and local seismicity in western Anatolia", *Geophys. J. Int., Vol.* 166, pp.1259–1269, 2006.

Alçiçek, M.C., N. Kazanç, M. Özkul, "Multiple rifting pulses and sedimentation pattern in the Cameli Basin, southwestern Anatolia, Turkey", *Sediment. Geol.*, Vol. 173, pp. 409–431, 2005.

Al-Lazki, A., D. Seber, E. Sandvol, N. Türkelli, R Mohamad and M. Barazangi, "Tomographic Pn Velocity and Anisotropy Structure beneath the Anatolian plateau (eastern Turkey) and surrounding regions", *Geophys. Res. Lett.,* Vol. 30, 2003.

Al-Lazki, A. I., E. Sandvol, D. Seber, M. Barazangi, N. Türkelli and R. Mohammad, "Pn tomographic imaging of mantle lid velocity and anisotropy at the junction of the Arabian, Eurasian and African plates", *Geophysical Journal International*, Vol. 158, pp. 1024–1040, 2004.

Amaaru, M.L., "*Global travel time tomography with 3-* Utrecht University, 2007.

Angus D.A., D. C. Wilson, E. Sandvol and J. F. Ni, "Lithospheric structure of the Arabian and Eurasian collision zone in Eastern Turkey from S-wave receiver functions", *Geophys. J. Int.,* Vol. 166 (3), pp. 1335–1346, 2006.

Armijo R., F. Flerit, G. King, B. Meyer, "Linear elastic fracture mechanics explains the past and present evolution of the Aegean", *Earth Planet Sci Lett.*, Vol. 217, pp. 85–95, 2003.

Bakırcı, T., K. Yoshizawa and M. F. Özer, "Three-dimensional S-wave structure of the upper mantle beneath Turkey from surface wave tomography", *Geophys. J. Int.,* Vol. 190, pp. 1058-1076, 2012.

Barka, A.A., R. Reilinger, "Active tectonics of the Mediterranean region: deduced from GPS, neotectonic and seismicity data", *Annali di Geophis*, Vol. XI, pp. 587–610, 1997

Barka, A., R. Reilinger, F. Saroglu, and A.M.C. Sengor, "The Isparta angle: Its importance in the neotectonics of the eastern Mediterranean region", in O. Piskin, M. Ergun, M.Y. Savascin, and G. Tarcan, eds., *International Earth Sciences Colloquium of the Aegean Region, 9-14 October 1995, Izmir-Gulluk, Turkey, Proceedings*, **1**, pp. 3-17, 2005.

Ben-Avraham, Z., A. Ginzburg, J. Makris, and L. Eppelbaum, "Crustal Structure of the Levant Basin, eastern Mediterranean, *Tectonophysics*", Vol. 346, pp. 23-43, 2002.

Bensen, G.D.., M. H. Ritzwoller, M. P. Barmin, A. L. Levshin, F. Lin, M. P. Moschetti, N. M. Shapiro and Y. Yang, "Processing seismic ambient noise data to obtain reliable broad-band surface wave dispersion measurements", *Geophys. J. Int,* 169, pp. 1239–1260, 2007.

Bijward, H., W. Spakman, and E. R. Engdahl. "Closing the gap between regional and global travel time tomography", *J. Geophys. Res*, 103, pp. 30,055– 30,078, 1998.

Biryol, B.C., S. L. Beck, G. Zandt, A. A. Özacar, "Segmented African Lithosphere Beneath The Anatolian Region Inferred From Teleseismic P-Wave Tomography", *Geophys. J. Int.,* Vol. 184, pp. 1037-1057, 2011.

Biryol, C.B., G. Zandt, S. L. Beck, A. A. Özacar, H. E. Adiyaman and C. R. Gans, "Shear wave splitting along a nascent plate boundary: the North Anatolian Fault Zone", *Geophysical Journal International*, Vol. 181, pp. 1201–1213, 2010.

Bohnhoff, M., J. Makris, D. Papanikolaou and G. Stavrakakis G, "Crustal investigation of the Hellenic subduction zone using wide aperture seismic data", *Tectonophysics*, Vol. 343, pp. 239–262, 2001.

Boschi, L., and A. M. Dziewonski, "Highand low-resolution images of the Earth's mantle: Implications of different approaches to tomographic modeling". *J. Geophys. Res.*, 104 (B11), 25,567–25,594, 1999.

Bourova, E., I. Kassaras, A. H. Pedersen, T. Yanovskaya, D. Hatzfeld, and A. Kiratzi, "Constraints on absolute *S* velocities beneath the Aegean Sea from surface wave analysis." *Geophys. J. Int.* pp. 1006–1019 doi: 10.1111/j.1365-246X.2005.02565.x, 2005.

Bozkurt, E., "Neotectonics of Turkey-a synthesis", *Geodin. Acta,* Vol. 14, pp. 3– 30, 2001.

Bruneton, M., H. A. Pedersen, V. Farra, N. T. Arndt, P. Vacher, U. Achauer, A. Alinaghi, J. Ansorge, G. Bock, W. Friederich, M. Grad, A. Guterch, P. Heikkinen, S. E. Hjelt, T. L. Hyvonen, J. P. Ikonen, E. Kissling, K. Komminaho, A. Korja, E. Kozlovskaya, M. V. Nevsky, H. Paulssen, N. I. Pavlenkova, J. Plomerova, T. Raita, O. Y. Riznichenko, R. G. Roberts, S. Sandoval, I. A. Sanina, N. V. Sharov, Z. H. Shomali, J. Tiikkainen, E. Wielandt, K. Wilegalla, J. Yliniemi and Y. G. Yurov, "Complex lithospheric structure under the central Baltic Shield from surface wave tomography". *J. Geophys. Res.*, 109 (B10303), 2004.

Bruneton, M., V. Farra, A. H. Pedersen and the SVEKALAPKO Seismic Tomography Working Group, "Non-linear surface wave phase velocity inversion based on ray theory", *Geophys. J. Int*, 151, pp. 583–596, 2002.

Bullen, K. E., and B. A. Bolt, "An Introduction to the Theory of Seismology 4th ed. xvii + 499 pp. Cambridge, London, New York, New Rochelle, Melbourne, Sydney: *Cambridge University Press*, 1985.

Cambaz, D., and H. Karabulut, "Love-wave group velocity maps of Turkey and surrounding regions", *Geophys. J. Int.,* Vol. 181, pp. 502-520, 2010.

Calixto, F. J., E. Sandvol, S. Kay, P. Mulcahy, B. Heit, X. Yuan, B. Coira, D. Comte, and P. Alvarado, "Velocity structure beneath the southern Puna plateau: Evidence for delamination", *Geochemistry, Geophysics, Geosystems*, 14 (10), pp. 4292-4305, 2013.

Ceylan, S., J. Ni, J. Y. Chen, Q. Zhang, F. Tilmann, and E. Sandvol, "Fragmented Indian plate and vertically coherent deformation beneath eastern Tibet", *Journal of Geophysical Research*, 117 (B11303), doi:10.1029/2012jb009210, 2012.

Cho, K.H., R. B. Hermann, C. J. Ammon and K. Lee, "Imaging the crust of the Korean peninsula by surface wave tomography", *Bull. seism. Soc. Am*, 97 (18), pp. 198-207, 2006.

Clayton, R. W, "Seismic Tomography (abstract)", Eos. Trans.Am. Geophys. Union ,65, 236, 1984.

Çevikbilen-Yolsal, S., T. Taymaz, "Earthquake source parameters along the Hellenic subduction zone and numerical simulations of historical tsunamis in the Eastern Mediterranean", *Tectonophysics*, 536, pp. 61-100, 2012.

De Boorder H., W. Spakman, S. H. White, M. J. R. Wortel, M.J.R, "Late Cenozoic mineralization, orogenic collapse and slab detachment in the European Alpine Belt", *Earth Planet. Sci. Lett.*, Vol. 164, pp. 569–575, 1998.

Debayle, E., and B. L. N. Kennett, "The Australian continent upper mantle: Structure and deformation inferred from surface waves", J. Geophys. Res., 105, 25, pp. 423–25,450, 2000.

Delph, J. R., C. B. Biryol, S. L. Beck, G. Zandt and K. M. Ward, "Shear wave velocity structure of the Anatolian Plate: anomalously slow crust in southwestern Turkey", *Geophys. J. Int*., 202, pp. 261–276 doi: 10.1093/ gji/ggv141, 2015.

Dilek, Y., "Collision tectonics of the Mediterranean region: Causes and consequences", *Geological Society of America, Special Paper* 40, DOI: 10.1130/2006.2409(01), 2006.

Dilek, Y., and S. Altunkaynak, "Geochemical and temporal evolution of Cenozoic magmatism in western Turkey: mantle response to collision, slab break-off, and lithospheric tearing in an orogenic belt", *J. Geol. Soc. London, Special Publications*, Vol. 311, pp. 213 – 233, 2009.

Dilek, Y., and E. A. Sandvol, "Seismic structure, crustal architecture and tectonic evolution of the Anatolian-African Plate Boundary and the Cenozoic Orogenic, Belts in the Eastern Mediterranean Region", *J. Geol. Soc. London, Special Publications,* Vol. 327, pp. 127 – 160, 2009.

DiLuccio, F., M. E. Pasyanos, "Crustal and upper-mantle structure in the eastern Mediterranean from the analysis of surface wave dispersion curves", *Geophys. J. Int.,* Vol. 169, pp. 1139–1152, 2007.

Dumont, J.F., E. Kerey E., "L'accident de Kırkkavak, un de´crochement majeur dans le Taurus occidental", , Vol. 16, pp. 1071–1073, 1975.

Ekstrom, G., J. Tromp, and E. W. F. Larson, "Measurements and global models of surface wave propagation", *J. geophys. Res.,* 102, pp. 8137–8157, 1997.

Endrun, B., S. Lebedev, T. Meier, C. Tirel, W. Friederich, "Complex layered deformation within the Aegean crust and mantle revealed by seismic anisotropy", *Nat. Geosci.,* 4, pp. 203-207, 2011.

Engdahl, E.R., R. D. van der Hilst and R. Buland, "Global teleseismic earthquake relocation with improved travel times and procedures for depth relocation", *Bull. Seism. Soc. Am.*, Vol. 88, pp. 722–743, 1998.

Erduran, M., B. Endrun and T. Meier, "Continental vs. Oceanic Lithosphere beneath the Eastern Mediterrranean Sea-Implications from Rayleigh Wave Dispersion Measurements", *Tectonophysics*, Vol. 457, pp. 42-52, 2008.

Erduran, M., "Teleseismic inversion of crustal S-wave velocities beneath the Isparta Station", *J. Geodynamics.,* Vol. 47, pp. 225–236, 2009.

Faccenna, C., O. Bellier, J. Martinod, C. Piromallo, and V. Regard, "Slab detachment beneath eastern Anatolia: A possible cause for the formation of the North Anatolian fault", *Earth Planet. Sci. Lett.*, Vol. 242, pp. 85-97, 2006.

Faccenna, C., L. Jolivet, C. Piromallo, and A. Morelli, "Subduction and the depth of convection in the Mediterranean mantle", *J. Geophys. Res.*, Vol. 108(B2), 2003.

Faccenna, C., T. W. Becker, C. P. Conrad, L. Husson, "Mantle convection in the Middle East: Reconciling Afar Upwelling, Arabia indentation and Aegean trench rollback", *Earth Planet. Sci. Lett,* 375, pp. 254-269, 2013.

Forsyth, D. W., S. Webb, L. Dorman, and Y. Shen, "Phase velocities of Rayleigh waves in the MELT experiment on the East Pacfic Rise", *Science*, 280, 1235–1238, 1998.

Forsyth, D. W., and A. Li, "Array-analysis of two-dimensional variations in surface wave phase velocity and azimuthal anisotropy in the presence of multi-pathing interference", in SeismicEarth: Array Analysis of Broadband Seismograms, Geophys. Monogr. Ser., vol. 157, edited by A. Levander and G. Nolet, pp. 81–97, AGU, Washington, D. C, 2005.

Friederich, W., and E. Wielandt, "Intepretation of seismic surface waves in regional networks: Joint estimation of wavefield geometry and local phase velocity: Method and tests", *Geophys. J. Int*, 120, 731– 744, 1995.

Friederich, W., "Propagation of seismic shear and surface waves in a laterally heterogeneous mantle by multiple forward scattering", *Geophys. J. Int.,* 136, 180–204, 1999.

Gans, C.R., S. L. Beck, G. Zandt, C. B. Biryol, and A. A. Özacar, "Detecting the limit of slab break-off in Central Turkey: New high-resolution *Pn* tomography results", *Geophys. J. Int.,* Vol. 179, pp. 1566-1572, 2009.

Glover, C., and A.D. Robertson, "Neotectonic intersection of the Aegean and Cyprus tectonic arcs: extensional and strike-slip faulting in the Isparta Angle, SW Turkey", *Tectonophysics*, Vol. 298, pp. 103–132, 1998.

Glover, C., and A. H. F. Robertson, "Role of extensional processes and uplift in the Plio-Quaternary sedimentary and tectonic evolution of the Aksu Basin, southwest Turkey", *J. Geol. Soc., London*, Vol. 155, pp. 365-368, 1998.

Gök, R., M. E. Pasyanos, and E. Zor, "Lithospheric structure of the continent–continent collision zone: eastern Turkey", *Geophys. J. Int.,* Vol. 169, pp. 1079–1088, 2007.

Gök, R., E. A. Sandvol, N. Türkelli, D. Seber, and M. Barazangi, "Sn attenuation in the Anatolian and Iranian plateau and surrounding regions", *Geophysical Research Letters*, Vol. 30(24), 2003.

Gök, R., N. Türkelli, E. Sandvol, D. Seber, and M. Barazangi, "Regional wave propagation in Turkey and surrounding regions", *Geophys. Res. Lett.*, Vol. *27*, pp. 479- 432, 2000.

Govers, R., M. J. R. Wortel, "Lithosphere tearing at STEP faults: Response to edges of subduction zones", *Earth Planet. Sci. Lett.,* Vol. 236, pp. 505–523, 2005.

Grand, S. P., "Mantle shear wave tomography and the fate of subducted slabs". *Phil. Trans. R. Soc. London.*, 360, pp. 2475–2491, 2002.

Grand, S. P., R. van der Hilst, and S. Widiyantoro, "Global seismic tomography: a snapshot of convection in the Earth" *GSA Today*, **7**(4), pp. 1–7, 1997.

Gülen, L., "Isotopic characterization of Aegean magmatism and geodynamic evolution of the Aegean subduction", in *Proceedings of the International Earth Science Colloquium on the Aegean Region,* Izmir, Turkey, Vol. 2, pp. 143–167, 1990.

Hatzfeld, D., E. Karagianni, I. Kassaras, A. Kiratzi, E. Louvari, H. Lyon-Caen, K. Makropoulos, P. Papadimitriou, G. Bock, and K. Priestley, "Shear wave anisotropy in the upper-mantle beneath the Aegean related to internal deformation", *J. Geophys, Res.*, Vol. 106, pp. 30,737-30,753, 2001.

Huang, Z., W. Su, Y. Peng, Y. Zheng, and H. Li, "Rayleigh wave tomography of China and adjacent regions", J. Geophys. Res., 108(B2), 2073, doi:10.1029/2001JB001696, 2003.

Humphreys, E. D., and R. W. Clayton, "Tomographic image of the southern California mantle", J. *Geophys. Res*., 95, pp. 19,725– 19,746, 1990.

Humphreys, E. D., and B. H. Hager, "A kinematic model for the late Cenozoic development of southern California crust and upper mantle", *J. Geophys. Res*., 95, 19, pp. 747–19,762, 1990.

Jolivet, L., J. P. Brun, S. Gautier, S. Lellemand, and M. Patriat, "3D kinematics of extension in the Aegean from the early Miocene to the present: insight from the ductile crust", *Bulletin de la Societe Geologique de France*, Vol. 165, pp. 195–209, 1994.

Jolivet, L., and C. Faccenna, "Mediterranean extension and the Africa-Eurasia collision. Tectonics", Vol. 19, pp. 1095–1106, 2000.

Jolivet, L., C. Faccenna, B. Goffe´, E. Burov, and P. Agard, "Subduction tectonics and exhumation of high-pressure metamorphic rocks in the Mediterranean orogens", *Am J Sci*, Vol. 303, pp. 353–409, 2003.

Kahle, H. G., M. Cocard, Y. Peter, A. Geiger, R. Reilinger, S. McClusky, R. King, A. Barka, and G. Veis, "The GPS strain rate field in the Aegean Sea and western Anatolia", *Geophysical Research Letters*, Vol. 26, pp. 2513–2516, 1999.

Karagianni, E. E., D. G. Panagiotopoulos, G. F. , Panza, P. Suhadolc, C. B. Papazachos, A. Kiratzi, D. Hatzfeld, K. Makropoulos, K. Priestley, and A. Vuan, "Rayleigh wave group velocity tomography in the Aegean area", *Tectonophysics,* Vol. 358, pp. 187–209, 2002.

Karagianni, E. E., C. B. Papazachos, D. G. Panagiotopoulos, P. Suhadolc, A. Vuan, and G. F. Panza, "Shear velocity structure in the Aegean area obtained by inversion of Rayleigh waves", *Geophys J Int*, Vol. 160, pp. 127–143, 2005.

K´arason, H., and R. D. van der Hilst, "Tomographic imaging of the lowermost mantle with differential times of refracted and diffracted core phases (PKP, Pdiff)". *J. Geophys. Res.*, 106(B4), pp. 6569–6587, 2001.

Kempler, D., and Z. Ben-Avraham, "The tectonic evolution of the Cyprus arc", *Annales Tectonicae*, Vol. 1, pp. 58–71, 1987.

Kempler, D., and Z. Garfunkel, "Structures and kinematics in the northeastern Mediterranean: a study of an irregular plate boundary", *Tectonophysics*, Vol. 234, pp. 19–32, 1994.

Kennett, B. L. N., E. R. Engdahl, and R. Buland, Constraints on seismic velocities in the Earth from traveltimes. *Geophys. J. Int*, 122, pp. 108–124, 1995.

Kennett, B. L. N., S. Widiyantoro, and R. D. van der Hilst, R, "Joint seismic tomography for bulk sound and shear wave speed in the Earth's mantle", *J. Geophys. Res.*, 103, pp. 12469– 93, 1998.

Kenneth, B. L. N., and K. Yoshizawa, "A reappraisal of regional surface wave tomography", *Geophys. J. Int,* 150, pp. 37–44, 2002.

Kennett, B. L. N. and A. Gorbatov, "Seismic heterogeneity in the mantle - strong shear wave signature of slabs from joint tomography", *Phys. Earth Planet. Int.*, 146, pp. 87–100, 2004.

Keskin, M., "Magma generation by slab steepening and breakoff beneath a subduction–accretion complex: An alternative model for collision-related volcanism in Eastern Anatolia, Turkey", *Geophys. Res. Lett.,* Vol. 30, pp. 8046 – 8050, 2003.

Khair, K., N. G. Tsokas, "Nature of the Levantine (eastern Mediterranean) crust from multiple-source Werner deconvolution of Bouguer gravity anomalies", *Journal of Geophysical Research*, Vol. 104, pp. 25,469-25,478, 1999.

Kiratzi, A., and E. Louvari, "Focal mechanisms of shallow earthquakes in the Aegean Sea and the surrounding lands determined by waveform modeling: a new database", *J. Geodyn.,* Vol. 36, pp. 251–274, 2003.

Kiratzi, A. A., and C. B. Papazachos, "Active deformation of the shallow part of the subducting lithospheric slab in the Southern Aegean", *Journal of Geodynamics*, Vol. 19, pp. 65 – 78, 1995.

Kissel, C., and A. Poisson, "Étude paléomagnetique préliminaire des formations cénozoïques des Bey Daglari (Taurides occidentales, Turquie)", *Comptes Rendus Acadademie Science Paris*, Vol. 304, pp. 343–348, 1987.

Kissel, C., O. Averbuch, D. Frizon de Lamotte, O. Monod, and S. Allerton, "First paleomagnetic evidence of a post-Eocene clockwise rotation of the western Taurus belt, east of the Isparta reentrant (southwestern Turkey)", *Earth and Planetary Science Letters*, Vol. 117, pp. 1–14, 1990.

Knopoff, L., "Observation and inversion of surface-wave inversion", *Tectonophysics*, 13, 497-519, 1972.

Koçyigit, A., and A. A. Özacar, "Extensional neotectonic regime through the NE edge of the Outer Isparta Angle, SW Turkey: new field and seismic data", *Turk J Eart Sci*, Vol. 12, pp. 67–90, 2003.

Koçyiğit, A., E. Ünay, and G. Saraç, "Episodic graben formation and extensional neotectonic regime in west Central Anatolia and the Isparta Angle: a case study in the Aksehir–Afyon graben, Turkey", *Tectonics and Magmatism in Turkey and the Surrounding Area, Bozkurt E, Winchester JA, Piper JDA (eds), Special Publication Geological Society: London,* Vol. 173, pp. 405–421, 2000.

Koulakov, I., and S. V. Sobolev, "Moho depth and three-dimensional *P* and *S* structure of the crust and uppermost mantle in the Eastern Mediterranean and Middle East derived from tomographic inversion of local ISC data", *Geophys. J. Int.*, 164, pp. 218-235, doi:10.1111/j.1365 246X.2005.02791.x, 2005.

Lay, T., and T. Wallace, "Modern Global Seismology", *Academic Press*, ISBN: 978-0-12-732870-6, 1995.

Lei, J., and D. Zhao, "Global P-wave tomography: On the effect of various mantle and core phases", *Phys. Earth Planet. Int.*, 154, pp. 44– 69, 2006.

Le Pichon, X., C. Kreemer, "The Miocene-to-Present kinematic evolution of the Eastern Mediterranean and Middle East and its implications for dynamics", *Annu. Rev. Earth. Sci.,* 38, pp. 323-351, 2010.

Li, X., A. G. Bock, R., Vafidis, H. P. Kind, W. Harjes, K. Hanka, M. Wylegalla, V. D. Meijde, and X. Yuan, "Receiver function study of the Hellenic subduction zone: Imaging crustal thickness variations and the oceanic Moho of the descending African lithosphere", *Geophys. J. Int*., Vol. 155, pp. 733– 748, 2003.

Li, A., D. W. Forsyth, and K. M. Fischer, "Shear velocity structure and azimuthal anisotropy beneath eastern North American from Rayleigh wave inversion", *J. Geophys. Res.,* 108(B8), 2362, doi: 10.1029/ 2002JB002259, 2003.

Li, A., 2011, "Shear wave model of southern Africa from regional Rayleigh wave tomography with 2-D sensitivity kernels", *Geophys J. Int*, 185(2), pp. 832-844, doi:10.1111/j.1365-246X.2011.04971.x, 2011.

Li, X., H. Li, Y. Shen, M. Gong, D. Shi, E. A. Sandvol, and A. Li, "Crustal Velocity Structure of the Northeastern Tibetan Plateau from Ambient Noise Surface-Wave Tomography and Its Tectonic Implications", *Bulletin of the Seismological Society of America*, Vol. 104, No. 3, pp. 1045-1055 ,doi: 10.1785/0120130019, 2014.

Maggi, A., K. Priestly, "Surface waveform tomography of the Turkish–Iranian plateau", *Geophys. J. Int.,* Vol. 160, pp. 1068–1080, 2005.

Makris, J., Z. Ben-Avraham, and A. Behle, "Seismic reflection profiles between Cyprus and Israel and their interpretation". *Geophysical Journal of the Astronomical Society,* 75, pp. 575-591, 1983.

Marone, F., M. V. D. Meijde, S. van der Lee, and D. Giardini, "Joint inversion of local, regional, and teleseismic data for crustal thickness in the Eurasia–Africa plate boundary region", *Geophys. J. Int*. 154, pp. 499–514, 2003.

McClusky, S., S. Balassanian, A. Barka, C. Demir, S. Ergintav, I. Georgiev, O. Gurkan, M. Hamburger, K. Hurst, H. Kahle, K. Kastens, G. Kekelidze, R. King, V. Kotzev, O. Lenk, S. Mahmoud, A. Mishin, M. Nadariya, A. Ouzounis, D. Paradissis, Y. Peter, M. Prilepin, R. Reilinger, I. Sanli, H. Seeger, A. Tealeb, M. N. Toksöz, and G. Veis, "Global Positioning System constraints on plate kinematics and dynamics in the eastern Mediterranean and Caucasus", *Journal of Geophysical Research*, Vol. 105, pp. 5695–5719, 2000.

McClusky, S., R. Reilinger, S. Mahmoud, D. Ben Sari, and A. Tealeb, "GPS constraints on Africa (Nubia) and Arabia plate motions", *Geophys. J. Int.*, Vol. 155, pp. 126–138, 2003.

McKenzie, D.P., "Active tectonics of the Alpine–Himalayan belt: the Aegean Sea and surrounding regions", *Geophys. J. Royal Astron. Soc.*, Vol. 55, pp. 217–254, 1978.

Meier, T., M. Rische, B. Endrun, A. Vafidis, and H. P. Harjes, "Seismicity of the Hellenic subduction zone in the area of western and central Crete observed by temporary local seismic networks", *Tectonophysics*, Vol. 383, pp. 149-169, 2004.

Montagner, J. P., and H. C. Nataf, "A simple method for inverting the azimuthal anisotropy of surface waves", *Journal of Geophysical Research: Solid Earth*, 91 (B1), pp. 511-520, doi:10.1029/JB091iB01p00511, 1986.

Moschetti, M.P., M. H. Ritzwoller, and N. M. Shapiro, "Surface wave tomography of the western United States from ambient seismic noise: Rayleigh group velocity maps", *Geochemistry, Geophysics, Geosystems,* Vol: 8 (8), 2007.

Muyzert, E., and R. Snieder, "The Influence of Errors in Source Parameters on Phase-Velocity Measurements of Surface Waves", *Bull. Seismol. Soc. Am.* 86, pp. 1863-1872, 1996.

Nyst, M., and T. Thatcher, "New constraints on the active tectonic deformation of the Aegean", *J. geophys. Res.*, Vol. 109, B11406, 2004.

Özacar, A. A., H. Gilbert, G. Zandt, "Upper mantle discontinuity structure beneath East Anatolian Plateau (Turkey) from receiver functions", *Earth Planet. Sci. Lett.*, Vol. 269, pp. 426–434, 2008.

Özacar, A. A., G. Zandt, H. Gilbert, and S. L. Beck, "Seismic images of crustal variations beneath the East Anatolian Plateau (Turkey) from teleseismic receiver functions", *J. Geol. Soc.,* Vol. 340, pp. 485-496, 2010.

Papazachos, B. C**.,** A. and A. Kiratzi, "A detailed study of the active crustal deformation in the Aegean and surrounding area", *Tectonophysics*, Vol. 253, pp. 129-153, 1996.

Papazachos, B. C., and G. Nolet, "P and S deep velocity structure of the Hellenic area obtained by robust nonlinear inversion of travel times", *J. Geophys. Res.*, Vol. 102, pp. 8349-8367, 1997.

Papazachos, B. C., V. G. Karakostas, C. B. Papazachos, and E. M. Scordilis, "The geometry of the Wadati-Benioff zone and lithospheric kinematics in the Hellenic arc", *Tectonophysics*, Vol. 319, pp. 275–300, 2000.

Pasyanos, M. E., W. R. Walter, and S. E. Hazler, "A surface wave dispersion study of the Middle East and North Africa for monitoring the Comprehensive Nuclear-Test-Ban Treaty", *Pure Appl. Geophys.*, 158, pp. 1445– 1474, 2001.

Pasyanos, M. E and W. R. Walter, "Crust and upper-mantle structure of North Africa, Europe and the Middle East from inversion of surface waves", *Geophys. J. Int.* (2002) 149, pp. 463–481, 2002.

Pasyanos, M.E, "A variable resolution surface wave dispersion study of Eurasia, North Africa, and surrounding regions", *Journal   *, Vol: 110, B12301, 2005.

Pasyanos, M. E., A. A. Nyblade, "A top to bottom lithospheric study of Africa and Arabia", *Tectonophysics*, 444, pp. 27–44, 2007.

Paul, A., H. Karabulut, A. K. Mutlu and G. Salaün, "A comprehensively and densely sampled map of shear-wave azimuthal anisotropy in the Aegean-Anatolia region", *Earth Planet. Sci. Lett*, 389, pp. 14-22, 2014.

Piromallo, C., and A. Morelli, "P wave tomography of the mantle under the Alpine-Mediterranean area", *J. Geophys. Res.*, Vol. 108(B2), 2065, 2003.

Poisson, A., R. Wernli, E. K. Sagular, and H. Temiz, "New data concerning the age of the Aksu Thrust in the south of the Aksu valley, Isparta Angle (SW Turkey) consequences for the Antalya Basin and the Eastern Mediterranean", *Geol. J.*, Vol. 38, pp. 311–327, 2003.

Press, W. H., S. A. Teukolsky, W. T. Vetterling, and B. P. Flannery, "*Numerical Recipes   *, 2nd ed., 963 pp., Cambridge Univ. Press, New York, 1992.

Price, S., and B. Scott, B, "Fault block rotations at the edge of a zone of continental extension: southwest Turkey", *J. Struct. Geol.*, Vol. 16, pp. 381–392, 1994.

Reilinger, R.E., S. C. McClusky, M. B. Oral, W. King, and M. N. Toksöz, "Global Positioning System measurements of present-day crustal movements in the Arabia–Africa-Eurasia plate collision zone", *J. Geophy. Res.*, Vol. 102, pp. 9983–9999, 1997.

Ritzwoller, M. H., N. M. Shapiro, A. L. Levshin, and G. M. Leahy, "Crustal and upper mantle structure beneath Antarctica and surrounding oceans", *J. Geophys. Res.*, 106, pp. 30,645– 30,670, 2001.

Ritzwoller, M. H., N. M. Shapiro, M. P. Barmin, and A. L. Levshin, "Global surface wave diffraction tomography", *J Geophys. Res.*, 107 (B12), 2335, doi:10.1029/2002JB001777, 2002.

Robertson, A.H.F, "Mesozoic–Tertiary sedimentary and tectonic evolution of Neotethyan carbonate platforms, margins and small ocean basins in the Antalya Complex, southwest Turkey." *In Special Publication of the International Association of Sedimentologists 20*, Frostick LE, Steel RJ (eds) , pp. 415–465, 1993.

Robertson, A.H.F, "Tectonic significance of the Eratosthenes Seamount: a continental fragment in the process of collision with subduction zone in the eastern Mediterranean (Ocean Drilling Program Leg 160)", *Tectonophysics*, Vol. 298, pp. 63–82, 1998.

Robertson, A. H. F., O. Parlak, and T. Ustaömer, "Melange genesis and ophiolite emplacement related to subduction of the northern margin of the Tauride–Anatolide continent, central and western Turkey" *In*: van Hinsbergen, D. J. J., Edwards, M. A., Govers, R. (eds) Collision and Collapse at the Africa–Arabia– Eurasia Subduction Zone, *J. Geol. Soc., London*, *Special Publications*, Vol. 311, pp. 9–66, 2009.

Robertson, A. H. F., A. Poisson, and Ö. Akıncı, "Developments in research concerning Mesozoic-Tertiary Tethys and Neotectonics in the Isparta Angle, SW Turkey", *Geol. J.,* Vol. 38 (3–4), pp. 195–234, 2003.

Rychert, C. A., K. M. Fischer, and S. Rondenay, "A sharp lithosphere- asthenosphere boundary imaged beneath eastern North America", *Nature*, 436, pp. 542– 545, 2005.

Sahin, S., B. Xueyang, N. Turkelli, E. A. Sandvol, U. M. Teoman, and M. Kahraman, "Lg Attenuation in Western Turkey and the Surrounding Regions", SSA 2009 Annual Meeting, California, USA, 2009.

Sabra, K. G., P. Gerstoft, P. Roux, W. A. Kuperman, and M. C. Fehler, "Surface wave tomography from microseism in southern California", *Geophys. Res. Lett.,* 32, L14311, doi:10.1029/2005GL023155, 2005.

Saito, M., "DISPER80: A subroutine package for the calculation of seismic normal-mode solutions", in *Seismological Algorithms*, edited by D. J. Doornbos, pp. 293–319, Elsevier, New York, 1988.

Salaün, G., H. A. Pedersen, A. Paul, V. Farra, H. Karabulut, D. Hatzfeld, C. Papazachos, D. M. Childs, C. Pequegnat, and SIMBAAD Team, "High-resolution surface wave-tomography of the Aegean-Anatolia region: constraints on upper mantle structure", *Geophys. J. Int.,* 190, pp. 406–420, 2012.

Sandvol, E., N. Türkelli, E. Zor, R. Gök, T. Bekler, C. Gürbüz, D. Seber, and M. Barazangi, "Shear wave splitting in a young continent-continent collision: An example from Eastern Turkey", *Geophys. Res. Lett.,* Vol. 30(24), pp. 8041, 2003.

Sapaş, A., and A. B. Güney, "Shear wave splitting in the Isparta Angle, southwestern Turkey: anisotropic complexity in the mantle", *J .Earth Syst. Sci.,* Vol. 118, pp. 71–80, 2009.

Saunders, P., K. Priestley, T. Taymaz, "Variations in the Crustal Structure beneath Western Turkey", *Geophys. J. Int.*, Vol. 134, pp. 373-389, 1998.

Savaşçın, M. Y., and T. Oyman, "Tectono–Magmatic Evolution of Alkaline Volcanics at the Kırka–Afyon–Isparta Structural Trend, Sw Turkey", *Tr. J. of Earth Sciences*, Vol. 7, pp. 201-214, 1998.

Schmid, C., S. Van Der Lee, D. Giardini, "Delay times and shear wave splitting in the Mediterranean region", *Geophys. J. Int.,* Vol. 159, pp. 275–290, 2004.

Segev, A., M. Rybakov, V. Lyakhovsky, A. Hofstetter, G. Tibor, V. Goldshmidt, and Z. Ben- Avraham, "The structure, isostasy and gravity field of the Levant continental margin and the southeast Mediterranean area", *Tectonophysics*, Vol. 425, pp. 137–157, 2006.

Şengör, A. M. C., N. Görür, F. Saroğlu, "Strike-slip faulting and related basin formation in zones of tectonic escape: Turkey as a case study", *In*: Biddle, K. T., and Christie-Blick, N. (eds), Strike-slip Faulting and Basin Formation, *Soc. Econ. Paleont. Miner. Spec. Publ.*, Vol. 37, pp. 227-264, 1985.

Şengör, A. M. C., S. Özeren, T. Genç, and E. Zor, "East Anatolian high plateau as a mantle supported, north-south shortened domal structure", *Geophys. Res. Lett.,* Vol. 30 (24), pp. 8045, 2003.

Seyitoglu, G., B. C. Scott, C. C. Rundle, "Timing of Cenozoic extensional tectonics in west Turkey", *Journal of the Geological Society London*, Vol. 149, pp. 533–538, 1992.

Shapiro, N. M., M. Campillo, L. Stehly, and M. H. Ritzwoller, "High resolution surface wave tomography from ambient seismic noise", *Science,* 307, pp. 1615–1618, 2005.

Shaw, B., J. Jackson, "Earthquake mechanisms and active tectonics of the Hellenic subduction zone", *Geophys. J. Int*, 181, pp. 966-984, 2010.

Smith, M. L., and F. A. Dahlen, "The azimuthal dependence of Love and Rayleigh wave propagation in a slightly anisotropic medium", *J. Geophys. Res*, 78, pp. 3321– 3333, 1973.

Sodoudi, F., R. Kind, D. Hatzfeld, K. Priestley, W. Hanka, K. Wylegalla, G. Stavrakakis, A. Vafidis, H. P. Harjes, and M. Bohnhoff, 2006, "Lithospheric structure of the Aegean obtained from P and S receiver functions", *J. Geophys. Res.*, Vol. 111, B12307, pp. 1-23, 2006.

Spakman, W., and G. Nolet, "Imaging algorithms, accuracy and resolution in delay time tomography", In N. Vlaar, G. Nolet, M. Wortel, and S. Cloetingh, editors, *Mathmatical Geophysics*, pp. 155–187, 1988.

Spakman, W., S. van der Lee, and R. D. van der Hilst, "Travel-timetomography of the European-Mediterranean mantle down to 1400 km", *Phys. Earth planet. Int.,* 79, pp. 3–74, 1993.

Spetzler, J., J. Trampert, and R. Snieder, "The effect of scattering in surface wave tomography", *Geophys. J. Int.*, 149, pp. 755– 767, 2002.

Stein, S., C. A. Stein, "Thermo-mechanical evolution of oceanic lithosphere: implications for the subduction process and deep earthquakes", In: Bebout, E., Scholl, D. W, Kirby, S. H, Platt, J. P., Subduction Top to Bottom, *Geophysical Monograph*, Vol. 96, American Geophysical Union, Washington, 1996.

Stixrude, L., and C. Lithgow-Bertelloni, "Mineralogy and elasticity of the oceanic upper mantle: Origin of the low-velocity zone", *J. Geophys. Res.*, 110, B03204, doi:10.1029/2004JB002965, 2005.

Tarantola, A., and B. Valette, "Generalized non-linear problems solved using the least-squares criterion", *Rev. Geophys.*, 20, pp. 219– 232, 1982.

Tatar, M., D. Hatzfeld, J. Martinod, A. Walpersdorf, M. Ghafori-Ashtiany, and J. Chery, "The present day deformation of the central Zagros from GPS measurements", *Geophysical Research Letters*, Vol. 29, pp. 1927-1930, 2002.

Taymaz, T., J. Jackson, D. McKenzie, D, "Active tectonics of the north and central Aegean Sea", *Geophys. J. Int.*, Vol. 106, pp. 433–490, 1991.

Taymaz, T., and O. Tan, "Source parameters of June 6, 2000 Orta-Çankırı (Mw = 6.0) and December 15, 2000 Sultandağ-Akşehir (Mw = 6.0) earthquakes obtained from inversion of teleseismic P- and SH- body waveforms", In: *Scientific activities 2001 symposia*, Istanbul Technical University the Faculty of Mines, Extended Abstracts, Istanbul, pp. 96–107, 2001.

Taymaz, T., O. Tan, S. Özalaybey, H. Karabulut, "Source characteristics of February 3, 2002 Çay-Sultandağ Earthquake (Mw=6.5) sequence in SW-Turkey: a synthesis of seismological observations of body-waveforms, strong motions, and aftershock seismicity survey data", *1st International Symposium of Istanbul Technical University the Faculty of Mines on Earth Sciences and Engineering*, Istanbul-Turkey. Abstracts: 60, 2002.

Taymaz, T., Y. Yılmaz, and Y. Dilek, "The Geodynamics of the Aegean and Anatolia: Introduction", In*: The Geodynamics of the Aegean and Anatolia (eds. Tuncay Taymaz, Yücel Yılmaz , Yıldırım Dilek), *J. Geol. Soc., London, Special Publications*, Vol. 29, pp. 1-16, 2007.

Ten Veen, J., J. Woodside, T. C. Zitter, J. Dumont, J. Mascle, and A. Volkonskaia, "Neotectonic evolution of the Anaximander Mountains at the junction of the Hellenic and Cyprus arcs", *Tectonophysics*, Vol. 391, pp. 35-65, 2004.

Tezel, T., T. Shibutani, and B. Kaypak, "Crustal structure variation in western Turkey inferred from the receiver function analysis", *Tectonophysics*, Vol. 492, pp. 240-252, 2010. Thurber, C.H., "Local earthquake tomography: velocities and Vp / Vs – theory", Seismic Tomography: Theory and Practice edited by H.M. Iyer and K. Hirahara, published by Chapman & Hall, 2-6 Boundary Row, London, 1993.

Tiberi, C., M. Diament, H. Lyon-Caen, H., and T. King, "Moho topography beneath the Corinth Rift area (Greece) from inversion of gravity data", *Geophys. J. Int.*, Vol. 145, pp. 797–808, 2001.

Tirel, C., F. Gueydan, C. Tiberi, and J. Brun, "Aegean crustal thickness inferred from gravity inversion. Geodynamical implications", *Earth Planet. Sci. Lett.*, Vol. 228, pp. 267–280, 2004.

Tiryakioğlu, İ., M. Floyd, S. Erdoğan, E. Gülal, S. Ergintav, S. Mcclusky, and R. Relinger, "GPS Constraints on active deformation in the Isparta Angle Region of SW Turkey", *Geophys. J. Int.*, Vol. 195, issue 3, pp. 1455-1463, 2013.

Tokçaer, M., S. Agostini, and Y. M. Savasçın, "Geotectonic setting and origin of the Youngest Kula Volcanics (Western Anatolia), with a New Emplacement Model", *Turkish J. Earth Sci.,* 14, pp. 145–166, 2005.

Türkelli, N., E. Sandvol, E. Zor, R. Gök, T. Bekler, A. Al-Lazki, H. Karabulut, S. Kuleli, T. Eken, C. Gürbüz, S. Bayraktutan, D. Seber, and M. Barazangi, "Seismogenic zones in Eastern Turkey", *Geophys. Res. Lett.,* Vol. 30, pp. 8039, 2003.

Udias, A., "Principles of Seismology", *Cambridge University Press*, ISBN: 9780521624787, 2000.

Van der Hilst, R. D., S. Widiyantoro, and E. R. Engdahl, "Evidence of deep mantle circulation from global tomography", *Nature*, 386, pp. 578– 584, 1997.

Van Der Meijde, M., S. Van Der Lee, and D. Giardini, "Crustal structure beneath broad-band seismic stations in the Mediterranean region", *Geophys. J. Int.*, Vol. 152, pp. 729–739, 2003.

Van Hinsbergen, D. J. J., E. Hafkenscheid, W. Spakman, J. E. Meulenkamp, and R. Wortel, "Nappe stacking resulting from subduction of oceanic and continental lithosphere below Greece", *Geology*, Vol. 33, pp. 325–328, 2005.

Warren, L. M., S. L. Beck, C. B. Biryol, G. Zandt, A. A. Özacar and Y. Yang, "Crustal velocity structure of Central and Eastern Turkey from ambient noise tomography", *Geophys. J. Int*, 194(3), pp. 1941-1954, 2013.

Wdowinski, S., Z. Ben-Avraham, R. Arvidsson, and G. Ekstrom, "Seismotectonics of the Cyprian Arc", *Geophys. J. Int.*, Vol. 164, pp. 176-181, 2006.

Weeraratne, D. S., D. W. Forsyth, K. M. Fischer, and A. A. Nyblade, "Evidence for an upper mantle plume beneath the Tanzanian craton from Rayleigh wave tomography", *J. Geophys. Res.*, 108(B9), pp. 2427, 2003.

Westaway, B., "Present-day kinematics of the Middle East and eastern Mediterranean", *Journal of Geophysical Research*, Vol. 99, pp. 12071–12090, 1994.

Widiyantoro, S., R. D. Van Der Hilst, and F. Wenzel, "Deformation of the Aegean slab in the mantle transition zone", *International Journal of Tomography, Statistics*, Vol. D04, pp. 1–14, 2004.

Wielandt, E., "Propagation and structural interpretation of non-plane waves", *Geophys. J. Int*, 113, pp. 45–53, 1993.

Woodhouse, J H., and A. Dziewonski, "Mapping the Upper Mantle: Three Dimensional Modelling of Earth Structure by Inversion of Seismic Wavefronts", *J. Geophys. Res*., 89, pp. 5953-5986, 1984.

Wortel, M. J. R., and W. Spakman, "Subduction and slab detachment in the Mediterranean-Carpathian region", *Science*, Vol. 290, pp. 1910–1917, 2000.

Yağmurlu, F., M. Y. Savaşçın, and M. Ergun, "Relation of alkaline volcanism and active tectonism within the evolution of Isparta Angle, SW Turkey", *Journal of Geology*, Vol. 105, pp. 717–728, 1997.

Yang, Y., and D. W. Forsyth, "Rayleigh wave phase velocities, small-scale convection, and azimuthal anisotropy beneath southern California", *Journal of Geophysical Research*, 111(B7), pp. 1978-2012, 2006a.

Yang, Y., and D. W. Forsyth, "Regional tomographic inversion of the amplitude and phase of Rayleigh waves with 2-D sensitivity kernels", *Geophys. J. Int.* (166), pp. 1148-1160, 2006b.

Yang, Y., M. H. Ritzwoller, A. L. Levshin, and N. M. Shapiro, "Ambient noise Rayleigh wave tomography across Europe", *Geophys. J. Int.,* 168, pp. 259–274, 2007.

Yao, H., R. D. Van Der Hilst, and M. V. De Hoop, "Surface-wave tomography in SE Tibet from ambient seismic noise and two-station analysis: I.—Phase velocity maps", *Geophys. J. Int.*, 166, pp. 732–744, 2006.

Yoshizawa, K., and B. L. N. Kennett, "Determination of the influence zone for surface wave paths", *Geophys. J. Int.*, 149, pp. 441–454, 2002.

Zhu, L., B. J. Mitchell, N. Akyol, I. Çemen, and K. Kekovali, "Crustal thickness variation in the Aegean region and its implications for the extension of continental crust", *J. Geophys. Res.,* 111, B01301, 2006.

Zitter, T. A. C., J. M. Woodside, and J. Mascle, "The Anaximander Mountains: a clue to the tectonics of southwest Anatolia", *Geol. J.,* Vol. 38, pp. 375–394, 2003.

Zhang, Q., E. A. Sandvol, J. Ni, J. Y. Chen, "Rayleigh wave tomography of the northeastern margin of the Tibetan Plateau", *Earth and Planetary Science Letters*, Vol. 304, pp. 103-112, 2011.

Zhou, Y., F. A. Dahlen, and G. Nolet, "Three-dimensional sensitivity kernels for surface wave observables", *Geophys. J. Int.*, 158, 142– 168, 2004.

Zor, E., "Tomographic evidence of slab detachment beneath eastern Turkey and the Caucasus", *Geophys. J. Int.,* Vol. 175, pp. 1273-1282, 2008.

Zor, E., E. Sandvol, C. Gürbüz, N. Türkelli, D. Seber, and M. Barazangi, "The Crustal Structure of the East Anatolian Plateau from Receiver Functions", *Geophys. Res. Lett.*, Vol. 30, p. 8044, 2003.